

POLITECNICO DI TORINO

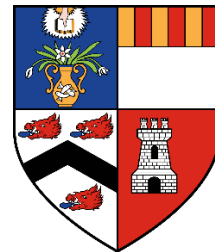
MASTER COURSE: INGEGNERIA PER L'AMBIENTE ED IL  
TERRITORIO

Master Thesis

**Determining soil moisture with an integrated  
monitoring and modelling approach in a  
humid area in NE Scotland**



Politecnico di Torino



University of Aberdeen

Supervisors:  
Professor Pierluigi Claps,  
Lecturer Josie Geris

Candidate:  
Alice Poli

a.a. 2018/2019

# Contents

1. Introduction.....	5
1.1. Background.....	5
1.2. State of the art.....	7
1.3. Main aim and objectives.....	8
2. Methodology.....	9
2.1. Site description and field data collection.....	9
2.1.1. Description of the study area.....	9
2.1.2. Monitoring of the site.....	12
CRS equipment description.....	14
Description of the soil moisture probes (ML2 and PR2).....	15
2.1.3. Sampling campaign for the soil water retention curve.....	18
2.1.4. CRS: Measurement principles and calibration.....	20
Theory.....	21
Radius of influence.....	22
Sample depth.....	23
Correction.....	24
Calibration.....	25
2.2. Characterization of soil hydraulic properties.....	29
2.2.1. Soil water retention curve – theoretical basis.....	29
2.2.2. Laboratory experiments.....	32
Particle size analysis.....	32
Procedure to determine the water retention curve.....	35
2.3. Investigation of soil moisture dynamics of single units.....	40
Potential evapotranspiration assessment.....	40
2.3.1. Field data observation.....	42
2.3.2. Modelling.....	46

Hydrus-1D, PC-PROGRESS .....	46
Calibration.....	48
The concept of equifinality .....	51
Models of the cropped fields and the pasture.....	51
Evaluation of the models of the two units.....	53
2.4. Investigation of CRS-scale soil moisture dynamic.....	53
2.4.1. CRS model .....	53
2.5. Comparison of the dynamics of the two units and the CRS-scale dynamic.....	55
3. Results.....	56
3.1. Soil hydraulic properties.....	56
Texture results .....	56
3.1.1. Water retention curve .....	57
Estimated parameters .....	57
Shape of the curves .....	61
3.2. Soil moisture dynamics in the two units.....	70
3.2.1. Modelling results of the two units.....	70
Evaluation of the models of the two units .....	75
3.3. Simulated large scale dynamics.....	77
Evaluation of the CRS model.....	77
1.1. Comparison of the results of the CRS model and of the models of the two units.....	81
4. Discussion of the results .....	82
4.1. Discussion of the soil hydraulic properties and texture results .....	82
Texture .....	82
4.1.1. Discussion of the water retention curve results.....	82
Estimated parameters .....	82
Discussion about the variability of the curves .....	83
4.2. Discussion about the models of the two units .....	84
Discussion of the evaluation of the two models.....	85

4.3.	Discussion about the CRS model .....	85
	Discussion about the evaluation of the CRS model .....	86
4.4.	Discussion about the comparison of the modelling results .....	86
5.	Conclusion .....	87
6.	Bibliography .....	88
7.	Aknowledgements.....	91

# 1. Introduction

## 1.1. Background

Soil moisture is a fundamental state variable for understanding hydrological processes in the vadose zone. It depends on but also affects weather and climate conditions by controlling the exchange of water and energy fluxes at the land surface and it has a crucial impact on the health of crops (Vereecken et al. 2010).

The study of soil moisture within a catchment is also crucial for understanding the storage-discharge relationship of the system, as discharge is directly dependent on the timing and amount of water that the catchment can store (Creutzfeldt et al. 2014). Indeed, the rainfall-runoff response at the catchment scale is mainly controlled by soil moisture, especially in wet environments where runoff processes due to saturation excess are dominant (Robinson et al. 2008). For example, Rodríguez-Blanco et al. (2012) found that antecedent soil moisture conditions were at least as crucial as the rainfall amount, when they analysed the hydrological response to precipitation events of a humid catchment in Northern Spain.

Soil moisture data can also be effectively used to estimate soil hydraulic parameters by inverse hydrological modelling using softwares, such as Hydrus, PC\_Progress (Rivera Villarreyes et al., 2014; Brunetti et al., 2018).

Soil hydraulic parameters are the parameters that define the “soil water retention curve” (Figure 1.1) through empirical equations such as Brooks and Corey’s (1966) and Van Genuchten’s (1980) equations. These equations describe the relationships between suction head, hydraulic conductivity and soil moisture content. The paths of water in unsaturated porous media depends on these relationships (Tarboton 2003).

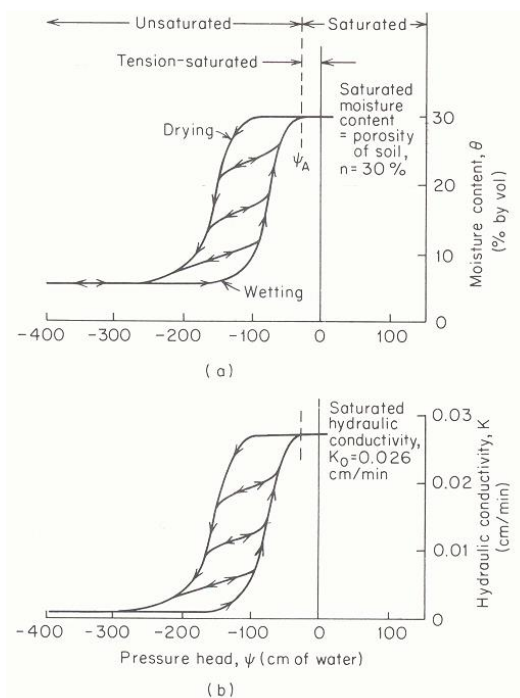


Figure 1.1 – Water retention curves (Tarboton 2003)

However, soil moisture is highly variable in time and space. One of the reasons is that it is influenced by multiple factors (e.g. soil, vegetation, atmospheric conditions) that could also be variable in time and/or space. It follows that spatial heterogeneity of hydraulic states and the complexity of the processes are an obstacle to understanding the moisture dynamics of the

catchment system as a whole and to the prediction of its response (Creutzfeldt et al. 2014). Indeed, for practical applications, it's often necessary to use information from point scales to make predictions at larger scales, which in fact request a higher amount of information (i.e. extrapolating results at small extents to larger area). However, the factors which influence soil moisture could be different at different scales (Western et al., 2002). It follows that scaling is an important issue that research needs to address (Beven, 2016).

Peters-Lidard et al.(2017) encouraged exploring scaling and similarity by a data-intensive approach as a decisive way to advance hydrological science. Similarly Vereecken et al. (2015) stressed the importance for the hydrological community to investigate the organizational principles that control heterogeneity and process complexity and promoted the improvement of data assimilation for the development and validation of the models.

It follows that the problem should be addressed with a combined approach that includes both the refinement of computational models and the improvement and exploration of new monitoring techniques. In fact new technologies in monitoring and data assimilation which are currently gaining momentum could offer new opportunities to address the scaling problem with a data-driven approach (Peters-Lidard et al. 2017).

Robinson et al. (2008) reviewed advances in soil moisture measuring techniques for watershed scale. He pointed out that, although there had been a development of point-scale sensors and of remote sensing providing measurements at continental scale, there was still an existing gap at the intermediate scale. Since that time, new technologies that could be promising for filling this gap have been developed. Some examples of them are multi-receiver electromagnetic induction sensors (EMI), multi receiver ground penetrating radar (GPR) (Vereecken et al, 2015), and the recent Cosmic Ray Sensor (CRS) (e.g. Creutzfeldt et al., 2014; Ling Lv et al., 2014). Also Zreda et al. (2008) encourages the use of cosmic-ray neutron probe, combined with other techniques, to fill the gap between point measurements and airborne or satellite imaging.

The CRS is a device that indirectly monitors average topsoil water content in a non-invasive way, over wide areas covering up to 30 hectares. Thanks to its large footprint, it provides more spatial representativeness, offering a valid alternative to the traditional point approach (International Atomic Energy Agency 2017).

## 1.2. State of the art

As written above, the CRS is a new promising technology that may fill the existing gap at intermediate-scale measurements. Hence, it's subject of many recent studies and most of them have combined it with point-scale measurements and hydrological modelling, as it was done in this thesis. Some examples are Ling Lv et al. (2014) and Rivera Villarreyes et al.(2014); the first was conducted in a mixed forest, while the second one concerns a sunflower farm. Both of them involved the use of the software Hydrus-1D (PC-Progress), that is the one chosen for this thesis. Rivera Villarreyes et al. (2014) demonstrated that CRS could be effectively used to inversely estimate soil hydraulic parameters that could be representative of the sensor scale. He additionally simulated soil water storage at the CRS-scale and found it to have a good correlation with point-scale values, although they had different support volumes. In addition to that, local soil hydraulic properties were inversely estimated from local measurements. Estimated CRS-scale properties resulted to be within the range of variation of local properties.

However, we wonder if the comparison of CRS-scale and local data, as well as estimated soil hydraulic properties, might give very different results if different land uses were concerned.

Also Brunetti et al. (2018) investigated the potential of CRS data for the inverse estimation of hydraulic parameters, in a grassland catchment in Germany. CRS data were found to be effective in estimating soil hydraulic parameters and the concurrent use of it and other kinds of soil moisture data was promoted to reduce the uncertainty related to the estimates.

From the outline above it's clear how the potential and operating of CRS is subject to ongoing research. However, among the recent studies, just a few of them concerned managed landscapes (Rivera Villarreyes et al., 2014 is an example) and even less regarded cropped fields (Baroni et al., 2018, which is conducted in two crop fields in Germany, is one of the few ones).

However many studies showed that land use could affect soil hydraulic properties (as summarized by Ma et al., 2017) and assert that there is a need to investigate human impact on catchment system (Beven 2016). To my knowledge, none of the studies conducted about the CRS included different land uses within its footprint.

The present study combines CRS data, point-scale measurements and modelling with Hydrus-1D to study soil moisture patterns in a managed landscape. The CRS is installed at the intersection of three fields characterized by different land uses (two of the fields are cropped and the other one is a pasture) and by two different soil types (poorly-draining soil -non-calcareous gleys- and freely draining Humus-iron podzol; Boorman, Hollis and Lilly, 1995). Therefore, this study could offer

new insights into how local patterns integrate to larger-scale CRS measurements when multiple land uses and different soil types are involved.

### **1.3. Main aim and objectives**

#### *Main aim*

The main aim of the thesis is to better understand heterogeneities in soil hydraulic properties of different units of the study site, characterized by different land uses (i.e. two different crops and a pasture) and different soil types, and to see if data from a Cosmic Ray sensor (CRS) integrate local soil moisture dynamics to larger scale.

#### *Objectives*

The first objective is to characterise the different soil hydraulic properties of three units within the CRS footprint and to understand better their variability within each field and between the different fields.

Each unit is characterized by a different land use: there are two different crops and a pasture. In addition to that, the soil type of the two cropped fields is different than the one in the pasture: the first one is poorly-draining soil (non-calcareous gleys), while the second one is a freely draining Humus-iron podzol (Boorman et al. , 1995).

The second objective is to explore soil moisture dynamics for the two most dominant of these units by using combination of point-scale field data and modelling.

The point-scale data consisted in water content values estimated from samples, ML2 and PR2 theta probes (*Delta-T*). The model that was used is Hydrus 1D (PC-Progress).

The third objective is to estimate large scale soil moisture dynamics by using both measurements from the CRS and modelling (Hydrus-1D, PC-Progress).

Finally, the fourth objective is to compare soil moisture dynamics estimated for each unit (objective 2) to the simulated larger-scale dynamic (objective 3).



## 2. Methodology

### 2.1. Site description and field data collection

#### 2.1.1. Description of the study area

The study area is located within an agricultural catchment and it coincides with the footprint of a Cosmic Ray Sensor (CRS; Figure 2.1). It has an elevation ranging from 85 to 105 m a.s.l and an extent that is related to the soil moisture, so it's not constant. Indeed, the radius of influence of the CRS varies from 242 to 255 m.

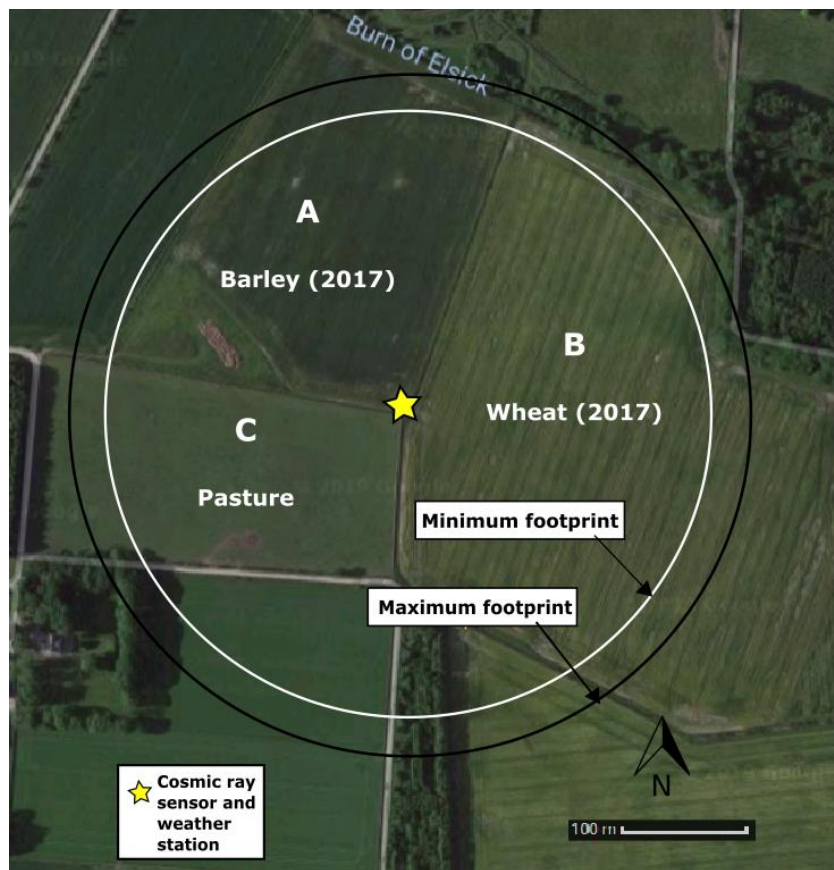


Figure 2.1 - Cosmic Ray Sensor location and footprint. The radius of influence changes from 242 (white line) to 255 m (black line). Three land uses are included in the footprint: two crops and a pasture. The land uses illustrated in the figure refer to the year 2017 (the crops swop every year).

The agricultural catchment that includes the study site is Elsick Burn and it's situated in NE Scotland; it has an extent of 10 km<sup>2</sup> and an elevation ranging from 20 to 165 m. a.s.l (Figure 2.2). The average annual precipitation over the catchment is 700 mm and the estimated annual potential evapotranspiration is 350 mm (poster Geris et al.). It's currently being urbanized, including a motorway and a new town that will affect a large part of the area (Figure 2.2).

The catchment has been monitored since October 2013 by the University of Aberdeen, as a part of a research project about flow pathways and storage in peri-urban landscapes, and it's currently the subject of a PhD project (namely, Katya Dimitrova's PhD project).

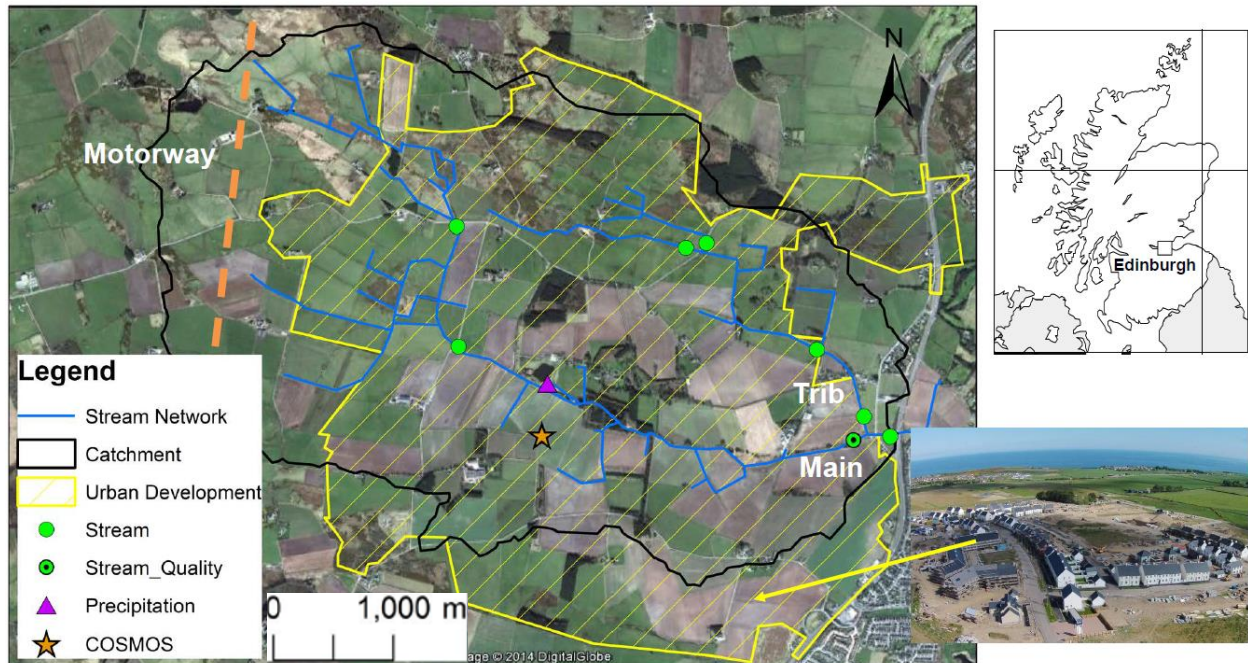


Figure 2.2 - Elsieck catchment, indicating the location of the sites which have been monitored since 2013, and showing the location of the new motorway and the future extent (yellow hashed area) and start of the urbanisation (right lower inset). The position of the system including the CRS and a weather station (COSMOS) is also reported in the map. Poster by Geris et al.

The study area includes three different units, with the characteristics summed up in Table 2.1.

For each unit, a weight that represents it in the CRS measurement was estimated, according to the unit's extent. The narrow intersection between the fields, covered by grass, was assumed to contribute of 1% to the CRS measurement. The land uses reported in the table refer to the year 2017 and are not the same of 2018 because a crop rotation is applied every year. To simplify the terminology, from this point on I will refer to the fields by using the land use of 2017.

Table 2.1 - Characteristics of the three units included in the footprint.

Unit	Assumed weight in the CRS measurement (%)	Land use in 2017	Soil type
A	25%	Barley	Poorly-draining soil (non-calcareous gleys)
B	49 %	Wheat	
C	25 %	Pasture	Freely draining Humus-iron podzol

To have some information about the soil in that area, the HOST - Hydrology of soil types - report was consulted (Boorman *et al.*,1995), which is a classification that was conducted in all the UK, based on data both about the soils and their distribution, and the hydrological response of catchments. As reported in Table 2.1, according to HOST, one class was identified for the two cropped fields and another one for the pasture:

- Cropped fields: they are characterized by a loamy substrate (later confirmed by a texture analysis) and “prolonged seasonal saturation and hence a dominantly horizontal flow with only some leakage through the permeable substrate to groundwater”. This model motivates the importance of surface soil moisture in the production of discharge in this area.
- The pasture, instead, is “underlain by either a slowly permeable or an impermeable substrate (such as glacial lodgement till or hard coherent rock) at depths greater than 1 m”. “However, the soils described by the model have no inhibition to drainage within the first metre and exhibit vertical unsaturated and by-pass flow through macro-pores to the depth of the underlying substrates. A groundwater table or aquifer is not normally present in these substrates”. From a geophysical survey, that had been conducted in the study area, a glacial drift was identified below 1 m depth and no aquifer was identified above 5 m depth, confirming part of the HOST model for the pasture.

The models representing the two classes are displayed in Figure 2.3.

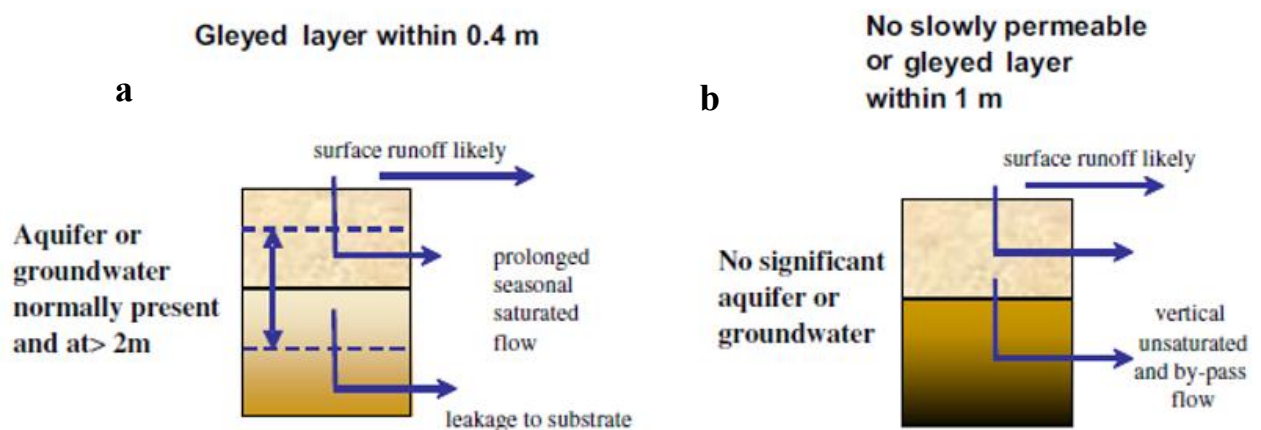


Figure 2.3 – a. Soil type in the two cropped fields, according to HOST classification ((Boorman et al., 1995)); b. Soil type in the pasture, according to HOST.



### 2.1.2. Monitoring of the site

The CRS monitoring of the site started in 2015 and was then extended in 2017 with a weather station (COSMOS, COsmic-ray Soil Moisture Observing System, Figure 2.5); also a tipping rain gauge (ARG100, EML, Figure 2.4) and more detailed point scale measurements were added in the same year. Hence, when my project started, a good amount of CRS and point-scale data had already been collected, as described below.

In addition to that, soil moisture PR2 *Delta-T* probes were installed; they have detected soil water content every 30 minutes at 4 depths (10, 20, 30 and 40 cm), in the biggest crop field and at the intersection between the fields (near the CRS station).

Point scale measurements have also been taken once a week on average, since 2017, in the three fields and at the intersection of fields, by using ML2 and PR2 *Delta-T* theta probes.

To calibrate the CRS, four sampling campaigns were carried out, during the 2017 growing season (April – November 2017) and in July 2018 (as more thoroughly reported in section 2.1.4). This was in agreement with Ling Lv et al. (2014) which suggested to calibrate the sensor more than once and under different weather conditions. The water content determined by these samples was used in the present thesis for the calibration of two Hydrus-1D models.

To characterise soil hydraulic properties of the different units, as a part of my thesis project, on 26/09/2018, 48 soil samples were collected to estimate the water retention curve in the laboratory.



Figure 2.4 - Tipping rain gauge, ARG100, EML, with a sensitivity of 0.2 mm/tip.

Table 2.2 sums up the soil moisture data available for the site and the way they were obtained, while Table 2.3 reports the additional data collected as a part of the present thesis project. Finally, Table 2.4 lists the atmospheric data available for the study area.

Table 2.2 – Description of soil moisture monitoring.

<b>Method of measurement</b>	<b>Period and frequency of the monitoring</b>	<b>Position</b>	<b>Description</b>
CRS	Every 30 minutes, from November 2015 until now.	Intersection between the fields	Continuous monitoring of all the study area (Radius from 242 to 255 m). Sampling depth varies from 9 to 26 cm.
ML2 Theta-Probe	Once a week on average, from April 2017 until now.	Randomly distributed points in the Wheat, Barley and Pasture field and along the intersection between the fields	Ten point-scale measurements were taken in each field and at the intersection, then the averages and standard deviations were calculated. Sampling depth = 6 cm
PR2, profile Theta-Probe	Every 30 minutes, from April 2017 to now	One PR2 in the Wheat field and one at the intersection between the fields	Measurements taken every 30 minutes in two preinstalled access tubes, at 10, 20, 30 and 40 cm depths.
	Once a week on average, from April 2017 to now	Pre-installed access tubes in the Wheat, Barley and Pasture fields and along the intersection between the fields	One of the two available PR2 probes has been moved once a week on average to take three measurements (at 10, 20, 30 and 40 cm depth) in each pre-installed access tube. Then the averages and standard deviations were calculated
Determination of water content from samples (from the calibration of the CRS)	18/04/2017; 27/07/2017; 29/11/2017; 25/07/2018;	Along transects in the Wheat, Barley and Pasture fields and along the intersection between the fields	Collection of 18 samples in each field, at the depths 0-5, 5-10 and 10-15 cm, at the distances 5, 25 and 75 m from the CRS. Additional collection of 9 samples along the intersection between the fields.
Determination of water content from samples	26/09/2018	Wheat field	Further collection of 9 samples from the wheat field, at the depths 0-5, 5-10 and 10-15 cm, at the distances 5, 25 and 75 m from the CRS

Table 2.3 – Additional samples collected for this thesis project

Measured characteristic	Date of sampling	Number of samples	Description
Water retention curve	26/09/2018	44	44 samples were collected at different depths and at different distances from the CRS (Figure 2.10)

Table 2.4 - Atmospheric data which were available for the study site

Measured characteristic	Method of measurement	
Precipitation	From 2015 to 2017	Tipping rain gauge in the catchment of Elswick, about 1 km from the study site
	From 2017 until now	Tipping rain gauge close to COSMOS (Figure 2.4)
Atmospheric pressure Air temperature Net radiation Wind speed and direction Relative humidity of the air	Sensors in COSMOS Measurements taken every 30 minutes from 2015 until now	

### *CRS equipment description*

The model of the Cosmic ray sensor is CRS 1000/B (Hydroinnova) and since April 2017 it functions as a fully equipped weather station, called “COSMOS” (COsmic-ray Soil Moisture Observing System, Figure 2.5).

The system includes the following components:

- soil moisture sensors;
- a data logger, a battery and a modem to transmit the data, housed in an outdoor enclosure;
- a solar panel connected to the system;
- internal sensors for: air temperature, relative humidity, barometric pressure;
- external sensors for: air temperature, relative humidity, net radiation and an anemometer (for the intensity and direction of the wind).

The CRS is cabled to the data logger and the thermalized neutron counter is housed in an enclosure. The sensors, data logger, and housing box are mounted on a large steel pole anchored to the ground via a cement filled hole.

The soil moisture sensors are installed at a level of about 1.5 m from the ground, as indicated by the manufacturer.

(International Atomic Energy Agency 2017).

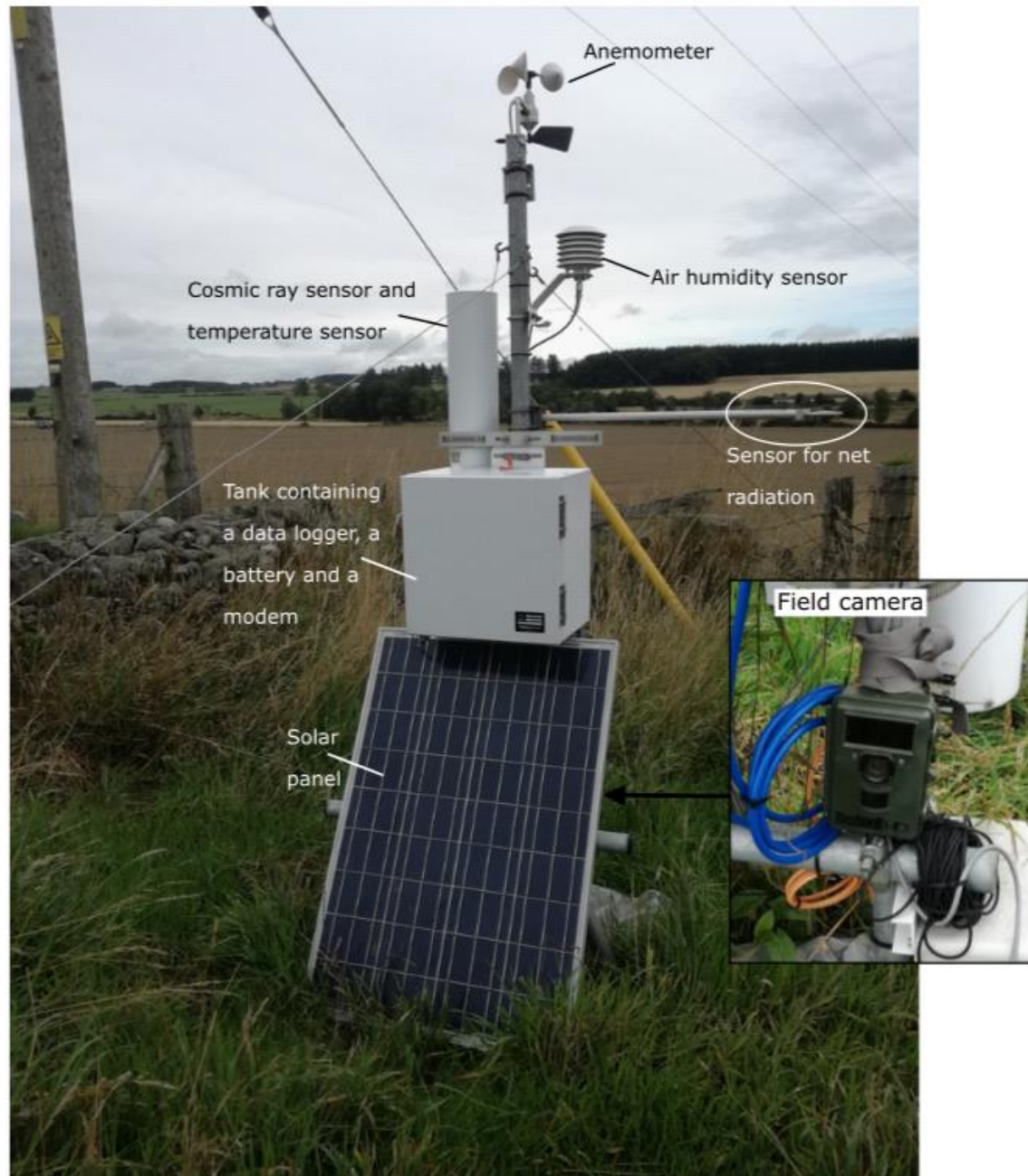


Figure 2.5 – COSMOS station. CRS 1000/B (Hydroinnova) was assembled together with other sensors and functions as a fully equipped weather-station. In addition to that, a field camera was installed and it photographs the field every 30 minutes.

### *Description of the soil moisture probes (ML2 and PR2)*

The Theta-Probes measure volumetric soil moisture content, by the responding to changes in the apparent dielectric constant. These changes are converted into a dc voltage, which is assumed to be proportional to volumetric soil moisture content. Volumetric soil moisture content is the ratio

between the volume of water present and the total volume of the sample and is expressed as a percentage (%vol) or a ratio ( $\text{m}^3/\text{m}^3$ ). (Delta-T Devices Ltd 1998)

## ML2

The instrument includes a waterproof housing, that contains the electronics, and, attached to it, at the bottom, four sharpened, stainless steel rods of 6 cm each (Figure 2.6).

The connection to a power supply and an output signal is provided by a cable. The results of the measurements are displayed on a HH2 Moisture Meter readout unit (*Delta-T*) that has to be connected to the probe during the measurements.

To measure soil moisture, the rods are completely inserted into the soil and readings are taken from readout unit. Since the length of the rods is 6 cm, the instrument measures the soil moisture of the top 6 cm of the soil.

The following factors can lead to an error in the measurement:

- air pockets around the rods: they can reduce the value of soil moisture measured;
- insertion angle: when immediate measurements are taken the probe should be vertical;
- stones or roots close to the rods, roots: they not only affect the measurement but could also bend the rods while they are being inserted in the soil.

For these reasons, attention is paid during the measurements and more than one measurement is taken, in different points.

This kind of probes measure soil moisture in a very small volume (about  $33 \text{ cm}^2$ ), hence the measurement is assumed to be point-scale.

Since 2017, the ML2 probe has been used to measure soil moisture once a week on average. The measurements have been taken in 10 different points in each field and in 10 points along the intersection between the fields (covered by grass). The spatial distribution of the measurements is random. For each field and for the intersection, the average and standard deviation of the ten measurements have been calculated.

(Delta-T Devices Ltd 1998)



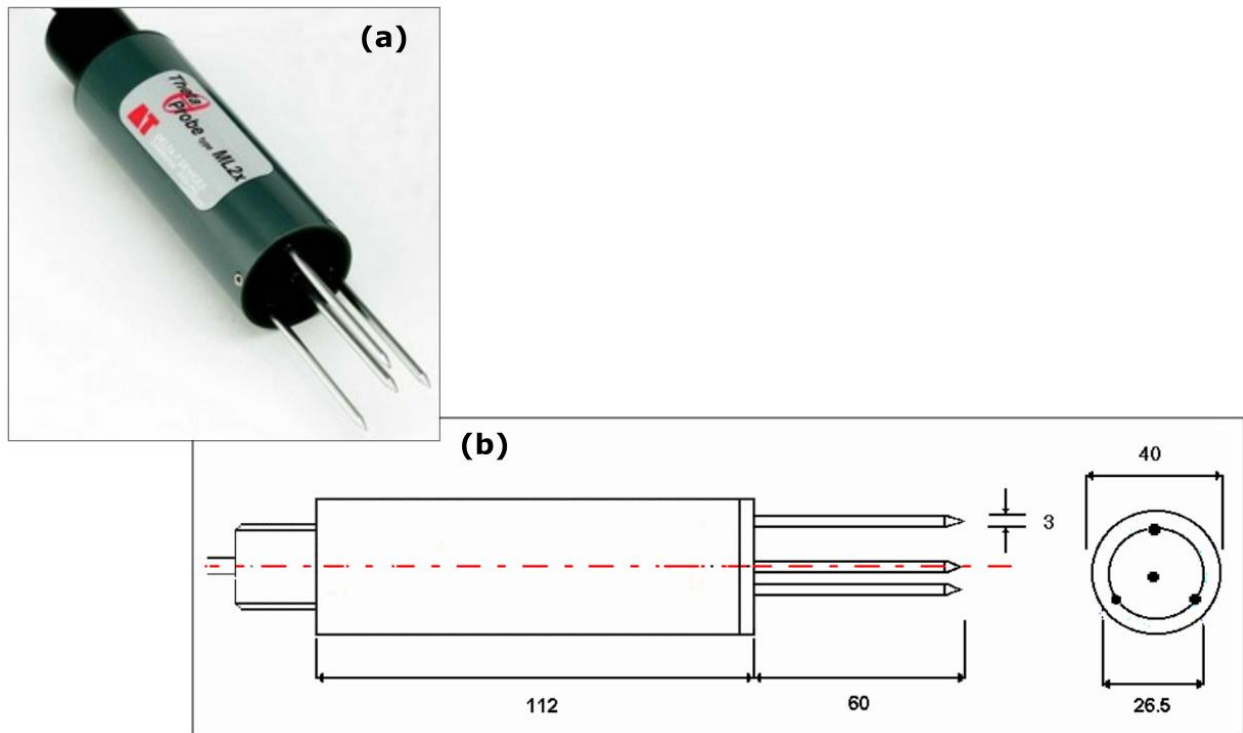


Figure 2.6 – a. ML2 soil moisture probe; b. Geometric characteristics of a ML2 Delta-T ThetaProbe; measures are in mm. (Delta-T Devices Ltd 1998)

## PR2

PR2 is a profile probe that measures soil moisture at different depths (10, 20, 30 and 40 cm) within the soil profile (Figure 2.7).

It's a sealed polycarbonate rod, of 25 mm diameter, with electronic sensors (that are four pairs of stainless-steel rings) arranged at fixed intervals of 10 cm along its length. Each sensor gives a voltage output which is converted into soil moisture, providing four values of soil moisture at each reading. The sampling volume is about 1 litre at each depth.

The probe needs to be inserted into an access tube (a fibreglass tube, provided by the manufacturer). The tube is previously installed by digging a hole in the ground with a drill.

Two PR2 were available in the fields; they have been used both for portable readings from many access tubes and for long-term monitoring of two access tubes, installed since 2017 in the wheat field and at the intersection between the fields. However, one of the two PR2 probes (the one in the wheat field) was found to be faulty and the data were consequently rejected.

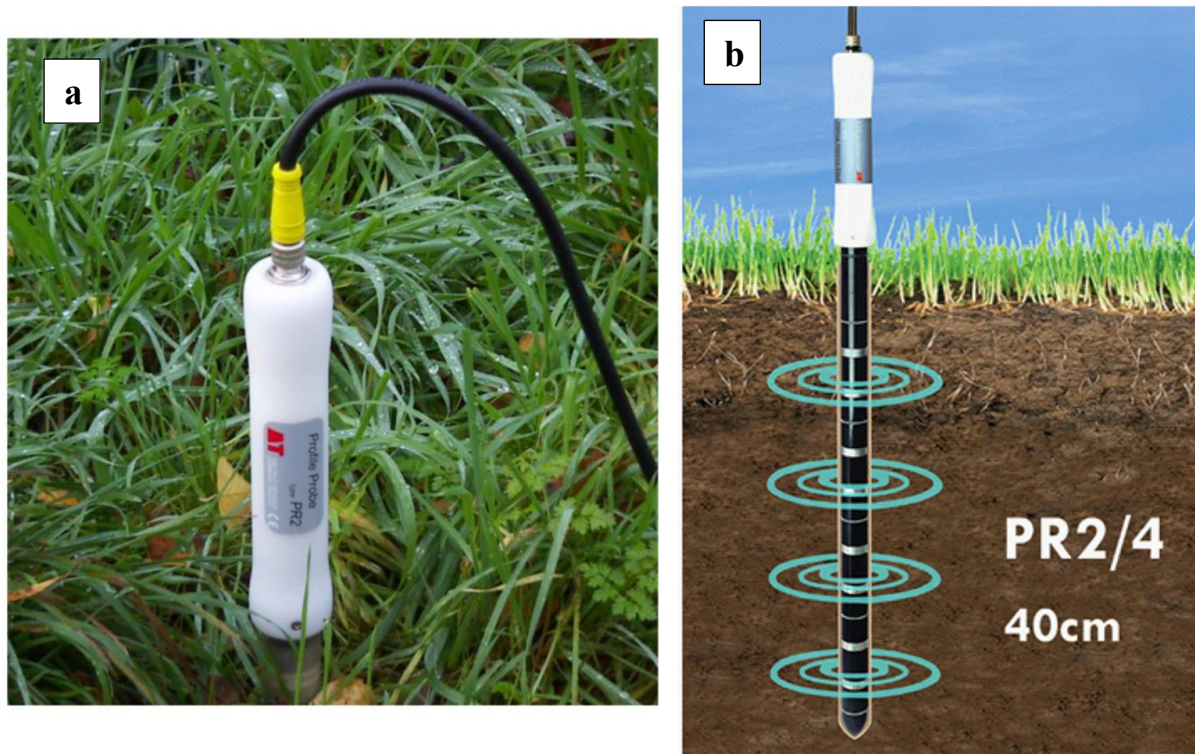


Figure 2.7 –PR2 profile probe inserted into the ground (a) and monitoring depths (b). (Delta-T Devices Ltd, 2016)

### 2.1.3. Sampling campaign for the soil water retention curve

On 26 September 2018 a sampling campaign was conducted in order to determine the soil water retention curve of the three different fields, at different depths.

Undisturbed soil samples were collected into rings with a diameter of 5.5 cm and a height of 4 cm (Figure 2.8), by using a sample ring kit with closed ring holder.

The bottoms of the rings have a cutting edge, allowing the ring to be forced into the soil without disturbing it.



Figure 2.8 – Rings for soil sampling. Diameter = 5.5 cm, height = 4 cm.

By using the sample ring kit, undisturbed soil samples were collected along seven vertical profiles. The distance between the centre of each sample was about 5 cm, hence each sample was assumed to be representative of a 5 cm range of depth. At some depths also some replicas were collected; they all were within a distance of 50 cm from the original hole, so that can be attributed to the same sampling point. The replicas collected for each point are reported in Table 2.5.

The seven sampling points were at distances of 5 and 25 m from COSMOS; their position is represented in Figure 2.9.

The aim was to characterize the first 15 cm of the soil of each point. However, to gain a better understanding of the deeper layers, for 5 of the 7 points a higher sampling depth was reached. That wasn't possible for all the points because some stones were present along the profile.

In the Barley field, the soil had been ploughed before the sampling and, after collecting the samples of the points E and F, the soil was prepared for the sowing. Therefore, an additional sampling was conducted (point G, Figure 2.9) in order to gain some insights into the changes in the behaviour of the first layers of soil caused by the treatment.

The set-up of the sampling is reported in Table 2.5.

Table 2.5 – Characteristics of the sampling points of the campaign for the soil hydraulic properties assessment

<b>Sampling point</b>	<b>Field use</b>	<b>Distance from COSMOS (m)</b>	<b>Sample depth (cm)</b>	<b>Number of samples</b>	<b>Depths of the replicas (cm)</b>
A	Wheat	5	0 to 35	11	0-5; 5-10; 10-15; 25-30; 30-35
B	Wheat	25	0 to 35	7	//
C	Pasture	5	0 to 15	3	//
D	Pasture	25	0 to 30	7	20-25
E	Barley	5	0 to 15	3	//
F	Barley	25	0 to 30	7	0-5
G - after treatment	Barley	25	0 to 30	6	//

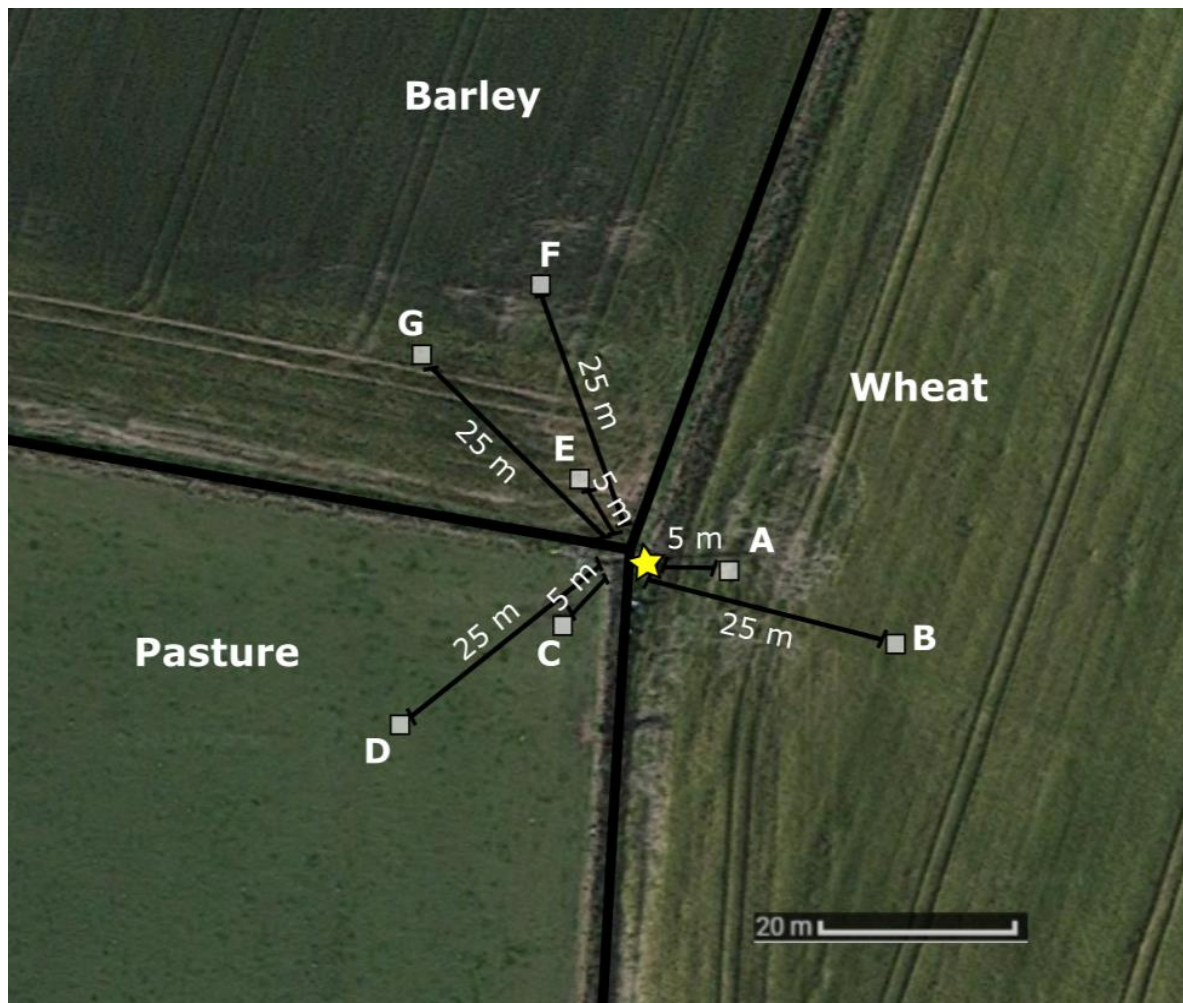


Figure 2.9 – Position of the seven sampling points to collect samples to determine the water retention curve. The star indicates the position of COSMOS.

#### 2.1.4. CRS: Measurement principles and calibration

The cosmic ray sensor (CRS) continuously detects water content in the upper layers of soil in a non-invasive way. The measurement obtained is a spatial average value of soil moisture over a lateral radius that is estimated to be about 260 m at sea level, although it's a bit lower in our study site.

The sensor relies on naturally occurring cosmic ray neutrons as a proxy for soil moisture. The neutron intensity is, indeed, inversely proportional to the amount of water that is near the land surface. So, the intensity of neutrons is detected by a sensor located about 1÷1,5 meters above the ground and then it's converted into a soil moisture value. Also barometric pressure, temperature and relative humidity are recorded and these data are used to correct the neutron count.

To convert neutron count to soil water content, an algorithm is used, that requires parameters obtained by field calibrations, as reported below.

(International Atomic Energy Agency 2017)

This section explains the physical principles behind the CRS technique, the measurement characteristics and the corrections needed, followed by a description of the instrument calibration.

## *Theory*

The following is a description of the physical principles, which are the base of the CRS measurements (according to International Atomic Energy Agency, 2017).

The sensor detects cosmic ray neutrons, which are a natural component of Earth's radiations and hence are ever present at the land surface. These neutrons are called "cosmic" only because they are a by-product of chain of reactions that are initiated by primary cosmic rays.

The initiating cosmic rays consist mainly of highly energetic protons and helium nuclei which originate in supernovas throughout the Milky Way. When they reach the atmosphere, they collide with air molecules and, as a consequence, their nuclei explode, producing protons, neutrons and other subatomic particles (Figure 2.10 A). These fragments traverse the atmosphere, initiating new interactions. Hence the radiation propagates as a cascade and, as this chain reaction progresses, the energy of the primary particles spreads through a growing number of secondary particles. Consequently, the average energy per particle decreases with depth, until the chain reaction can no longer propagate itself.

Fast neutrons are generated by cascade particles as they interact with nuclei in the atmosphere and in the upper few meters of the Earth's crust. The fast neutrons are then scattered in random directions, losing energy because of collisions with air and soil nuclei (Figure 2.10 B). After a certain number of these collisions, the neutrons lose most of their energy and are captured by nucleus in the air and in soil. Fast neutrons in soil are rapidly moderated by hydrogen, which at the land surface is mainly in the form of water. No other element has the same capacity of hydrogen to moderate fast neutrons. Elastic collisions with hydrogen caused the neutrons to be absorbed by certain nuclei or slowed to equilibrium. The cosmic ray sensor is on this unique ability of hydrogen to slow down neutrons. Soil moisture is then calculated, starting from the detected neutron count, through a calibration function. Cosmic ray neutrons are spatially distributed and can scatter large distances in air, allowing the sensor to have a footprint on the order of hundreds of meters.



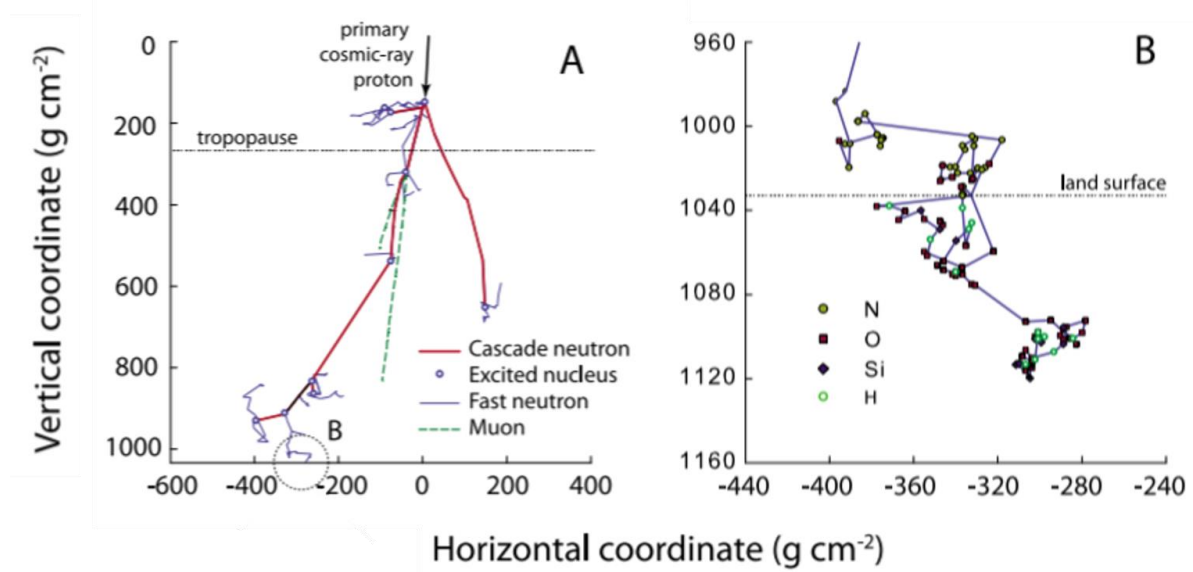


Figure 2.10 – A: Simulated particle cascade in the atmosphere. A proton of a primary cosmic ray collides with atmospheric nitrogen, initiating a particle cascade that reaches sea level. Collisions are marked by a circle; fast neutrons are generated at each of them. B: The fast neutron generated by the cascade, at the point circled in A, is scattered in random directions and eventually captured in the ground. (Desilets, Zreda, and Ferré 2010)

### *Radius of influence*

The extent of the CRS footprint is determined by the distance travelled by a fast neutron from the point in the ground where it is emitted to where it's detected (International Atomic Energy Agency 2017). Desilets and Zreda (2013) estimated the lateral footprint of a cosmic-ray probe and found that the Radius of the area from which 86% of the recorded neutrons originate is nearly 300 m in dry air. They also found out that:

- the footprint is affected by air density and by the height of the sensor above the ground, that hence could be set according to the manufacturer instructions;
- the dependence of the footprint extent on soil moisture is small, while the dependence of it on atmospheric humidity is significant.

However, recent work suggests that the radius of influence at sea level is actually lower than 300 m (Desilets, unpublished data). The updated radius was indeed found to be 264 m for dry soil in a dry atmosphere; this radius is referred to as  $R_0$  (International Atomic Energy Agency 2017).

Starting from this, the radius of influence under different conditions could be estimated as follows:

$$R = R_0 * f_{hum} * f_{bar}$$

Where:

- the factor  $f_{hum}$  takes into account the humidity of the atmosphere:

$$f_{hum} = -7.763 * 10^6 \frac{H}{\rho_{air}} + 1$$

where  $\rho_{\text{air}}$  is the atmospheric density ( $\text{g/cm}^3$ ) and  $H$  is the absolute humidity ( $\text{g/m}^3$ ), calculated as follows. The different units of  $H$  and  $\rho_{\text{air}}$  are adjusted by the factor  $10^6$ .

$$H = \frac{U(\%)}{100} \left( \frac{e_w k}{T + 273.16} \right)$$

where  $U$  is the relative humidity,  $T$  the air temperature (both detected by sensors),  $e_w$  is the saturation vapour pressure and  $k$  is a constant equal to  $216.68 \text{ g k J}^{-1}$ ;

$e_w$  is calculated as:  $e_w = 6.112 \exp \left( \frac{17.62T}{243.12+T} \right)$

- the factor  $f_{\text{bar}}$  takes into account the atmospheric pressure  $P$  (measured by a sensor) and it's calculated as follows (where  $P_0$  is 1013.3 mb):

$$f_{\text{bar}} = \frac{P_0}{P}$$

(International Atomic Energy Agency 2017).

For the study site, the radius of influence was estimated with the procedure reported above, resulting to vary from 242 to 255 m. The series of radius estimated for each day is reported in Figure 2.11, together with the soil moisture data and the sample depth.

### *Sample depth*

The effective measurement depth ( $z^*$ ) is affected by soil moisture and could be calculated according to Franz et al (2013):

$$z^* = \frac{5.8}{\frac{\rho_{bd}}{\rho_w} (\tau + SOC) + \theta + 0.0829}$$

where

- $\rho_{bd}$  is the bulk density of the dry soil ( $\text{g/cm}^3$ );
- $\rho_w$  is the density of liquid water and could be assumed equal to  $1 \text{ g/cm}^3$ ;
- $\tau$  represents the fraction of lattice water in the mineral grains and the bound water (g of water/g of dry minerals);
- SOC is the soil organic carbon (estimated from stoichiometry using measurements of total soil carbon and  $\text{CO}_2$ :  $\text{SOC} = \text{TC} - 12/44 \text{ CO}_2$ ). Its estimation was part of Katya Dimitrova's PhD project.

As a result, the sampling depth in Elswick is estimated to vary between 9 and 26 cm during the measurement period.

Figure 2.11 reports the daily soil moisture data obtained from the CRS measurements (that follows a correction and calibration procedure) and the corresponding radius of influence and sample depth.

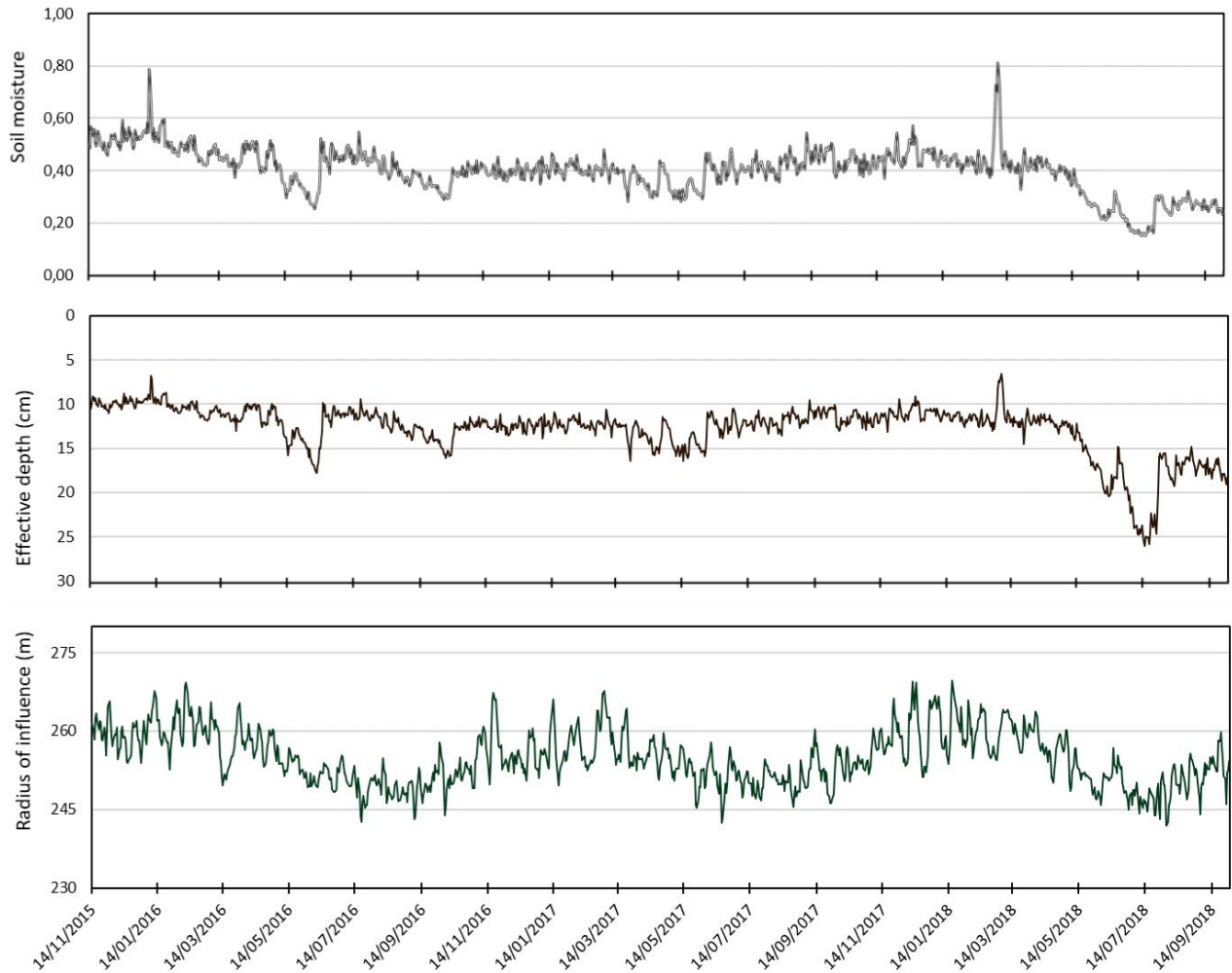


Figure 2.11 –Soil moisture, sample depth and sample radius estimated for the period of the measurements.

### *Correction*

The neutron count provided by the CRS sensor needs several corrections, that were applied by following the procedure indicated by Evans et al (2016).

The objective of the corrections is to take into account the following factors:

- the influence of atmospheric pressure (detected by a sensor included in COSMOS);
- the influence of atmospheric water vapour (by exploiting the data of relative humidity detected by a sensor included in COSMOS);



- the incoming neutron flux; for this correction, count rate data from Jungfraujoch monitoring station were used;
- the effect of vegetation, by deriving a biological water content time series for the footprint, based on vegetation samples and estimates of the height of crops (also pictures from the field camera were used for this);
- the effect of snow and overland water. The CRS detects not only the water in the soil, but also any water on the land surface, within its footprint. For this reason, the days when very high soil moisture values were found (that looked as outliers) were checked. On the days when field observations and pictures from the field camera reveal the presence of snow or overland flow, the corresponding data were rejected.

Finally, it should be noted that, even if the CRS detects soil moisture every 30 minute, data are affected by a large amount of noise, inevitably associated with this technique. Evans et al.(2016) suggests to average up the neutron counts at least to 6 hours. However, for humid environments and close to sea level, daily integration is suggested. Hence, only daily average values were used for the present site.

The corrections listed above have to be applied to the neutron count before applying the calibration function.

### *Calibration*

Four calibrations of the CRS have been conducted, as a part of Katya Dimitrova's PhD project. The work involved intense soil sampling within the sensor footprint; the spatial scheme of the sampling points is reported in Figure 2.12.

The procedure described by Heidbuchel et al. (2016) was followed, with some modifications. He suggested a sampling pattern involving three concentric circles around the CRS, intersected by six straight lines equally distant to each other. Samples have to be taken in the proximity of each intersection. The sampling pattern should ensure that each sample has equal weight towards the spatial mean of measured soil moisture, assuming that the sensitivity of the CRS decreases exponentially with distance.

The modifications introduced for the Elsieck site consisted in equal representation of each field during sampling, smaller sampling radius (from 0 to 75 m, as reported in Figure 2.12, instead of 200 m originally) and shallower depth (0-15 cm instead of 0-30 cm). This is in line with recent research on the topic by (Schrön et al. 2017) that suggests reduced footprint and sensing depth for humid environments such as NE Scotland.

The first three calibration campaigns were carried out in April, July and November 2017. They aimed to capture a wide range of soil water content and different stages of the crop growth. Additionally, a further sampling campaign was conducted in July 2018. This was in agreement with Ling et al. (2014), that recommended multiple calibrations of the instrument and under different climate conditions.

Each calibration presented the following sampling scheme:

- number of transects per field: 2;
- number of sampling points per transect: 3. They were at distances equal to 5, 25 and 75 m from COSMOS;
- Number of sampling depths per point: 3. They were 0-5, 5-10 and 10-15 cm.

The result consists in 18 points from each field.

In addition to that, also three sampling points were placed along the intersection between the barley and wheat field and three samples were collected from each of them.

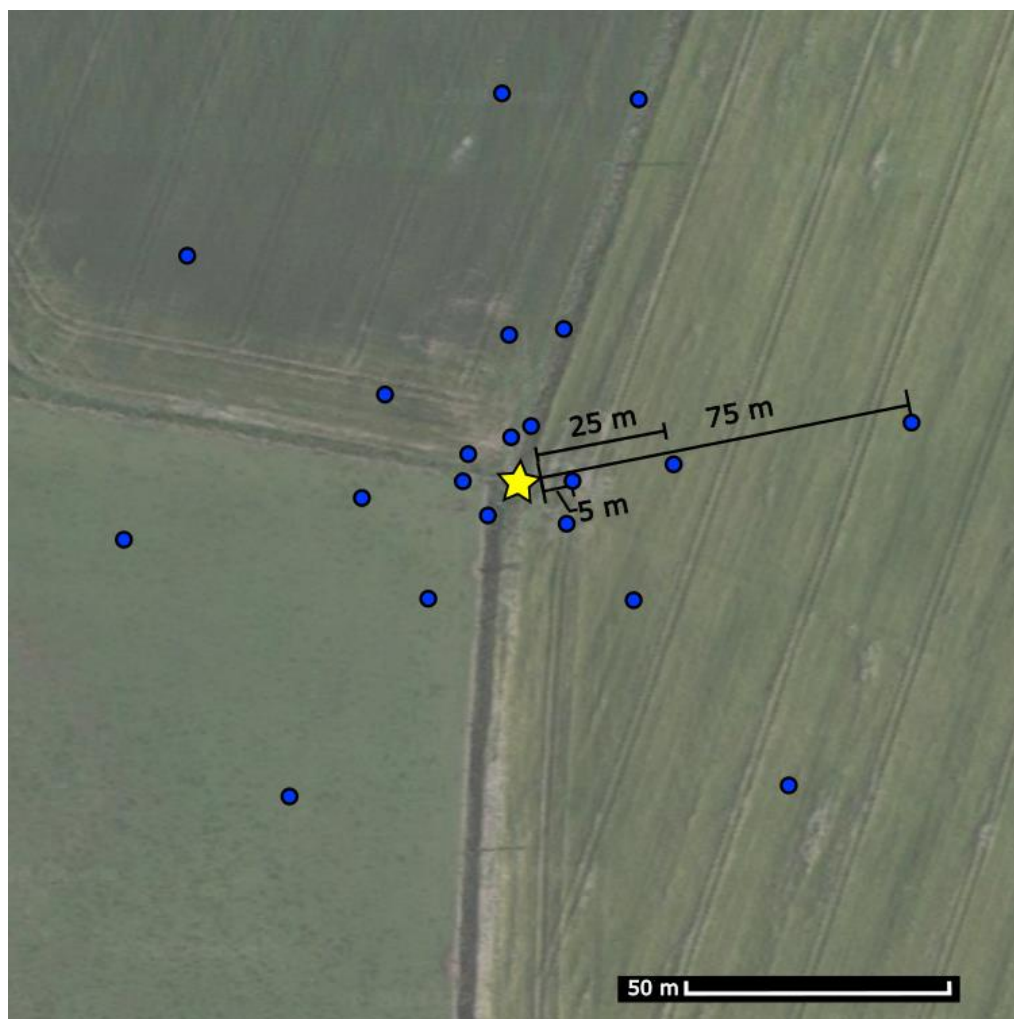


Figure 2.12 – Sampling scheme adopted for the calibration campaign

The calibration function, that relates the volumetric water content in the soil to the neutron count, is the one obtained by Desilets et al. (2010), and it's reported below.

$$\theta(N) = \left[ \frac{a_0}{\frac{N_c}{N_0} - a_1} - a_2 \right] * \rho_{bd} - W_L - (SOM + B_R)$$

where:

- $\theta$  is the volumetric water content;
- $a_0=0.0808$ ,  $a_1=0.372$ ,  $a_2=0.115$ , they are assumed to be constant;
- $N_c$  is the corrected neutron count;
- $N_0$  serves as a calibration parameter accounting for site and sensor-specific variations and representing neutron counts over dry soil at reference conditions during calibration;
- $W_L$  represents the lattice water;
- $SOM$  the organic matter;
- $BR$  the root biomass;
- $\rho_{bd}$  is the bulk density of the soil.

The last four parameters were calculated from the same samples collected during the calibration campaigns.  $N_0$ , instead, is adjusted with an iterative process, until the two sides of the equation are equal. In the present case,  $N_0$  was optimized based on average values of soil moisture determined from the samples, that were weighted with distance and depth, by using a Monte Carlo method. Once all the parameters of the function were estimated, the corrected neutron count was converted into soil moisture values. The results obtained are plotted together with the measured precipitation in Figure 2.13.

## CRS data

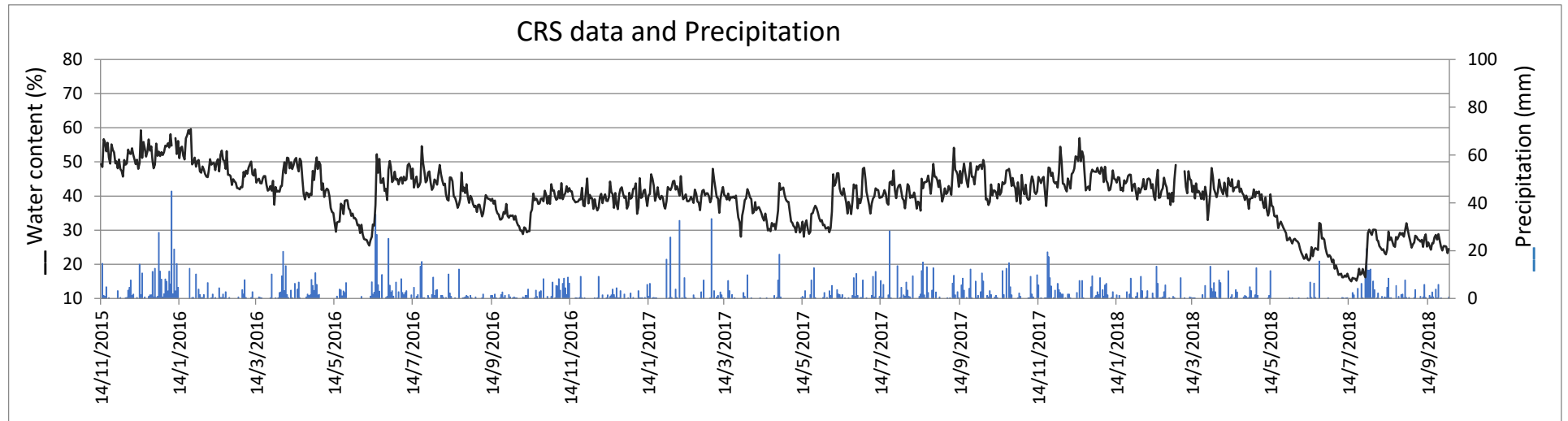


Figure 2.13 - CRS measurements and precipitation data (measured with the tipping rain gauge close to COSMOS from 2017 on, and with a rain gauge in a near site from 2015 to 2017)

## 2.2. Characterization of soil hydraulic properties

### 2.2.1. Soil water retention curve – theoretical basis

The water retention curve will be described in this section, according to Tarboton (2003).

The water retention curve indicates the relation between the water content in a certain volume of soil and the pressure head ( $\psi$ ). The term “pressure head” refers to one of the two components of the hydraulic head ( $h$ ):

$$h = z + p/\gamma = z + \psi;$$

being  $z$  the elevation (m),  $p$  the water pressure (Pa),  $\gamma$  the specific weight ( $\text{N/m}^3$ ) and  $\psi$  the pressure head (m), that is the pressure energy per unit weight of water.

The values that  $\psi$  normally assumes in a porous media are reported in Figure 2.14 c. Figure 2.14a shows an unsaturated zone near the surface and a saturated zone below; the border between them is the water table. Actually, there is also a narrow portion of soil that is saturated even if it's above the water table; it is called capillary fringe.

At the water table level, the fluid pressure in the pores is atmospheric and hence  $\psi=0$ . The saturated zone is characterized by positive pressure head ( $\psi > 0$ ), while in the unsaturated zone the pressure head is negative ( $\psi < 0$ ). Indeed, water in the unsaturated zone is held in the soil pores under tension due to surface-tension forces. Negative pressure head is also referred to as suction head because of this mechanism of water retention.

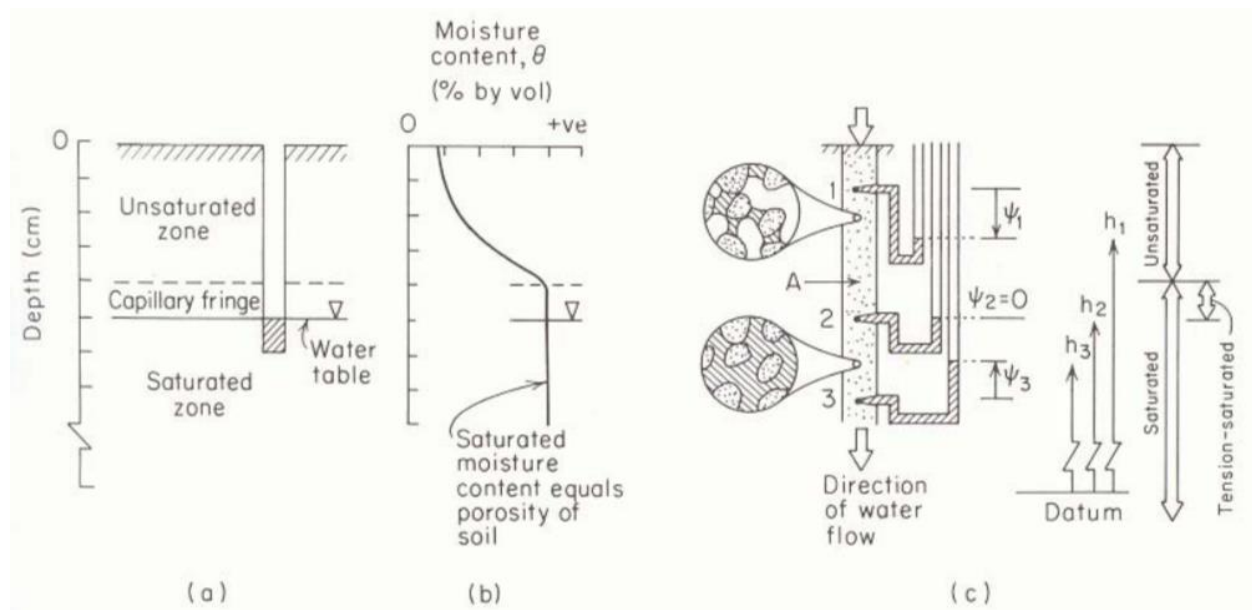


Figure 2.14 - Groundwater conditions near the ground surface. (a) Saturated, unsaturated zones and capillary fringe; (b) profile of moisture content versus depth; (c) pressure-head and hydraulic head relationships (Freeze/Cherry, Groundwater, 1979).

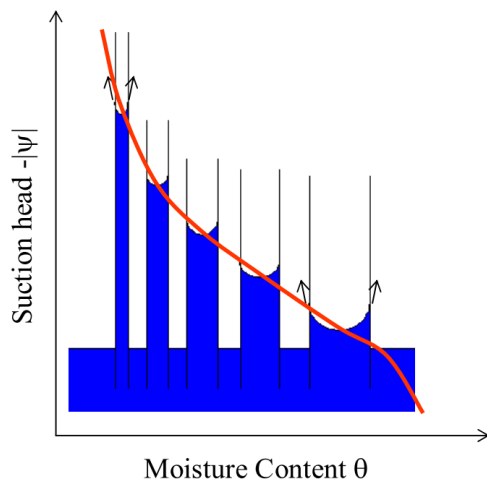


Figure 2.15 – Relationship between the capacity of soil pores to retain water and their size.

The capacity of soil pores to retain water depends on their size: small pores are able to sustain a larger suction head than larger pores. This happens because the ratio between the surface tension force and the pore cross section area is higher for small pores. So, the height to which water rises above the water table is greater for smaller pores; Figure 2.15 illustrates this effect. It follows that the soil moisture is a function of the suction head, because at high suction values just some of the pores (the smaller ones) can retain water.

Additionally, the paths for water to flow become fewer in number and more tortuous as the suction head increases, because the pores occupied by water are fewer and smaller. That leads to the fact that hydraulic conductivity decreases as suction head increases.

Figure 2.16 reports the curves representing the dependence of suction head (a) and hydraulic conductivity (b) on water content ( $\theta$ ); they are called soil water retention curves. Figure 2.16 c illustrates the same curves, but here  $\theta$  is expressed as the independent variable. The water retention curves are a specific property of each soil and their shape is related to the size distribution and structure of the pore space.

It has been empirically observed that the relationship between  $\psi$  and  $\theta$  is hysteretic: the shape of the curve is different for wetting and drying processes of the soil. As a consequence, also the relationship between  $K$  and  $\theta$  is hysteretic. Although hydrologically significant, hysteresis is very difficult to model mathematically and for this reason it's often disregarded in hydrological models. Indeed, it wasn't taken into account in the present thesis project.

The water retention curves present some characteristic points (Figure 2.16)

- One point represents the saturation condition:  $\theta$  equals the porosity,  $\psi$  is 0.
- From the saturation,  $\theta$  changes little as tension increases up to a point of inflection, that is characterized by the tension at which significant volumes of air begin to appear in the soil pores (air-entry tension,  $\psi_A$ ). These conditions of soil moisture, very close to saturation, reflect what happens in the capillary fringe.
- There is then a point, corresponding to high values of suction head, where water content is no longer reducible. The corresponding  $\theta$  is called residual moisture content ( $\theta_r$ ) and it's the amount of water that can't be drained from the soil because it's retained in disconnected pores and immobile films.

- Finally, there is the wilting point, that is the point corresponding to a value of suction equal to 15 000 cm. Plants can't exert suction higher than this value, so, when water content is as low as this point, plants wilt.

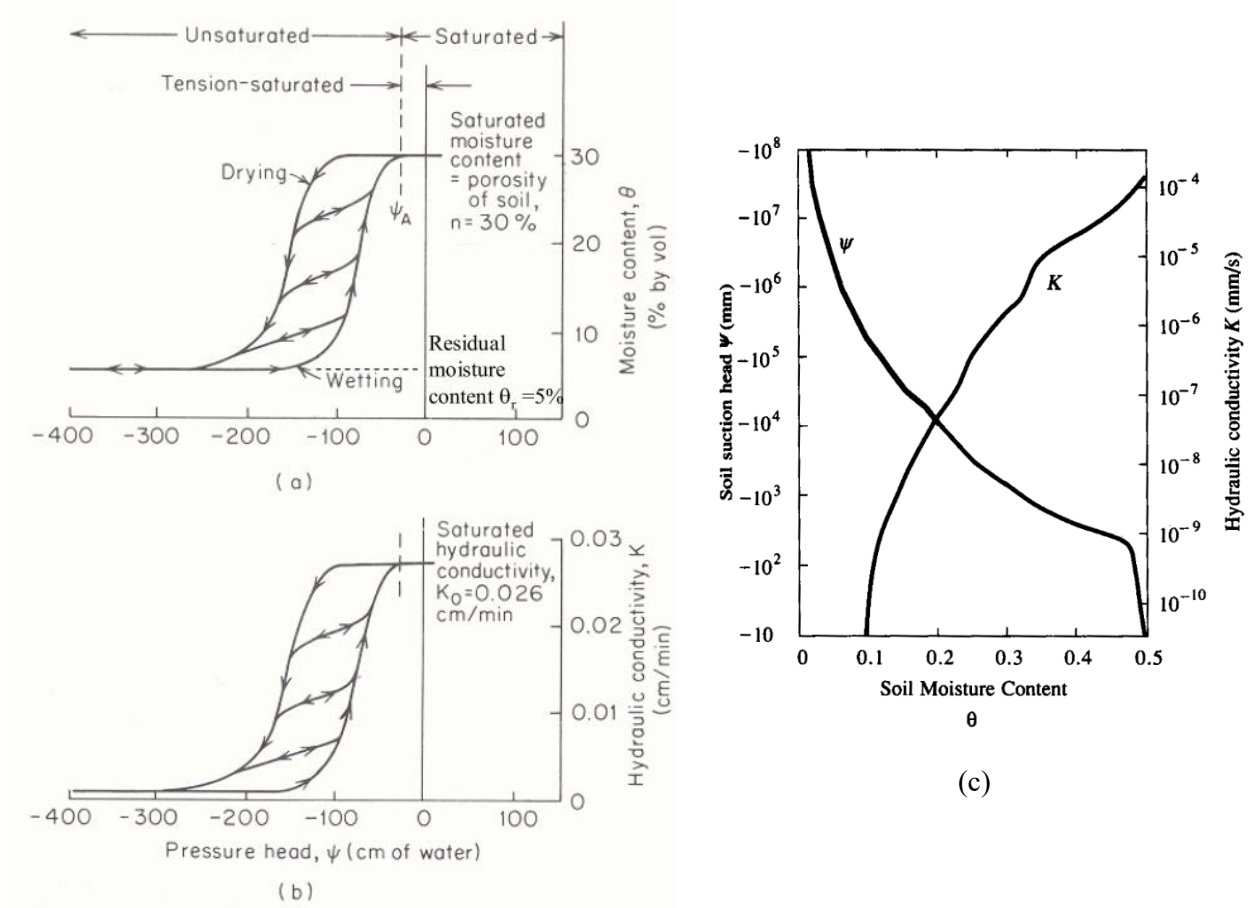


Figure 2.16 – a, b: Characteristic curves relating hydraulic conductivity and moisture content to pressure head for a sandy soil; c: soil water retention curves where  $\theta$  is expressed as the independent variable (Tarboton 2003)

The water retention curves can be determined experimentally (as reported in the following section) or they could be estimated from soil characteristics, such as soil texture. The USDA-ARS Salinity Laboratory has developed an algorithm, called Rosetta, that estimates these functions based on sand, silt and clay percentages in the soil. There are also empirical equations characterizing the curves above mentioned, that have been proposed by several authors, i.e. Brooks and Corey, Van Genuchten. In the present thesis, the Van Genuchten equation, in the Mualem form, was used to describe the water retention curve of the collected soil samples (Van Genuchten 1980):

$$\theta(\psi) = \theta_r + \theta_s - \theta_r[1 + (\alpha h)^n]^{1-1/n}$$

where;

- $\theta(h)$  is the measured volumetric water content at the suction  $\psi$  (that is positive for increasing suctions);
- $\theta_r$  is the residual water content, explained above;
- $\theta_s$  is the saturated water content;
- $\alpha$  ( $>0$ , in  $\text{cm}^{-1}$ ) is related to the inverse of the air entry suction;
- $n$  ( $>1$ ) is a measure of the pore-size distribution.

The corresponding equation for the hydraulic conductivity is:

$$K(S_e) = K_{sat} S_e^L \left\{ 1 - \left[ 1 - S_e^{n/(n-1)} \right]^{1-1/n} \right\}^2$$

where

- $S_e$  is the effective saturation:  $S_e = \theta(h) - \theta_r / \theta_s - \theta_r$ ;
- $K_{sat}$  is the hydraulic conductivity in saturation conditions (cm/day)
- $L$  is an empirical parameter usually assumed to be equal to 0.5.

### 2.2.2. Laboratory experiments

Some laboratory experiments were conducted to address the first objective.

The soil hydraulic parameters have been estimated for samples from the three units, at different depths by a laboratory experiment and then by fitting the Van Genuchten function to the experimental points. The fitting was obtained by using a Matlab code provided by the Postdoctoral researcher Lucile Verrot. For each field, a range of suitable values was obtained for each parameter of the Van Genuchten function.

In addition to that, to have a better understanding of the soil properties and of their variability, the texture have been estimated in the laboratory for the two soil types.

All the laboratory results later helped to set-up the Hydrus-1D model, specifically to make assumptions about the soil profile configuration and to decide suitable parameters ranges.

In this section, the laboratory experiment to determine soil texture is explained first; then the procedure to determine the soil hydraulic parameters is explained.

#### *Particle size analysis*

The texture analysis was conducted for the following samples, collected on September 2018:

- 6 samples from the wheat field, collected at the following depths: 0 to 5, 5 to 10, 10 to 15, 20 to 30, 30 to 40 and 40 to 50 cm;
- 3 samples collected from the pasture field, at the depths 0 to 5, 5 to 10 and 10 to 15 cm.



From field observations, the first 50 cm of soil of the pasture field is known to be homogeneous with depth, while in the wheat field the soil in the first 30 cm looks different from the deeper one. The objective of the present analysis is to determine if the observed difference corresponds to a difference in the texture.

The standard laboratory procedure of the University of Aberdeen was carried out to obtain the texture of the soil. It consists of two main phases:

- Sieving
- Sedimentation technique: pre-treatment and sedimentation in hydrometers.

Initially, the soil samples were dried in a oven at 105°C for 24 hours, to remove all the moisture. The samples were weighed with a balance sensitive to  $\pm 0.01$  g, before sieving with a 2 mm sieve. A wooden pestle with a flat bottom helped to push all the fine particles through the holes of the sieve, so that stones and gravel were removed from the rest. Then the two portions were weighed and the fine part was used for the following steps.

#### SEDIMENTATION TECHNIQUE

The following apparatus and reagents were used:

- glass cylinders with a capacity of 1 litre;
- sodium hexametaphosphate, 5% solution;
- water bath;
- ASTM hydrometer (Fisherbrand);
- interval timer;
- a plunger;
- thermometer.

First of all, about 50 g were selected from each sample and moved to a beaker; then they were covered with a volume of deionized water equal to the soil one. The samples were then treated with sodium hexametaphosphate to complex  $\text{Ca}^{++}$ ,  $\text{Al}^{3+}$ ,  $\text{Fe}^{3+}$  and other cations that bind clay and silt particles into aggregates. This pre-treatment aims to reduce the error due to the incomplete dispersion of soil clays, because they are cemented by various chemical agents and organic matter into aggregates of larger size. After sodium hexametaphosphate was added, the samples were stirred



Figure 2.17 – Sample frothing during the reaction with sodium hexametaphosphate.

and heated up in the water bath up to 80°C until they stopped reacting (namely they stopped frothing). The time needed for the reaction to stop depends on the soil organic matter (SOM); in our case, because of the high SOM, it needed more than one week. The SOM for Elsieck was indeed estimated to be 6% on average for the wheat field and 8% for the pasture field (Katya Dimitrova's PhD project). After that, each sample was moved to a cylinder that was filled with deionized water to a volume of 1000 ml.



Figure 2.18 – ASTM hydrometer (Fisherbrand)

The suspension was, then, stirred and one hydrometer was introduced in each cylinder; after 40 seconds the hydrometer reading was recorded. The same procedure was also done on a blank, that had been prepared by mixing 100 ml of the 5% dispersing solution and 900 ml of deionized water in a 1000 ml cylinder.

The second hydrometer reading was recorded after 7 hours. This measure should represent the amount of clay in suspension, as the silt should be settled to the bottom of the cylinder by this time. At the time of each hydrometer reading, also the blank temperature should be noted.

A correction of +0.2 unit for every °F above 67 °F and -0.2 for every °F above 67°F was added to the readings. In addition to that, the density of the blank was subtracted from the corresponding density readings of the samples.

Finally, the percentage of clay, silt and sand were calculated as follows:

$$\% \text{ clay} = \frac{\text{corrected hydrometer reading at 7 hours} * 100}{\text{weight of the sample}}$$

$$\% \text{ silt} = \frac{\text{corrected hydrometer reading at 40 seconds} * 100}{\text{weight of the sample}} - \% \text{ clay}$$

$$\% \text{ sand} = 100\% - \% \text{ silt} - \% \text{ clay}$$

The weights of the samples from the wheat field were reduced by 6%, while the ones from the pasture were reduced by 8% to take the soil organic matter into account.

### *Procedure to determine the water retention curve*

The laboratory analysis to determine the soil water retention curve was conducted on 44 samples collected from the three fields (Figure 2.9, Table 2.5). Each sample is contained in a ring of 5,5 cm diameter and 4 cm height.

The procedure involved multiple steps; at each step the samples were subjected to a suction that is higher than the one at the previous step. Each suction value was applied until the samples reached the equilibrium, namely they stopped losing weight. At this point, the samples are weighed in order to obtain the corresponding water content.

The following instruments were required:

- EcoTech pF Suction Plate module (Figure 2.19): it can apply a suction from 5 kPa to a maximum of 75 kPa;
- Blue Pressure Plate Vessel (Extractor, Figure 2.20): it can apply a suction from 50 kPa to a maximum of 3000 kPa;
- Silver Pressure Plate Vessel (Figure 2.20): it can apply a suction from 1000 to 1500 kPa.
- A two-place balance.
- An oven to dry the samples at 105 °C.

In addition to that, the following equipment was required:

- To prepare the samples: an elastic band and a nylon mesh for each sample;
- Deionised water.

Below is a list of the values of suction that were applied:

- 0 kPa, corresponding to saturation conditions;
- In the Suction plates: 5 and 10 kPa;
- In the blue pressure plate vessel: 3000 kPa;
- In the silver pressure plate vessel: 15000 kPa (corresponding to the wilting point).

In addition to that, a suction of 50 kPa was applied in the suction plate, but it wasn't possible to reach the equilibrium due to technical problems. Hence, it was necessary to move the samples directly to pressure plates. However, the samples were weighed before they were moved to the pressure plates and these values, representing the conditions before 50 kPa equilibrium, helped to check the reliability of the results.



Figure 2.19 - EcoTech pF Suction Plate module (<https://www.ecotech-bonn.de/>)



Figure 2.20 - Blue and silver pressure plate vessels.

### Saturation condition

As a first step, the rubber bands were used to secure the mesh at the base of each sample. Before this step, the samples, the meshes and the bands had been weighed.

Then the samples were saturated by placing them in the suction plates and soaking them in deionized water for 24 hours (Figure 2.21). The step could be done analogously in a simple bath.

After that, the samples were weighed: the points obtained correspond to a 0 kPa suction. Then, the suction plates were emptied and a certain suction was applied thorough them.



Figure 2.21 - Samples saturating in one of the suction plates.

### Suction plates operating

A suction plate (Figure 2.19) is made up of a polyamide membrane ( $0.45\mu\text{m}$ ) with a drainage system below and a protective polyester sheet above. This is connected to a vacuum pump with buffer vessels added to create a highly regulated vacuum. The vacuum pulls a suction through the membrane onto which the samples are placed. Water is removed from the samples into a reservoir according to the suction limit specified on a control panel. This action eventually equilibrates the applied suction with the water in the soil.

After saturation, a 5 kPa suction was applied to all the samples by these instruments. The samples were periodically weighed until they equilibrated to 0.1 g; this means that water loss from the samples had stopped. At this point, the weights were noted. The same procedure was repeated for 10 kPa suction and for 50 kPa. However, while 50 kPa were applied, the instrument started to occasionally stop working. Since it wasn't possible to identify the cause of the malfunctioning, it was necessary to quit this step and move the samples directly to the pressure plates, where higher suction values were applied.





Figure 2.22 – Strange phenomena: mushrooms growing on one of the samples in the suction plate during the analysis.

### Pressure plates

As mentioned above, a 3000 kPa suction was applied in the blue pressure plate vessel, while a 15000 kPa suction was applied in the silver one.

Due to technical reasons, during the laboratory experiment the samples were split into two groups, so half of them were moved to the blue pressure plate vessel (where a 3 bar suction was applied) and the other half to the silver pressure plate vessel (where a 15 bar suction was applied).

Before moving the samples to the silver vessel for the wilting point, the cores were broken and smaller reconstructed subsamples were created. The dimensions of the new rings are:

- Diameter = 2.8 cm;
- Height = 0.8 cm.

The silver vessel needs small cores because the time needed would be too long otherwise.

Each instrument consists of ceramic pressure plate cells, placed into a high-pressure vessel. Each cell has an upper ceramic plate, onto which samples are placed, and a lower neoprene diaphragm.

Water is forced through the plate due to the air pressure and collected through an outflow pipe.

The ceramic plates available have a porosity that is related to the pressure rating that is applied.

The plates were hence selected according to the pressure rating required, then they were soaked for 48 hours in deionized water before starting the experiment, because they need to be saturated to maintain a water continuum with the samples.

Once plates were in place and connected, the lid was sealed. The evolution of the experiment was checked by the water exiting through a tube at the side of the vessel (Figure 2.23). The samples reach equilibrium with the system when the water exiting is less than 0.1 mm/day per plate. At this point, the vessels were opened and the samples were weighed.



Figure 2.23 – Left: Sealing the silver vessel by tighten the screws; right: equilibrium is checked from the outflow.

### Determination of soil hydraulic parameters

Finally, the meshes and elastic bands were removed and the samples were dried in an oven at 105°C for 24 hours. After that, they were weighed to obtain the dry soil weight.

The volumetric water content at each step “i” was then determined as follows:

$$\frac{\text{Water weight}_i / \rho_{\text{water}}}{\text{Sample volume}} = \frac{(\text{Sample weight}_i - \text{Dry sample weight})}{\text{Sample volume}}$$

At this point, a sequence of points (Water content; Suction) was obtained for each sample. By using a Matlab code (provided by the Post-doc Lucile Verrot), the Van Genuchten – Mualem function was fitted to the points and a set of parameters ( $\theta_s$ ,  $\theta_r$ ,  $\alpha$  and  $n$ ) was obtained for each sample.

For the sampling points A, F and D (samples did the last step in the blue pressure plate vessel) the Van Genuchten function was fitted to the laboratory results corresponding to the suction values 0, 50, 100 and 3000 cm and an estimated point corresponding to 15000 cm suction. The assumption was that the water content at 15000 cm was the average of the values obtained in the laboratory for all the samples from the same field that did the last step in the the silver pressure plate. Since the wilting point is a rough value determined on samples of smaller volume, it’s correct to assume it to be the same of other samples of the same soil type; that was also done in other studies, such as Verrot et al. (2018).

Instead, for the sampling points B, C, E and G (samples in the silver pressure plate vessel), the Van Genuchten function was fitted to the laboratory results corresponding to the suction values 0, 50, 100 and 15000 cm (because no 3000 cm values were available).

## 2.3. Investigation of soil moisture dynamics of single units

The second objective was addressed first by analysing the point-scale measurements available and then by calibrating two Hydrus-1D models (one for the pasture, and the other one for the widest of the two cropped fields). For both the steps, the assessment of the potential evapotranspiration was needed and it was hence conducted in the way reported below.

### *Potential evapotranspiration assessment*

Evapotranspiration is a term that combines two processes involving water loss from land surface to the atmosphere:

- Evaporation: conversion of liquid water to water vapor, that is then removed from the soil or other source;
- Transpiration: vaporization of liquid water within a plant and its loss as a vapor through leaves.

Both the processes depend on air temperature, solar radiation, air humidity and wind speed.

Additionally, transpiration is also influenced by: crop characteristics and development and management practices. (Zotarelli et al., 2016)

The potential evapotranspiration (PET) indicates an upper limit to water losses by evapotranspiration and it's defined as the maximum evapotranspiration rate under unlimited water supply (Song et al. 2017). It was estimated from 2015 until the present as a part of Katya Dimitrova's PhD. The measurements provided by the sensors of COSMOS were exploited for this. The equation used is the FAO-56 Penman-Monteith equation (Allen et al. 1998):

$$PET = \frac{0.408\Delta(R_n - G) + \gamma \frac{900}{T + 273} u_2 (e_s - e_a)}{\Delta + \gamma(1 + 0.34u_2)}$$

Where:

- PET is the potential evapotranspiration rate (mm/d);
- $\Delta$  is the slope of saturated vapor pressure curve;
- $R_n$  is the net radiation flux ( $\text{MJ/m}^2\text{d}^{-1}$ );
- $G$  is the sensible heat flux into the soil ( $\text{MJ/m}^2\text{d}^{-1}$ );
- $T$  is the mean air temperature ( $^{\circ}\text{C}$ );



- $e_s$  is the mean saturated vapor pressure (kPa);
- $e_a$  is the mean daily ambient vapor pressure (kPa);
- $u_2$  is the wind speed (m/s) at 2 m above ground (that's more or less the position of the sensor).

It was then necessary to subdivide PET into potential evaporation and potential transpiration (because they are requested by the Hydrus model, reported in the following section). The following equations (Ritchie 1972) were used:

$$T_p = ET_p(1 - e^{-k \cdot LAI}) = ET_p SCF$$

$$E_p = ET_p e^{-k \cdot LAI} = ET_p(1 - SCF)$$

where:

- $ET_p$ ,  $T_p$ , and  $E_p$  are potential evapotranspiration, transpiration and evaporation, respectively;
- LAI is the leaf area index, later described;
- $SCF$  is the soil cover fraction;
- $k$  is a constant governing the radiation extinction by the canopy as a function of sun angle, the distribution of plants, and the arrangement of leaves and in the present case is assumed to be 0.463.

The leaf area index ( $m^2/m^2$ ) indicates the amount of leaf material in an ecosystem and it's defined as the total one-sided area of photosynthetic tissue per unit ground surface area. In this thesis, the value of leaf area index for the cropped fields was assumed to be equal to the function illustrated in Figure 2.24., that is the result of a monitoring study conducted in Europe (In et al. 2012).

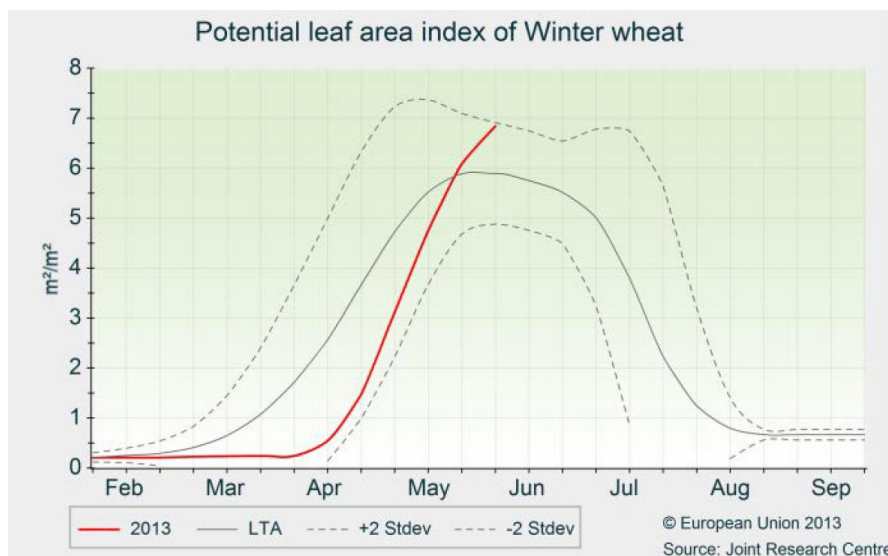


Figure 2.24 – Time variability of leaf area index for winter wheat in UK, according to In et al. (2012).

Instead, grasslands are characterized by a constant value of LAI. So, for the pasture, LAI was assumed to be constant and equal to 2.5, in agreement with the results obtained by a study presenting a global synthesis of this value (Asner, Scurlock, and Hicke 2003).

### **2.3.1. Field data observation**

The soil moisture data detected by the ML2 and PR2 probes and the ones obtained by the sampling campaigns were plotted together with the precipitation measurements and the estimated potential evapotranspiration (Figures from 2.25 to 2.29).

At this point, all the data from one of the two PR2 probes were rejected (the probe was later found to be faulty); for this reason, they are not reported in this section. The probe measured soil moisture at four depths in the wheat field, every 30 minutes since April 2017 and it was also used to take sporadic measurements (once a week on average) in other access tubes placed in the three fields and at the intersection between the fields. It follows that all these measurements were rejected.

Figure 2.25 illustrates the water content values in the three fields and at the intersection between the fields, obtained with the ML2 Theta-Probe, that measures soil moisture in the first 6 cm. Each dot reported in the graph is the average of 10 measurements taken in spatially-random distributed points in the corresponding field. To facilitate the interpretation, the measured precipitation and estimated potential evapotranspiration were also added in the same graph.

The figure shows a pretty high variability of the detected values between the fields, with generally higher values in the pasture and at the intersection between the fields (that is covered by grass as well). The values corresponding to the two cropped fields are generally more similar to each other.

Figure 2.26 reports the soil moisture measured at 4 different levels in the ground, every 30 minutes by the profile probe PR2 placed at the intersection between the fields. It's plotted together with the precipitation measurements and PET. Data are missing in some periods because the probe was found to be faulty and consequently removed and fixed. The graph shows a pretty high variability with depth. The most significance aspect, though, is that the overall trend of the PR2 measurements seems to confirm the ones taken with the ML2. It's relevant for the ML2 measurements to have a good reliability because they will be later used to evaluate all the hydrological models.

From the two figures mentioned above, three main periods with different characteristics are recognizable:

- from May to November 2017: precipitation in this period is characterized by frequent peaks and presents the maximum value registered during the period of interest (on 07/06/2017). Regarding soil moisture, the main trend roughly shows an increment of it during this period. Figure 2.26 shows that deeper layers respond less to single rainfall events.
- From December 2017 to the beginning of May 2018: the precipitation shows a lower frequency of peaks than in the previous period. The main trend of soil moisture seems to be constant;
- There is then a drought process, starting from May 2018, that soil moisture seems to be very sensitive to. Indeed, there is a marked decrease of soil moisture from May to July 2018 detected by every technique (also visible from Figures from 2.27 to 2.29). This matches a lack of precipitation, as expected.

Figures from 2.27 to 2.29 report the water content values obtained by samples collected in the wheat and barley fields and in the pasture, at the depths: 0-5, 5-10 and 10-15 cm. These samples are the ones used for the CRS calibration (Figure 2.11). In addition to that, water content data obtained by a further sampling campaign conducted in the wheat field (on 26/09/2018) were added (see Table 2.2).

These points will be used to calibrate two Hydrus-1D models, as reported in the following section. As shown in the figures, no samples were collected from December 2017 to July 2018 and, as a consequence, the period December-May 2018, characterized by a constant trend of soil moisture, is not represented by the calibration data, as well as the beginning of the drought process. This could possibly negatively affect the calibration results. On the other hand, these soil moisture values are characterized by a degree of certainty that can't be obtained by the theta probes, which are affected by several sources of error. Hence, the information contained in the data obtained from the samples shouldn't be misleading for the model.

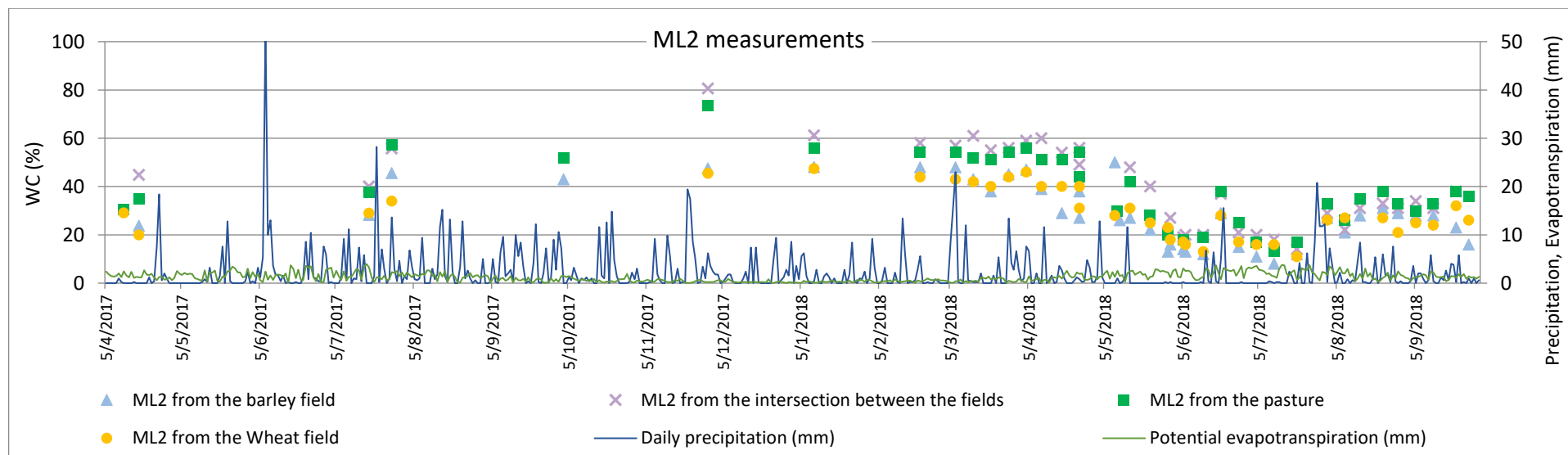


Figure 2.25 – Measurements taken with the ML2 probe, measured precipitation and calculated PET.

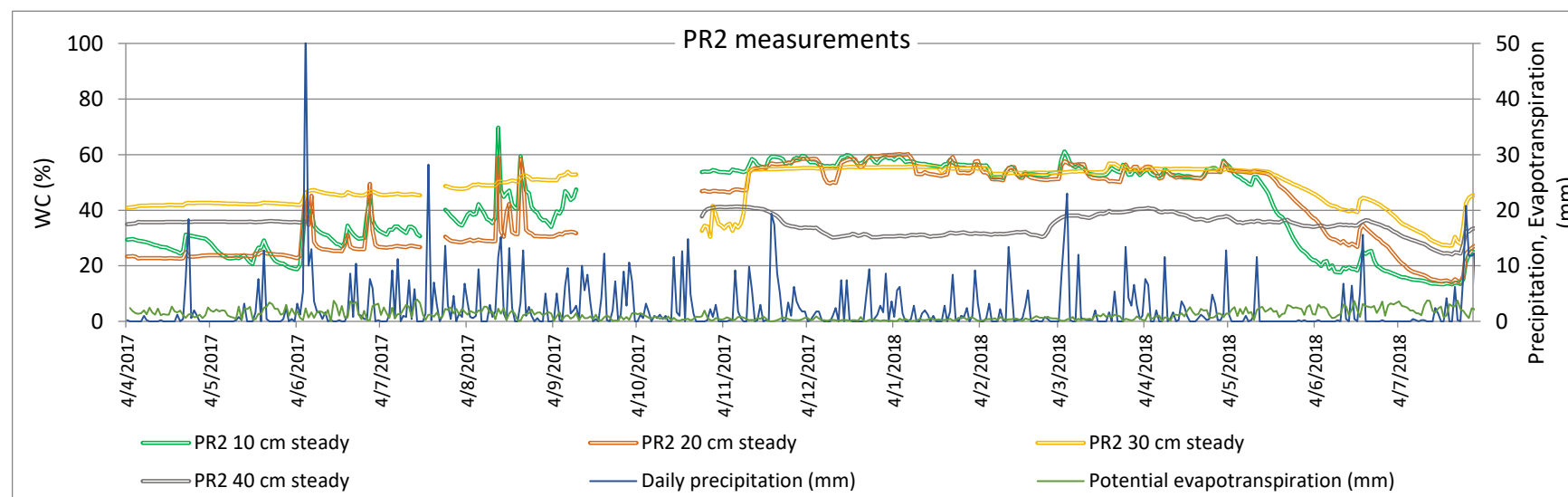


Figure 2.26 – Soil moisture values measured at 4 different depths, by the PR2 probe at the intersection between the fields, plotted together with measured precipitation and calculated PET.

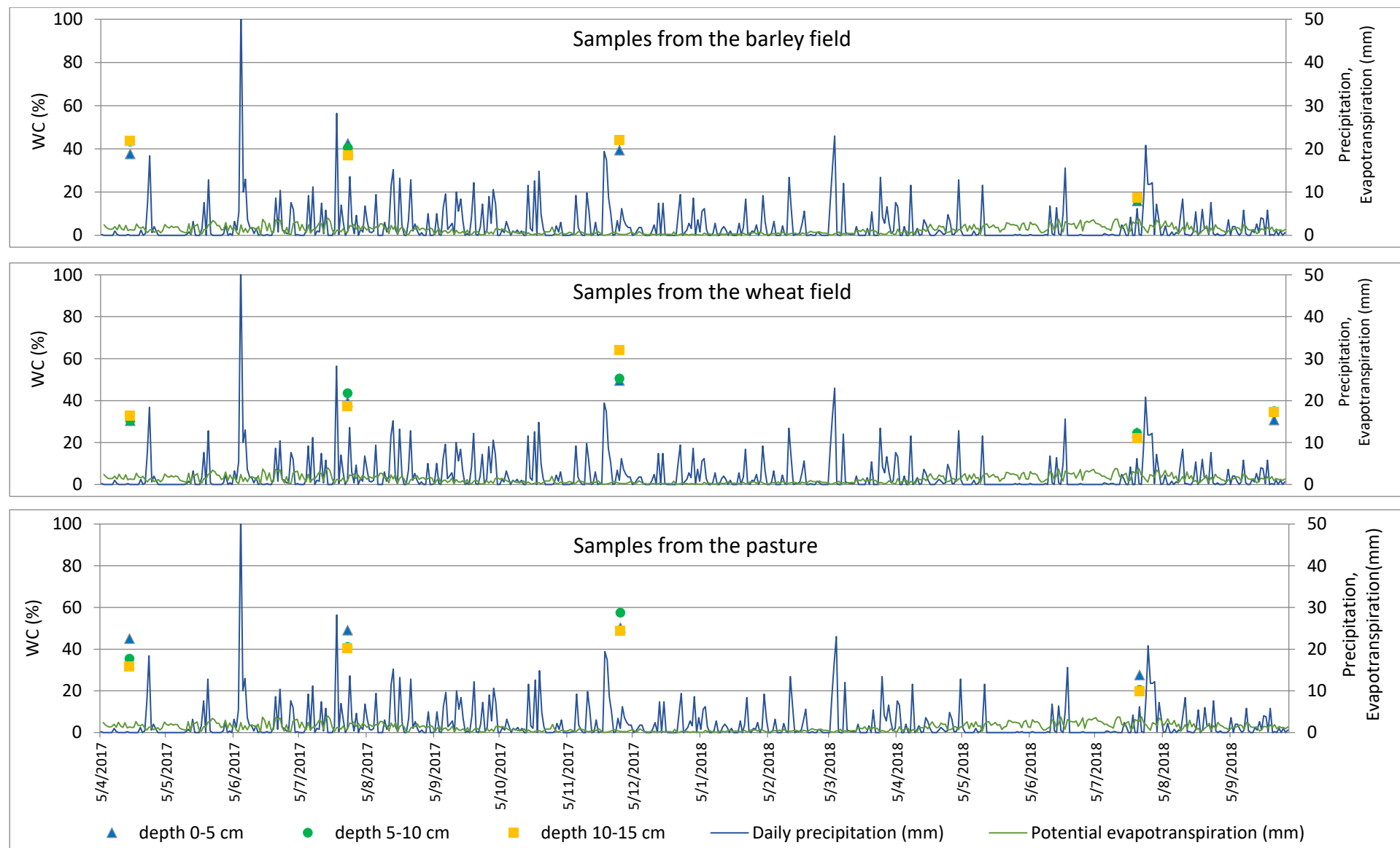


Figure 2.27, 2.28, 2.29 - Water content values obtained from the samples collected for the CRS campaign.

### 2.3.2. Modelling

#### *Hydrus-1D, PC-PROGRESS*

This section provides a description of the theoretical bases of the program Hydrus-1D (PC-PROGRESS), as reported by Šimůnek et al. (2013).

The program numerically solves the Richards' equations for saturated and unsaturated water flow and advection-dispersion equations for heat and solute transport. However, the heat and solute transport were not taken into account in the present thesis. The software additionally allows to take into account the effects of dual porosity and dual permeability, but this function was not exploited in the present thesis as well.

The basis of the software is the description of the one-dimensional water movement in a porous medium through a modified form of the Richard equations:

$$\frac{\partial \theta}{\partial t} = \frac{\partial}{\partial t} \left[ K \left( \frac{\partial h}{\partial x} + \cos \alpha \right) \right] - S$$

The present equation assumes that the air phase plays an insignificant role in the liquid flow processes and neglects the water flow due to thermal gradients. However, the software also gives the possibility to include the vapour transport. The variables of the equation are:

- $h$  is the pressure head;
- $\theta$  is the volumetric water content and it's a function of the pressure head;
- $t$  is the time;
- $x$  is the spatial coordinate;
- $S$  is the sink term, that takes into account the plant water uptake;
- $\alpha$  is the angle between the direction of the flow and the vertical axis; in the present case it's  $0^\circ$ , because the model was applied to a vertical soil column;
- $K$  is the unsaturated hydraulic conductivity and it's obtained as:  $K(h, x) = K_s(x)K_r(h, x)$ , being  $K_r$  the relative hydraulic conductivity and  $K_s$  the saturated hydraulic conductivity.

As previously written,  $\theta$  and  $K$  are functions of the water pressure head:  $\theta(h)$  and  $K(h)$ . Hydrus-1D gives the possibility to use five different curves to describe these relationships and among them, the Van Genuchten function was selected (soil water retention curves were described in section 2.2.1).

## Root water uptake

As mentioned above, the root water uptake is taken into account by the program through the sink term  $S$ , which represents the volume of water removed from a unit volume of soil per unit time because of plant uptake.

It can be calculated, according to Feddes et al. (1978), as:

$$S(h) = \alpha(h)S_p$$

where:

- $S_p$  is the potential water uptake rate ( $T^{-1}$ );
- $\alpha(h)$  is called stress response function and it's a dimensionless function of the pressure head of the water in the soil. The form of the function chosen for this thesis (Feddes 1978) is illustrated in Figure 2.30. From the figure it could be noted that the water uptake is assumed to be equal to zero close to saturation ( $h > h_1$ , that's an anaerobiosis point) and for conditions equal to or dryer than the wilting point ( $h < h_4$ ). The optimal value of water uptake is assumed to be obtained between the values  $h_2$  and  $h_3$  of the pressure head. Finally, water uptake linearly decreases with  $h$  between  $h_3$  and  $h_4$  and similarly increases between  $h_1$  and  $h_2$ .

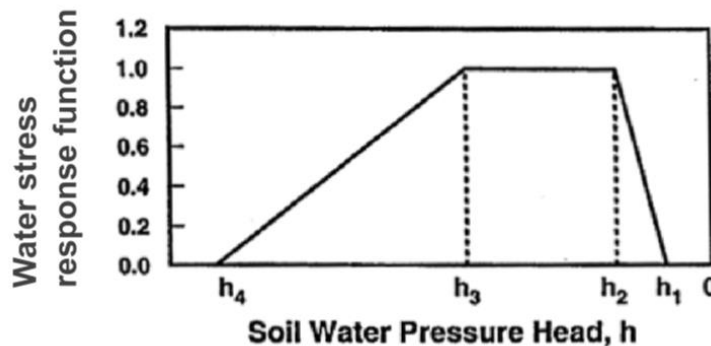


Figure 2.30 – Schematic representation of the plant water stress response function,  $\alpha(h)$ , as used by Feddes et al. (1978).

The  $h_1$ ,  $h_2$ ,  $h_3$  and  $h_4$  values of the pressure head and the potential evapotranspiration rates of the segments  $h_1$  to  $h_2$  and  $h_3$  to  $h_4$  are called Feddes' parameters. They depend on the kind of plants growing on the volume soil of interest; Hydrus-1D provides the values of these parameters corresponding to the most common land uses.

## Space and Time Discretization

A mass-lumped linear finite elements scheme is used for the discretization of the Richards' equation. So, a number of nodes ( $N$ ) has to be chosen during the setting of the model and according to that the soil profile is discretized. The profile is consequently divided into  $N-1$  contiguous



elements, with the ends of the elements corresponding to the nodes. Figure 2.31 illustrates the number of nodes set for the discretization of the soil profile in this thesis.

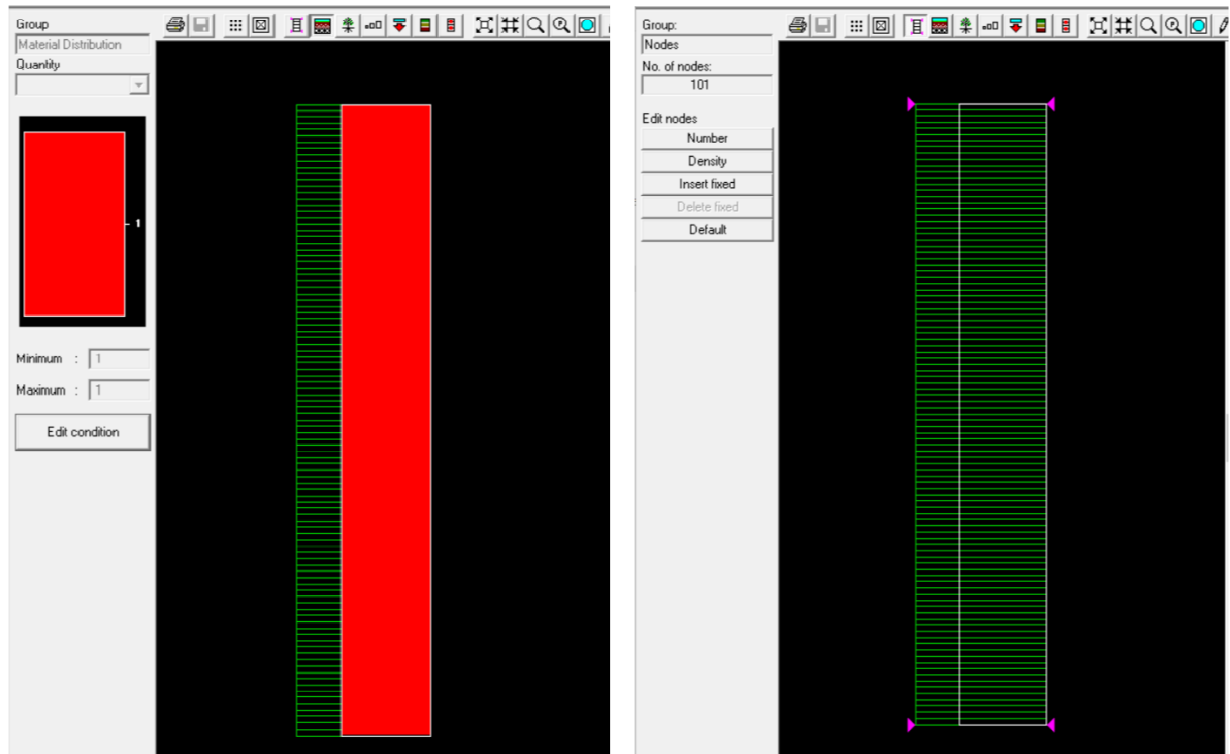


Figure 2.31 – Graphical editor of the soil profile on Hydrus – 1D. Left: one soil material was set for all the profile, for both the models later described. Right: the length of the soil profile was set to be 50 cm, and 2 nodes/cm were set.

## Calibration

The model can be used for both direct problems as well as inverse problems (when some of the parameters have to be estimated from observed data). The use of Hydrus for inverse problems is also called model calibration. To calibrate the model, an objective function is chosen and that quantifies the level of agreement between the measured and modelled data. This function is related to the parameters that have to be estimated, so a best-fit set of parameters can be determined by minimizing this objective function.

There are several different approaches to model calibration, with different degree of complexity. The calibration can, indeed, be carried out by using a quite simple, gradient-based, local optimization or more complex global optimization methods. The first approach could be applied by using the Marquardt-Levenberg method (directly implemented into the HYDRUS codes), while any global optimization method has to be run separately from HYDRUS (C. Zheng et al. 2013).

In the present thesis the second approach was adopted, by using a code that was run on Matlab (MathWorks) and that implemented the global optimization method of Monte Carlo. The code was provided by the Postdoctoral researcher Lucile Verrot.

## Objective function

The general form of the objective functions used for inverse applications of Hydrus-1D is the sum of three terms representing the following factors:

- the deviation between measured and calculated variables (measured data can be, for example, observed pressure head or water content values);
- the difference between independently measured and predicted soil hydraulic properties, such as  $\theta(h)$ ,  $K(h)$  or  $K(\theta)$ ;
- deviations between prior knowledge of the soil hydraulic parameters.

(C. Zheng et al. 2013)

The application of the inverse method in this thesis only comprises the first of the three terms.

The deviation between measured and simulated data could be assessed by using several indicators, such as Nash-Sutcliffe Efficiency, Root Mean Squared Error (RMSE), Mean Absolute Error and Coefficient of Determination; each one is sensitive to different characteristics of the errors and observed data.

The code used comprises the calculation of the widely used RMSE, providing a measure of the average error:

$$RMSE = \left( \frac{1}{n} \sum_{i=1}^n (O_i - M_i)^2 \right)^{0.5}$$

where:

- $O$  = observed data;
- $M$  = modelled data;
- $n$  = number of observation points.

It has to be noted that RMSE (or Root Mean Squared Deviation, RMSD) is dimensional and units are the same as the observed (or modelled) data. The optimal value of RMSE is 0.

RMSE is sensitive to large errors, that have more weight than small because of the squaring of deviations. This effect is reduced with large sample sizes. (Cort and Kenji 2005)

## Comparison of different calibration methods in favour of the Monte Carlo method

The Marquardt-Levenberg method implemented into the Hydrus code is a local optimization gradient method and requires initial estimates of the parameters that have to be optimized.

The objective function is calculated for some sets of parameters in the neighbourhood of the initial estimates and, according to the values obtained, an updated set of parameters' values is determined.

The new parameters are close to the set that previously produced the lower value of objective function. The risk of this method is that, for certain kinds of problems, the objective function could

be topographically very complex, without presenting a clear global minimum. It may instead have several local minima in the parameter space and the method could fail in finding the global minimum. It follows that the method could be very sensitive to the initial estimates of the parameters values and may bring to different local minimum depending on that. This kind of algorithms usually work quite well if only a limited number of parameters need to be estimated, while an alternative, global minimization method is necessary to optimize larger sets of parameters. (Zheng et al., 2013)

Since this thesis aimed to estimate the entire set of five hydraulic parameters, the robust global minimization method of Monte Carlo was chosen. The method was implemented by a Matlab code provided by the Postdoctoral researcher Lucile Verrot.

The calibrations with the Monte Carlo method involved multiple runs of Hydrus-1D using randomly chosen sets of parameters within predetermined ranges. The objective function was calculated for each set as a final step.

In order to gain a good match, 10000 runs of Hydrus-1D were launched by the code, in agreement with the majority of similar studies. It resulted in the Monte Carlo method to be very time-consuming (about 5 days were needed for each calibration).

The advantage of using randomly chosen parameter sets is that a large part of the parameter space is explored, increasing the probability of finding a global minimum, rather than a local one.

The sets of parameters are evaluated by calculating the objective functions only when all the runs are finished. As a consequence, this method has the disadvantage to be relatively inefficient if large areas of the parameter space result in unacceptable simulations. It indeed requests a large amount of time and computational expense, that are the main limit to its use in hydrological modelling. (Beven 2012).

The code used to apply the Monte Carlo method includes the following steps:

- it drives 10 000 runs of Hydrus-1D. For each run a set of parameters is chosen within pre-set ranges;
- once all the simulations are over, the objective function (RMSE) corresponding to each of them is calculated, by using the predicted soil moisture values and the observed data.
- the 5% best simulations (namely, the 5% with the minimum RMSE value) are selected and considered as “behavioural”;
- five dot plots are created (one for each parameter).

Dotty plots are scatter plots of parameter values against RMSE values, that represent a measure of model performance (Beven 2012). They hence allow to visualize how the objective function varies in the parameter space.

Each dot represents one run of the model and the ones corresponding to the behavioural simulations are represented in a different colour. Additionally, the optimum simulation is represented by a red dot.

### *The concept of equifinality*

The information given by the dotty plots are related to the concept of equifinality. This concept was thoroughly addressed by Beven (2006). He explained that finding many models equally giving good fits to observed data is common in hydrological modelling. Moreover, good fits are often found in wide regions of the parameter space, not only in the region of the “optimum”. This is what happened in the calibrations of the present thesis, as lately explained (Sections 3.2, 3.3).

He asserted that there are usually many acceptable representations of the system that shouldn't be easily rejected and, as a consequence, it shouldn't be assumed that a single correct representation could be found. This issue could also be addressed with the term of non-uniqueness in model identification or with non-identifiability, referring to the difficulty in finding the global best model and, hence, the true representation of the system.

This problem is typical of those calibrations with a shape of the objective function-surface having many local minima that don't differ much from the global one; the phenomena is reflected in the dotty plots. In these cases, there will not be a clear-cut boundary between acceptable and unacceptable simulations. Most calibration show indeed a spectrum of performances, varying from the best to the ones that are totally unacceptable. (Beven 2006)

Acceptable simulations are also called “behavioural”, in respect of the system being studied and the criteria to select them is the value of some performance measure (in this thesis is RMSE).

Because of the difficulty in finding a threshold, in this thesis the simulations which were the 5% best were considered as behavioural; all the rest were rejected.

### *Models of the cropped fields and the pasture*

Two calibrations were conducted with the Monte Carlo method:

- one was representative of the pasture;
- the other one was representative of the two cropped fields (so both the wheat and the barley fields).

The time-period was from 12/04/2017 to 30/09/2018 for both the models.

The input and settings of the two inverse models were the following:

- Atmospheric data: precipitation from April 2017 to September 2018, measured by the tipping rain gauge close to COSMOS; potential evaporation and transpiration were estimated as reported at the beginning of section 2.3.1 and are different for the two models;
- Soil profile: vertical soil profile, 0.5 m depth and with only one soil material (Figure 2.31). The choice was made according to the texture results, that showed the texture to be sandy loam at every depth, in both the fields.
- Feddes' parameters (to take into account the root water uptake): they were selected from a database provided by Hydrus, for the land uses "wheat" and "pasture";
- Water retention curve function: Van Genuchten – Mualem;
- Pre-set parameter ranges for the Monte Carlo runs (Table 2.6): they were set according to the water retention curve results obtained for the cropped fields and the pasture (section 2.2); the ranges were set a bit wider than the range of parameters values found for the samples. Instead, the range of saturated hydraulic conductivity, that wasn't estimated from the samples, was set according to a study in another Scottish site (Verrot 2018) with soil of the same texture.

Table 2.6 – Ranges of parameters that were set for the calibration of the models of the cropped fields and of the pasture.

Cropped fields					
	$\theta_r$	$\theta_s$	$\alpha$ (1/m)	n	Ks (m/day)
Min	0,0005	0,35	0,02	1,1	0.5
Max	0,085	0,65	35	2,3	2.5

Pasture					
	$\theta_r$	$\theta_s$	$\alpha$ (1/m)	n	Ks (m/day)
Min	0,0005	0,45	0,04	1,1	0.5
Max	0,03	0,65	4	2,2	2.5

- Observation points: water content values obtained from the sampling campaign conducted for the CRS calibration. They are 4 points in time, at three depths (assumed to be equal to the centre of the samples: 2.5, 7.5, 12.5 cm). Each point is the average of water content values obtained from six spatially-distributed points in the same field. In addition to that, for the wheat calibration, water content data obtained by a further sampling campaign (on 26/09/2018) were added (Table 2.2). They provided soil moisture values at the same three depths: 2.5, 7.5 and 12.5 cm. The calibration points are reported in Figures 2.28 and 2.29, plotted together with the measured precipitation and the calculated PET.

The objective function that was calculated for each simulation quantified the match between the simulated soil moisture at 2.5, 7.5 and 12.5 cm depths and the water content of samples at 0 to 5, 5 to 10 and 10 to 15 cm depth, respectively. The behavioural simulations were the 5% providing the better fits.

It should be noted that the result produced by the code was not only one simulation of soil moisture trend in time and depth, but an envelope of simulations, that encloses all the behavioural ones. The soil moisture data that better approximate the real conditions are supposed to be within this envelope.

### *Evaluation of the models of the two units*

To evaluate the two models, the envelopes of the simulated soil moisture at 2.5 cm depth were compared with the ML2 measurements. It should be noted that the ML2 probe measures soil moisture in the first 6 cm, hence the volume it considers could be assumed to be roughly equal to the one of the superficial calibration points (obtained by samples of the first 5 cm of soil).

The model representing the cropped fields was evaluated by using the ML2 measurements taken in the wheat field, while the pasture model by using the measurements from the pasture.

After that, the RMSE between the median of the simulated envelope and the ML2 values was calculated.

## **2.4. Investigation of CRS-scale soil moisture dynamic**

### **2.4.1. CRS model**

To address objective 3, a Hydrus-1D model was calibrated by using the soil moisture data obtained from the CRS measurements.

The calibration was conducted with the Monte Carlo method implemented by the same code used for the calibration of the two units, that was adapted to the CRS calibration though. Differently from the models of the two units, the objective function doesn't quantify the match between simulated and observed data just at one level of the soil column. It indeed quantifies the match between CRS data and the average of soil moisture values in a superficial portion of the soil column, that has a length that is equal to the CRS effective depth.

The period considered was from 05/01/2016 to 30/09/2018.

The input and settings of the calibration were the following:

- Atmospheric data: measured precipitation from January 2016 to September 2018 (data of 2016 were from a tipping rain gauge in a neighbouring site); potential evaporation and transpiration are the area-weighted averages of the ones estimated for the cropped fields and the ones estimated for the pasture (weight for the cropped fields: 0.74; weight for the pasture: 0.26; according to Table 2.1);
- Soil profile: vertical soil profile, 0.5 m depth and with only one soil material, according to the texture results and to the choices made for the models of the two units previously explained;
- Root water uptake: area-weighted averages of the Fedde's parameters of a wheat and pasture field were calculated (weight for the wheat: 0.74; weight for the pasture: 0.26; according to Table 2.1);
- Water retention curve function: Van Genuchten – Mualem;
- Parameter ranges: they have been set quite wide because the measurements are representative of a large and heterogeneous area, hence the range of values that could be expected is quite wide. The ranges were set according to literature values for soils with the same texture (sandy-loam) and saturated hydraulic conductivity was set according to a study in another Scottish site (Verrot 2018), like the models of the two units.

Table 2.7 – Ranges of hydraulic parameters set for the CRS calibration

	$\theta_r$	$\theta_s$	$\alpha$ (1/m)	n	Ks (m/s)
Min	0,005	0,37	0,5	1,1	0,5
Max	0,14	0,7	20	1,9	2,5

- Observation points: CRS data resulting from the correction and calibration procedures (Figure 2.13).

The Monte Carlo method involved 10000 runs of the software, as for the previous models. Since the time period considered for the CRS calibration was longer, the process needed about 10 days (more than the models of the two units).

The fitting of each simulation to the CRS data was checked in the following way:

- not only the CRS data, but also the effective depth ( $z^*$ ) of the measurement was an input requested by the code, for each day of the time period considered;
- an average of the soil moisture values simulated in the first  $z^*$  cm of soil was calculated for each day;
- the RMSE representing the differences between the values just mentioned and the CRS data was calculated for each Monte Carlo run;
- the 5% simulations with the minimum RMSE were selected as behavioural.



## **2.5. Comparison of the dynamics of the two units and the CRS-scale dynamic**

To address objective 4, an area-weighted average of the soil moisture trends in time which were simulated for the different units was calculated and compared with the CRS simulated trend, for the period from 12/04/2017 to 30/09/2018. The period coincided with the one considered for the models of the two units.

The weights were the portions of the CRS footprint occupied by pasture and crops, as previously reported in Table 2.1, and are reported below:

- weight for the trends of the cropped fields: 0.74;
- weight for the trends of the pasture: 0.26.

It should be noted that the weight originally attributed to the pasture was 0.25; then the weight corresponding to the narrow grass-stripe at the intersection between the wheat field and the others (0.1) was added to it.

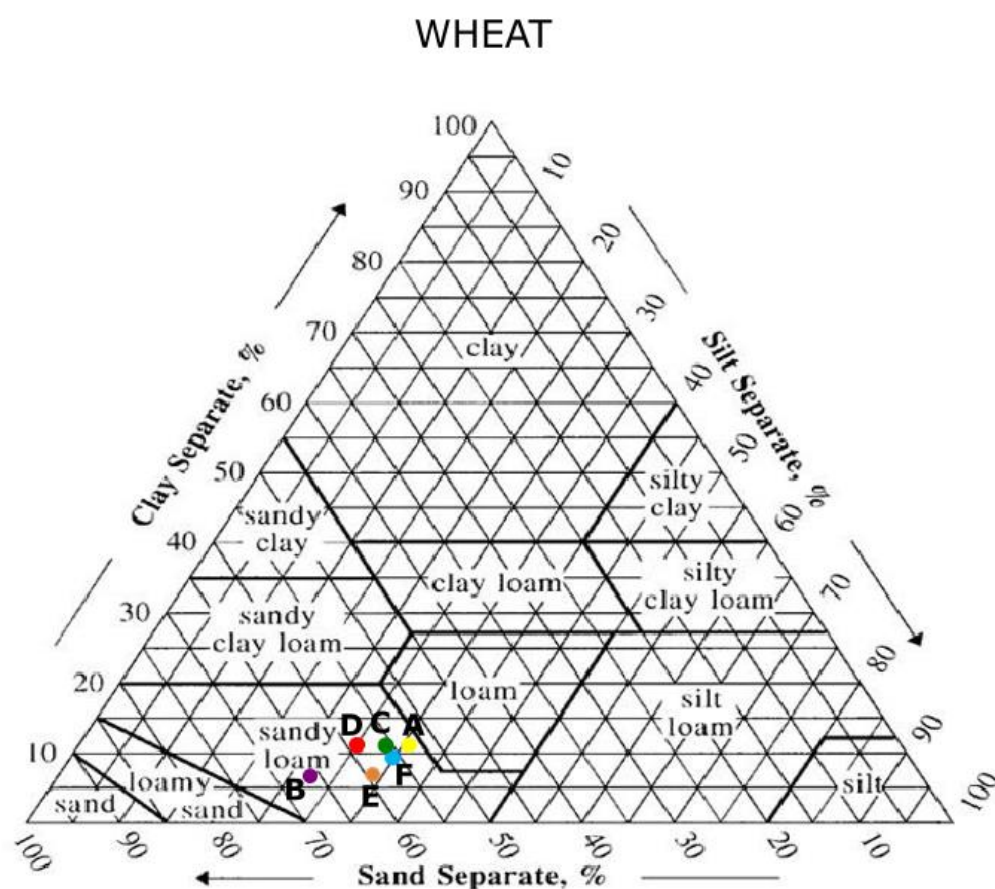
To observe the differences between them, the weighted average and the CRS simulated data were plotted together in the same graph, as reported in the “Results” chapter.

## 3. Results

### 3.1. Soil hydraulic properties

#### *Texture results*

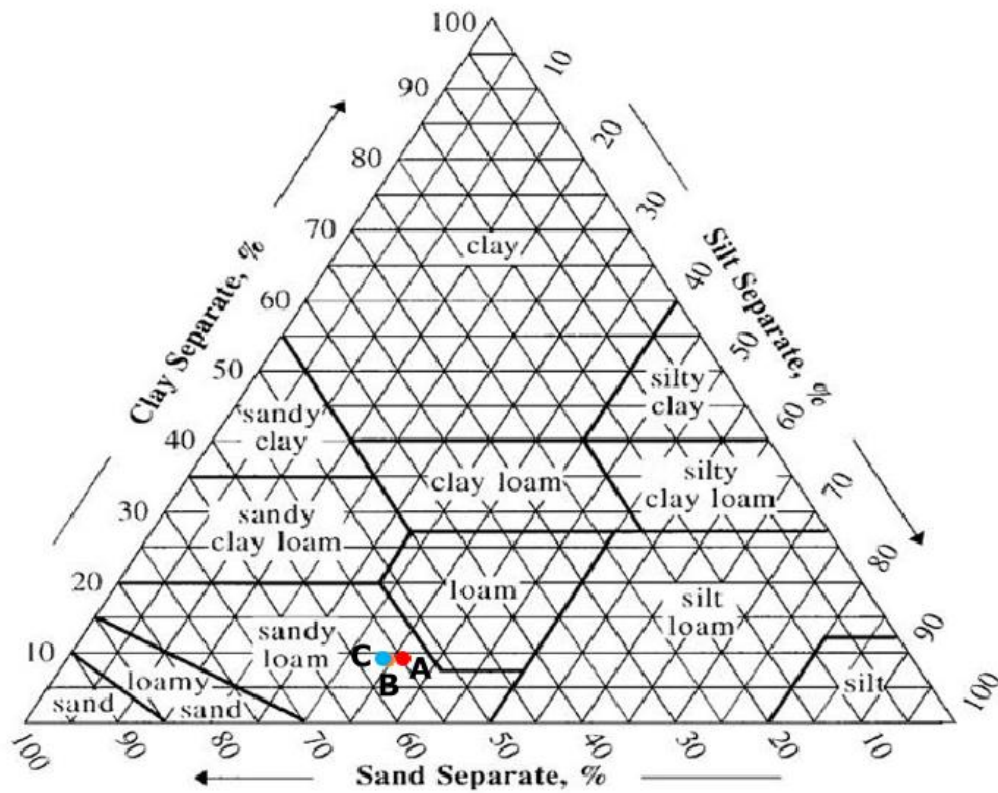
The results of the laboratory analysis to determine the texture are reported in the Figures 3.1, 3.2. As reported in the figures, the texture resulted to be sandy loam in both the fields and at all the analysed depths.



	Depth of the sample (cm)	Collection date	% of Clay	% of Silt	% of Sand	Texture
A	0-5	26/09/2018	10,7 %	36,0 %	53,3 %	Sandy loam
B	5-10	26/09/2018	6,4 %	27,5 %	66,1 %	Sandy loam
C	10-15	26/09/2018	10,7 %	33,7 %	55,7 %	Sandy loam
D	20-30	05/09/2018	10,7 %	30,5 %	58,8 %	Sandy loam
E	30-40	05/09/2018	6,5 %	34,3 %	59,2 %	Sandy loam
F	>40	05/09/2018	8,9 %	35,3 %	55,8 %	Sandy loam

Figure 3.1 – Texture results for the samples from the wheat field (USDA triangle).

## PASTURE



	Depth of the sample (cm)	Collection date	% of Clay	% of Silt	% of Sand	Texture
A	0-5	26/09/2018	8,7 %	36,5 %	54,8 %	Sandy loam
B	5-10	26/09/2018	8,6 %	34,9 %	56,5 %	Sandy loam
C	10-15	26/09/2018	8,7 %	34,4 %	56,9 %	Sandy loam

Figure 3.2 - Texture results for the samples from the pasture field (USDA triangle).

### 3.1.1. Water retention curve

#### *Estimated parameters*

Tables from 3.1 to 3.3 report the ranges of the parameters obtained by the fitting of the Van Genuchten function to all the laboratory results (including replicas). The minimum coefficient of determination of the fitting was 0.76 for the samples from the wheat field and 0.89 for the samples from the other units; for many samples it was very close to 1. Given the high value of  $R^2$ , we can assert that the fitting was good. These ranges were used to decide the ranges for the calibration of the cropped fields and of the pasture.

Table 3.1 – Ranges of the parameters obtained for the samples from the wheat field

Wheat				
	$\Theta_r$	$\Theta_s$	$\alpha$ (1/m)	n
Min	0,01	0,39	0,5	1,2
Max	0,08	0,54	1,7	2,0

Table 3.2 - Ranges of the parameters obtained for the samples from the barley field

Barley				
	$\Theta_r$	$\Theta_s$	$\alpha$ (1/m)	n
Min	0,01	0,36	0,5	1,2
Max	0,07	0,62	31,5	2,0

Table 3.3 - Ranges of the parameters obtained for the samples from the pasture

Pasture				
	$\Theta_r$	$\Theta_s$	$\alpha$ (1/m)	n
Min	0,01	0,49	0,5	1,2
Max	0,01	0,63	3,85	1,4

To have a better idea of the distribution of the results, also the box-and-whisker plots, representing all the estimated parameters, were created. They are reported in Figures from 3.3 to 3.6. The upper and lower edge of each box represent the first and third quartile, respectively, and the band inside the box is the median. The vertical whiskers indicate the variability outside the upper and lower quartiles: the upper one represents the minimum and the lower one the maximum value among all data. Outliers are plotted as individual points.

The considerations reported below could be done about the box-and-whiskers plots:

- $\Theta_r$ : the range of values obtained is wider for the cropped fields, while for the pasture a value of 0.01 was found for all the samples. In the barley field higher values of  $\Theta_r$  were found just for a few samples, while in the wheat field a wider distribution of this parameter was found, with several samples presenting  $\Theta_r$  values higher than 0.06;
- $\Theta_s$ : a wide distribution of this parameter was found in every field. It is worth comparing these results with porosity estimates made on samples from Elsieck. Porosity had been determined by Katya Dimitrova in the three units, as a part of her PhD project, presenting the ranges reported in Table 3.4. They were obtained by samples collected for the calibration of the CRS.

Table 3.4 – Ranges of the porosity values previously determined on samples from Elsieck.

	Porosity	
	Min	Max
Cropped fields	0,37	0,7
Pasture	0,4	0,76

- $\alpha$ : the widest distribution of this parameter was found in the barley field and, for this reason, the related boxplot is reported with a different scale. The maximum value among all ( $31.7 \text{ m}^{-1}$ ) was found for a sample from the barley field and, that was reported as an outlier. Also a sample from the wheat field, that is characterized by a  $\alpha=1.7$ , was reported as an outlier, because all the other values were within the range  $0,5 \div 0,75$ .
- $n$ : a wide range of values was found in both the cropped fields. For the wheat field, this was due to the fact that samples coming from two different sampling points showed very different values of this parameter. In the barley field, instead, a value of 2 was found only for two samples, while all the rest ranged between 1,2 and 1,4.

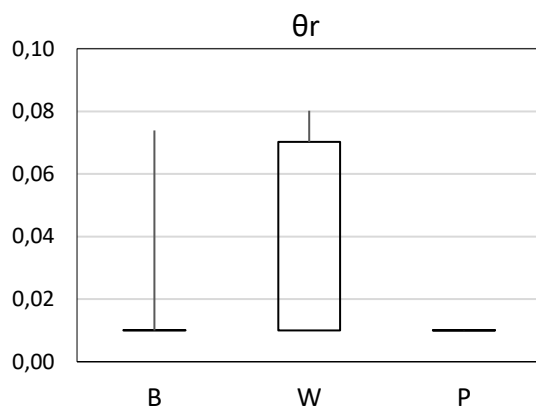


Figure 3.3 – Box-and-whiskers plots of  $\theta_r$  values in the three fields. B=barley field; W=wheat field; P=pasture.

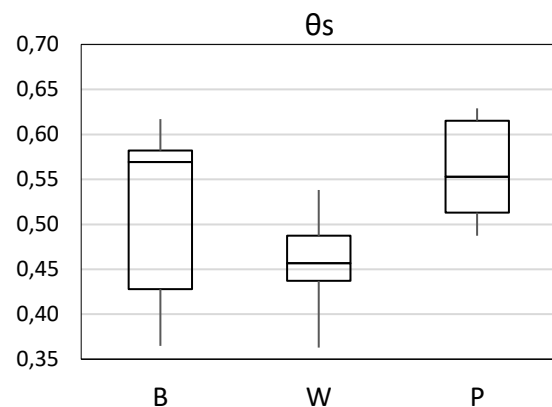


Figure 3.4 - Box-and-whiskers plots of  $\theta_s$  values in the three fields. B=barley field; W=wheat field; P=pasture.

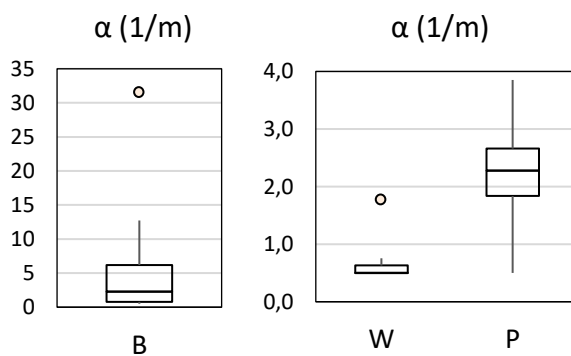


Figure 3.5 - Box-and-whiskers plots of  $\alpha$  values in the three fields. B=barley field; W=wheat field; P=pasture.

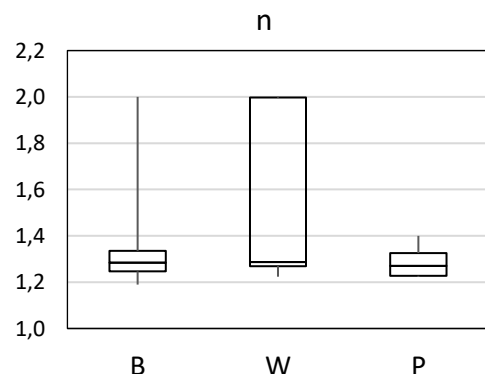


Figure 3.6 - Box-and-whiskers plots of  $n$  values in the three fields. B=barley field; W=wheat field; P=pasture.

### Comparison with literature values

The following table reports literature ranges of the hydraulic parameters for a sandy-loam soil (Rawls and Brakensiek 1985):

Table 3.5 – Literature values oh hydraulic parameters for a sandy-loamy soil.

Theta r		Theta s		$\alpha$ (1/m)		n	
Min	Max	Min	Max	Min	Max	Min	Max
0,024	0,106	0,35	0,56	1,6	29	1,14	1,62

The main differences are between the estimated and literature ranges are:

- Some values obtained for  $\theta_r$  are very low and out of literature ranges (in particular, all the values obtained for the pasture field);
- The  $\alpha$  values obtained for some samples are quite low and out of literature ranges.

The values obtained for the parameters  $\theta_s$  and  $n$  are more similar to the literature ones, although the maximum values obtained for both the parameters are out of literature ranges. However, the porosity (that can be assumed to be equal to  $\theta_s$ ) was already determined from other samples of the Elswick site (Table 3.4), giving very similar results.

### Comparison with data from another Scottish site

The results were then compared to the values obtained for the Mid-Pilmore site, that is an experimental field of the James Hutton Institute in east Scotland, United Kingdom, and, like our site, is characterized by sandy-loam soil at the surface (Verrot et al., 2018).

Table 3.6 – Ranges of the soil hydraulic parameters obtained in Pilmore (Verrot et al., 2018)

$\theta_r$		$\theta_s$		$\alpha$ (1/m)		n	
Min	Max	Min	Max	Min	Max	Min	Max
0,03	0,12	0,35	0,48	9	132	1,15	1,67

The comparison gives the following results, that are similar to the given by the comparison with literature values:

- The  $\theta_r$  value obtained for several samples is very low and out of the Pilmore-ranges;
- For several samples a high value of  $\theta_s$  was obtained, out of Pilmore ranges. However, these values were in agreement with other Elswick-data (Table 3.4), as written before;
- The range of values obtained for  $\alpha$  is lower than in Pimore;
- Some values obtained for  $n$  are quite high and out of Pilmore-ranges.

### *Shape of the curves*

The following figures represent the water retention curves obtained for the different sampling points, at different depths. The results obtained for replicas were reckoned not to bring significant extra information because they weren't significantly different from the corresponding samples. Hence, they are not displayed in the graphs, in order to allow a more straightforward interpretation of the rest of the results.

Figures from 3.7 to 3.11 illustrate the curves obtained at certain depths, from samples from the three fields. The colours of the curves indicate the field they correspond to and help to distinguish the variability within a field from the variability between fields.

The curves of point E and F in the barley field corresponding to the first 10 cm are not reported in Figures 3.7 and 3.8 because the related samples were disturbed, so they don't represent the natural soil properties (the soil had been ploughed before the samples were collected). Samples from point G, instead, were collected after a further treatment that made the superficial soil more homogeneous with the rest, hence they are reported in Figures 3.7 and 3.8.

At depths higher than 15 cm there are no curves corresponding to the points E and C because samples were collected only down to 15 cm in these points.

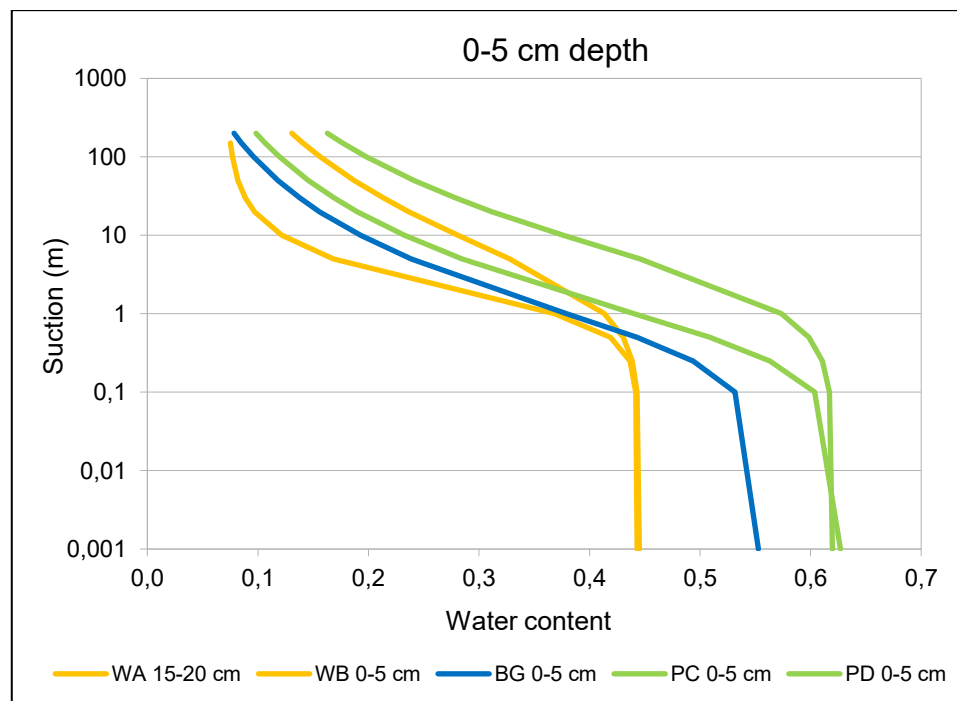


Figure 3.7 – Water retention curves of the first 5 cm of soil; the yellow curves are from the wheat field (points A and B), the blue one is from the barley field (point G) and the green ones are from the pasture (points C and D).



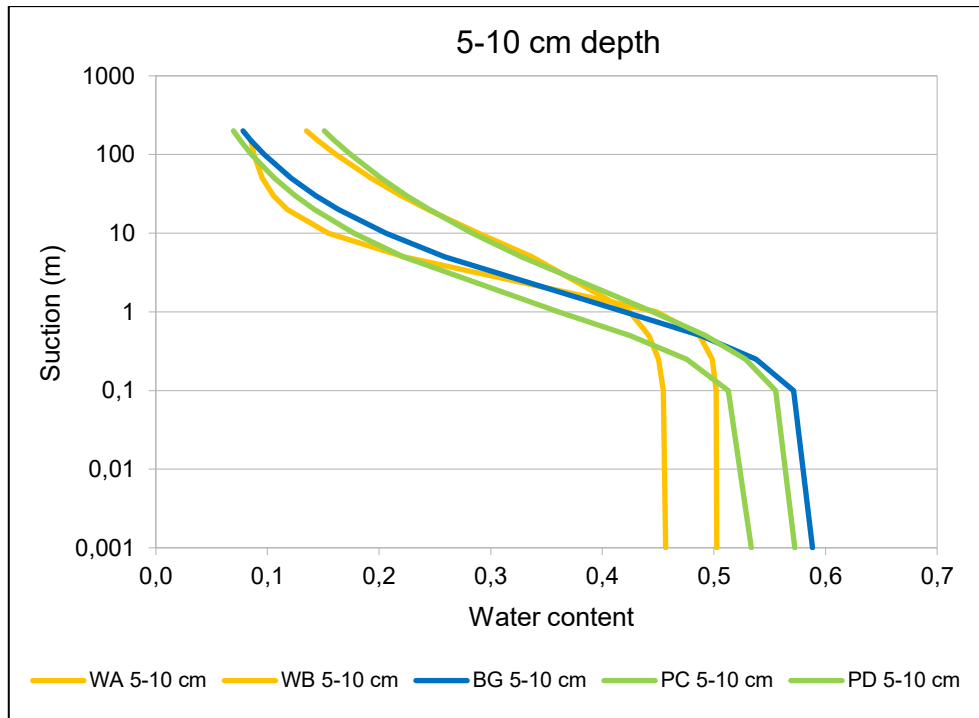


Figure 3.8 - Water retention curves at the depth 5÷10 cm, the yellow curves are from the wheat field (points A and B), the blue one is from the barley field (point G) and the green ones are from the pasture (points C and D).

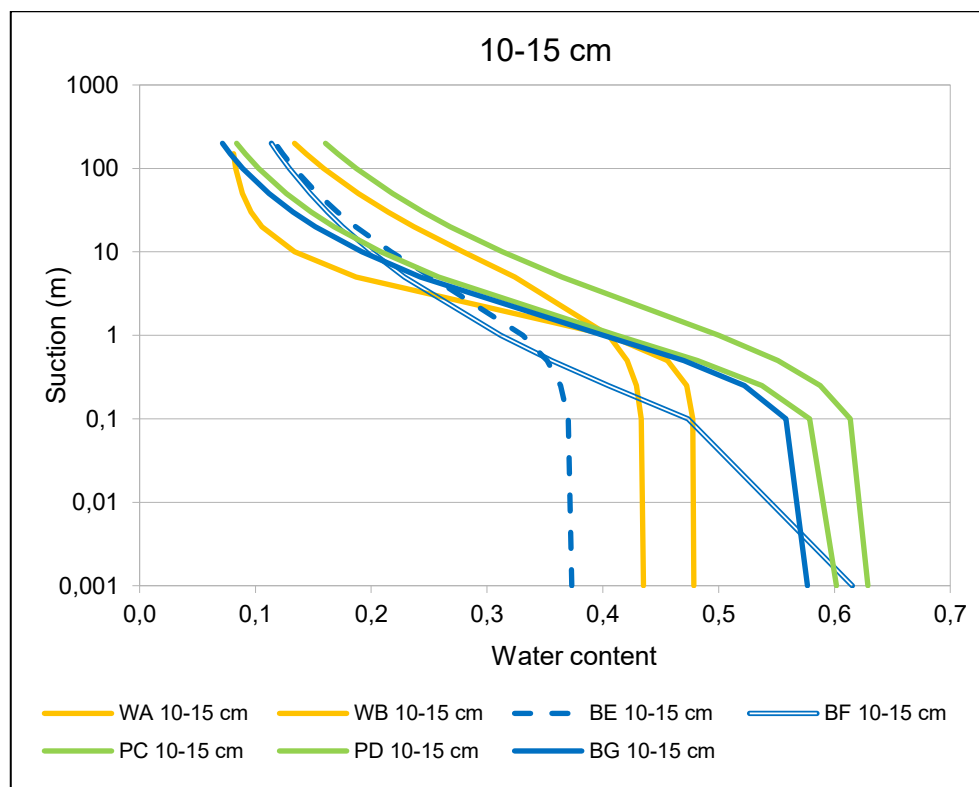


Figure 3.9 - Water retention curves at the depth 10÷15 cm, the yellow curves are from the wheat field (points A and B), the blue ones are from the barley field (point E, F and G) and the green ones are from the pasture (points C and D).

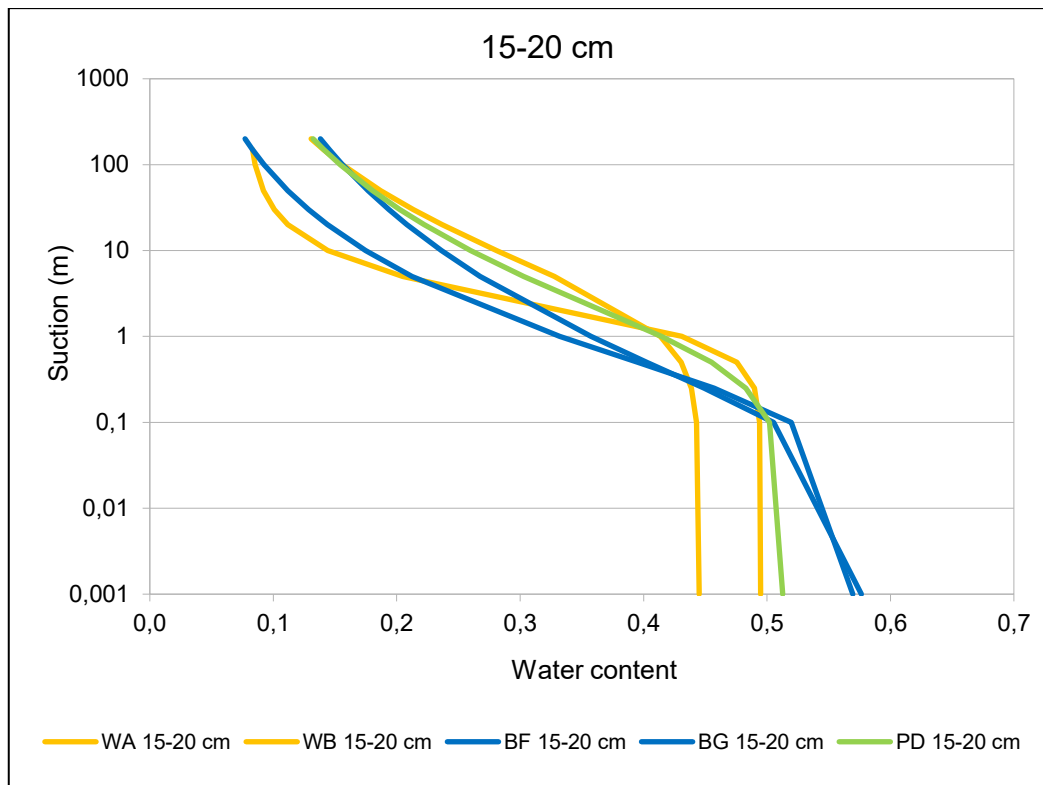


Figure 3.10 - Water retention curves at the depth 15÷20 cm, the yellow curves are from the wheat field (points A and B), the blue ones are from the barley field (points F and G) and the green one is from the pasture (point D).

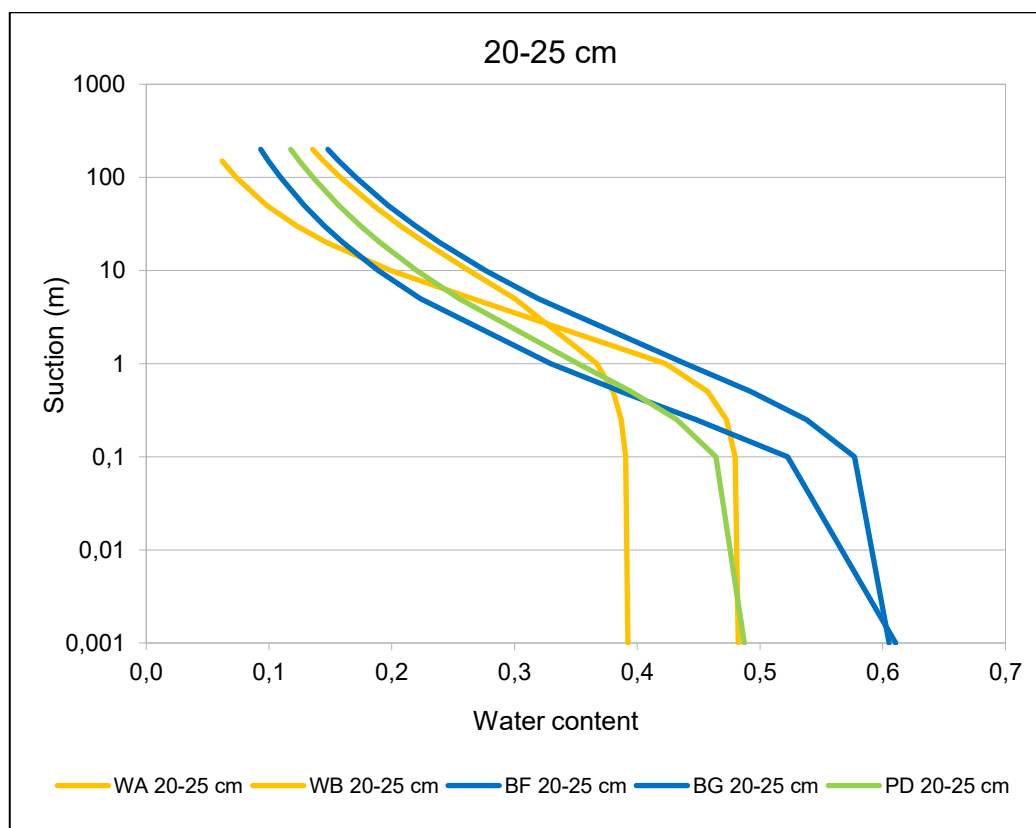


Figure 3.11 - Water retention curves at the depth 20÷25 cm, the yellow curves are from the wheat field (points A and B), the blue ones are from the barley field (points F and G) and the green one is from the pasture (point D).

In order to provide some insights into the vertical variability of soil hydraulic properties, the curves derived from each sampling point were plotted together in the Figures from 3.12 to 3.19. So, each figure represents different curves obtained from samples collected along a vertical profile.

Tables from 3.7 to 3.9 give information about the parameters obtained for each sampling point.

Figures 3.12 and 3.13 illustrate the curves corresponding to the samples collected from the two points in the wheat field:

- Point A: high variability of the parameter  $\theta_s$ , visible both from Figure 3.12 and in the boxplot of Table 3.7. The shape of the curves is similar, though. That's explained by the small variability of the rest of the parameters. No clear correlation between  $\theta_s$  and depth is recognizable.
- Point B: the variability of the parameters is similar to point A, although  $\theta_s$  presents a narrower range than point A.

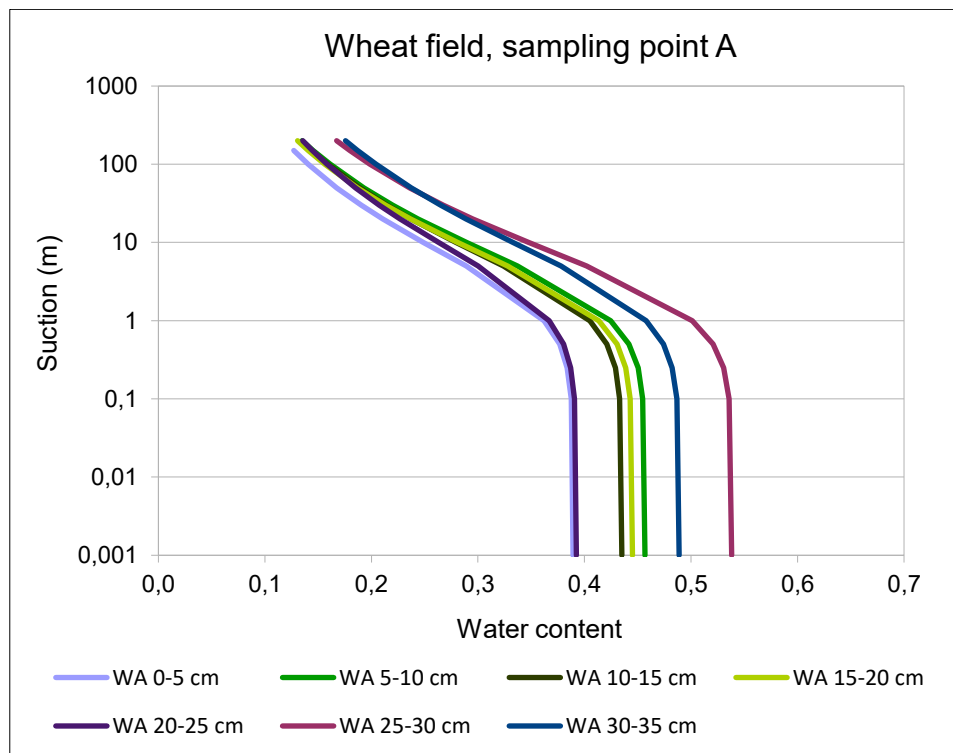


Figure 3.12 - Water retention curves corresponding to samples collected along the vertical profile of the sampling points A from the wheat field.

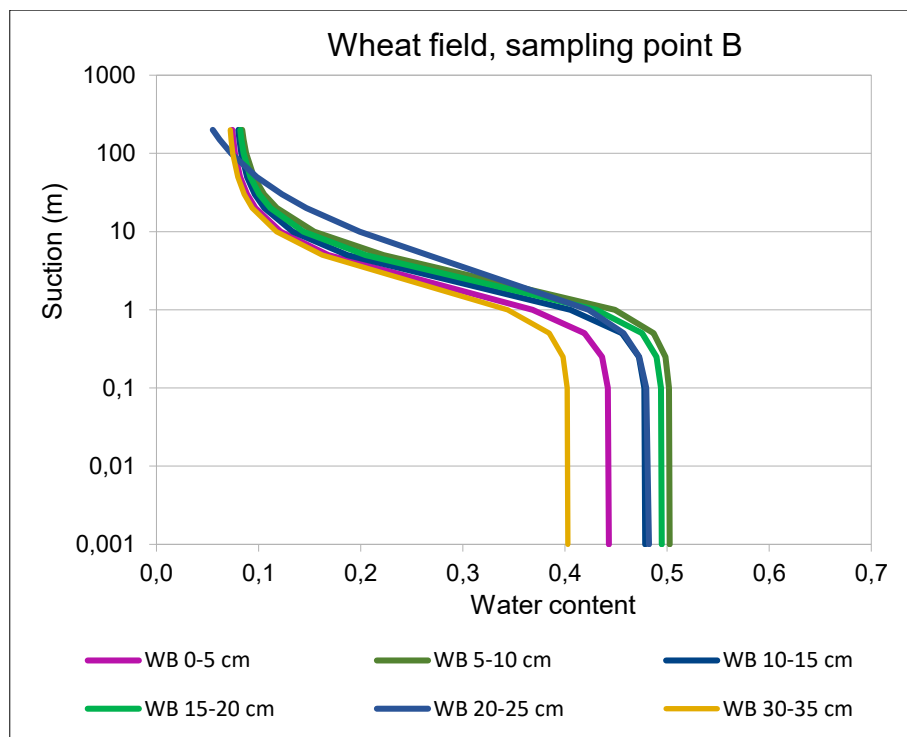


Figure 3.13 – Water retention curves corresponding to samples collected along the vertical profiles of the sampling point B from the wheat field.

Table 3.7 –Parameters obtained at the points A and B of the wheat field

$\theta_r A = 0.01$ for all the samples	<p style="text-align: center;"><math>\theta_r B</math></p>	<p style="text-align: center;"><math>\theta_s</math></p> <p style="text-align: center;">A                      B</p>
$\alpha A = 0.01$ for all the samples	<p style="text-align: center;"><math>\alpha (1/m) B</math></p>	<p style="text-align: center;">n B is 1.5 at 20-25 cm; and is 2 for all the rest of the samples</p> <p>n A = 1.24÷1.28</p>

Figures from 3.14 to 3.16 illustrate the curves for the samples collected from the three points in the barley field:

- Point E (Figure 3.14): a change of the soil characteristics is identifiable at 10 cm. That matches a change in the values of the parameters,  $\theta_r$  and  $n$  in particular (Table 3.8);
- Point F: Figure 3.15 shows a visible difference in behaviour between the soil of the first 10 cm and the deeper soil. A replica at 0÷5 cm confirms the shape of the superficial curves.

It should be noted that when the samples of points E and F were collected, the superficial soil was disturbed, because the field had been previously ploughed.

- Point G (Figure 3.16): in this point the variability of the curves is not high. These samples were collected after the soil was treated for sowing.

Table 3.8 - Parameters obtained at the points E, F and G of the barley field

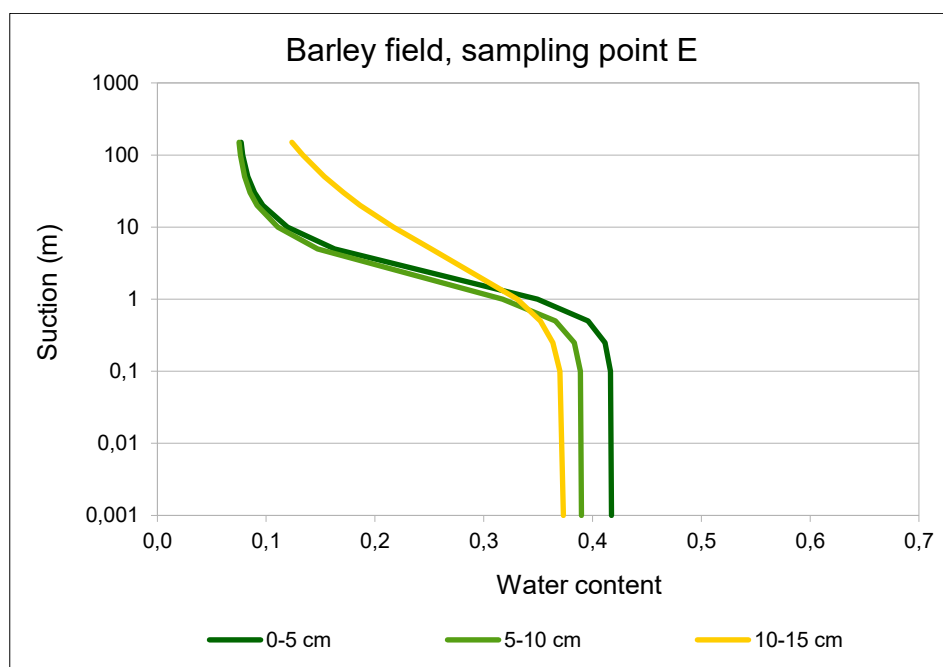
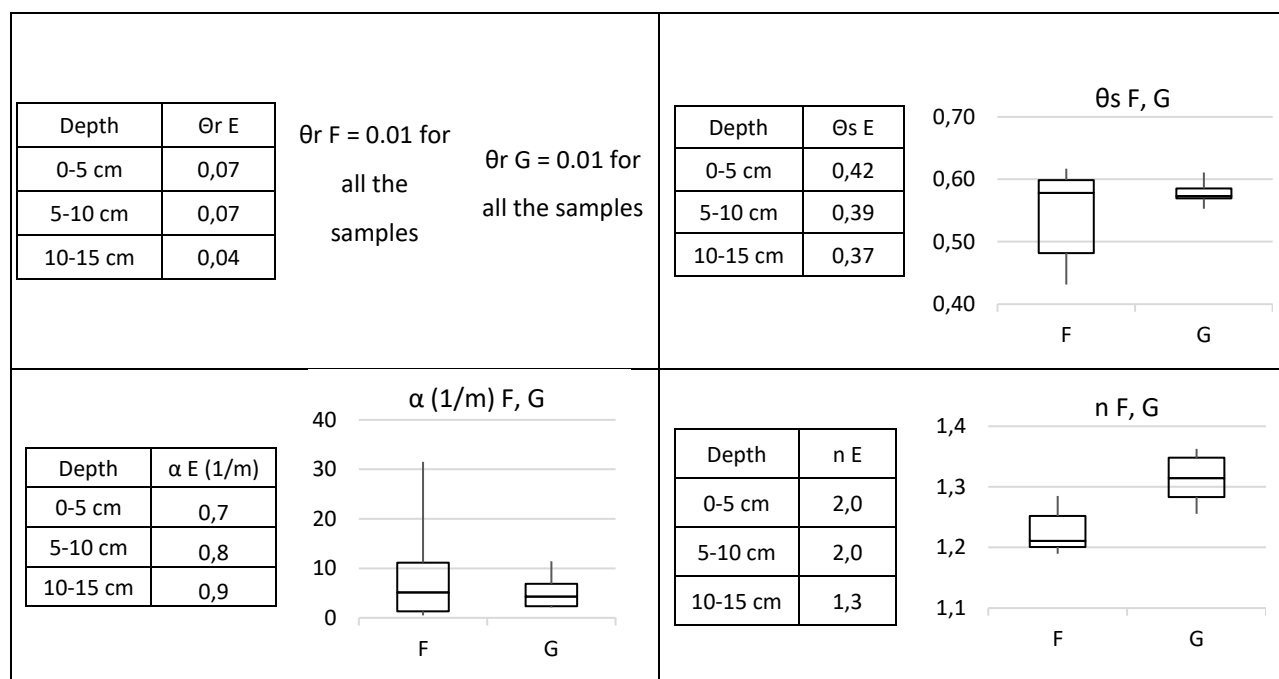


Figure 3.14 - Water retention curves corresponding to samples collected along the vertical profiles of the point E from the barley field. At the moment when samples were collected, the superficial soil was disturbed.

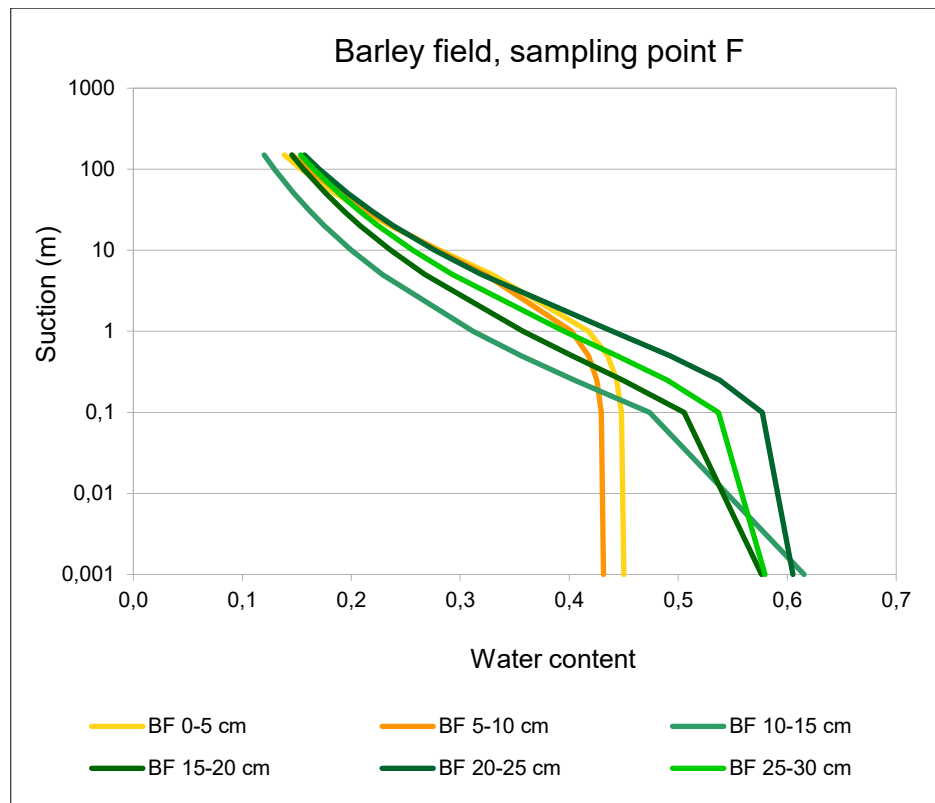
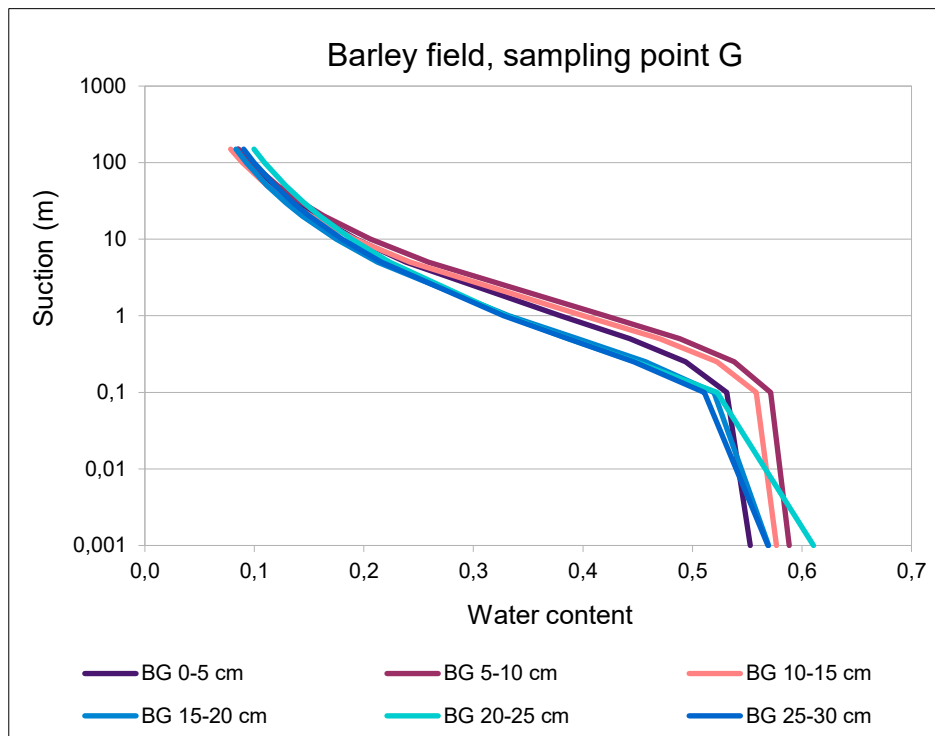


Figure 3.15 - Water retention curves corresponding to samples collected along the vertical profiles of the sampling point F from the barley field. At the moment when samples were collected, the superficial soil was disturbed.



Figures 3.16 - Water retention curves corresponding to samples collected along the vertical profiles of the sampling point G from the barley field. These samples were collected later than the ones of points E and F, after a further treatment.

In Figure 3.17 the envelopes of the results of point F and G are compared. The soil of point F that is deeper than 10 cm shows a very similar trend to the soil of point G and they are both very different from the surface soil of point F.

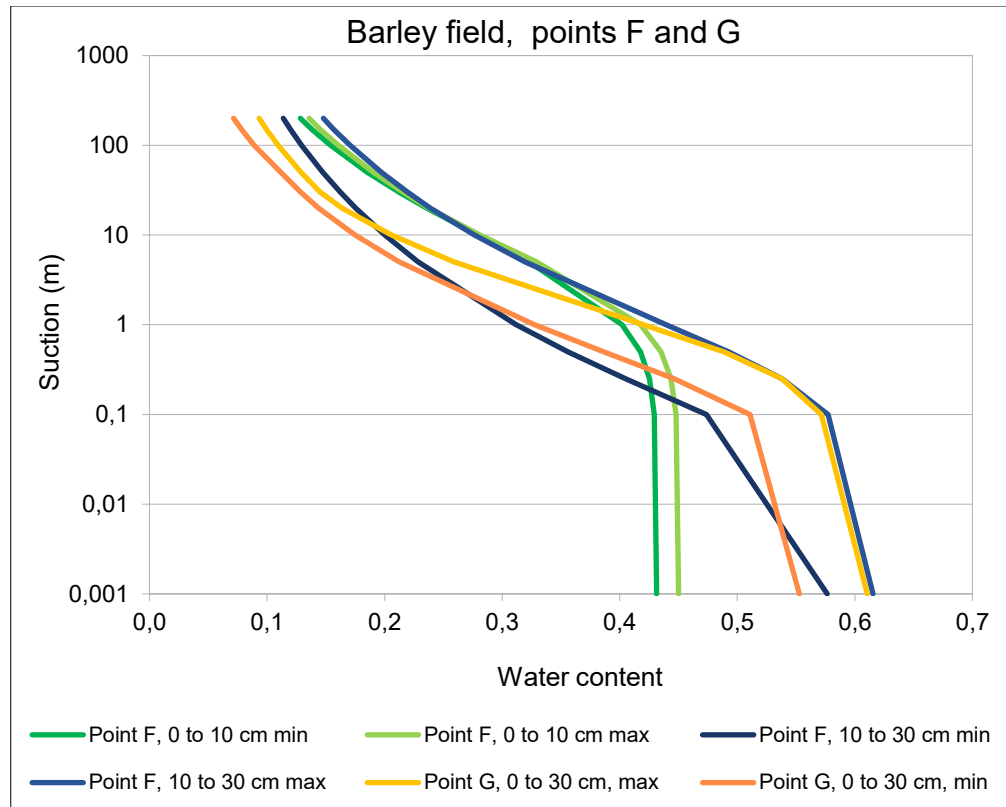


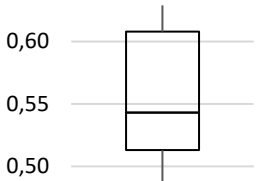
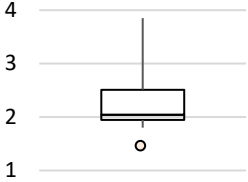
Figure 3.17 – Comparison of the envelopes of the water retention curves obtained at points F and G. The curves of the first 10 cm of point F are plotted separately in order to highlight their peculiarity.

Figures 3.18 and 3.19 represent the water retention curves of the samples collected from the pasture and Table 3.9 the corresponding soil hydraulic parameters.

- Point C (Figure 3.18): the curves in this point are quite similar to each other. Also the parameters have similar values.
- Point D (Figure 3.19): the curves in this point have similar shapes, although the one of the first 5 cm is slightly different from the rest. That matches a difference in the parameters ( $\alpha=0.5$ , while it's higher than 1,8 for the rest;  $n=1,3$  while it's 1,2 for all the rest).



Table 3.9 - Parameters obtained at the points C and D of the pasture

<p><math>\theta_r C = 0.01</math> for all the samples</p> <p><math>\theta_r D = 0.01</math> for all the samples</p>	<table border="1" data-bbox="842 324 1136 488"> <thead> <tr> <th>Depth</th><th><math>\theta_s C</math></th></tr> </thead> <tbody> <tr> <td>0-5 cm</td><td>0,63</td></tr> <tr> <td>5-10 cm</td><td>0,53</td></tr> <tr> <td>10-15 cm</td><td>0,60</td></tr> </tbody> </table> <div data-bbox="1177 241 1433 555"> <p><math>\theta_s D</math></p>  </div>	Depth	$\theta_s C$	0-5 cm	0,63	5-10 cm	0,53	10-15 cm	0,60
Depth	$\theta_s C$								
0-5 cm	0,63								
5-10 cm	0,53								
10-15 cm	0,60								
<p><math>\alpha C = 2.7</math> for all the samples</p>	<div data-bbox="539 645 788 922"> <p><math>\alpha (1/m) D</math></p>  </div> <p><math>n C = 1,3</math> for all the samples</p> <p><math>n D = 1,3</math> at 0-5 cm; = 1,2 for all the rest of the samples</p>								

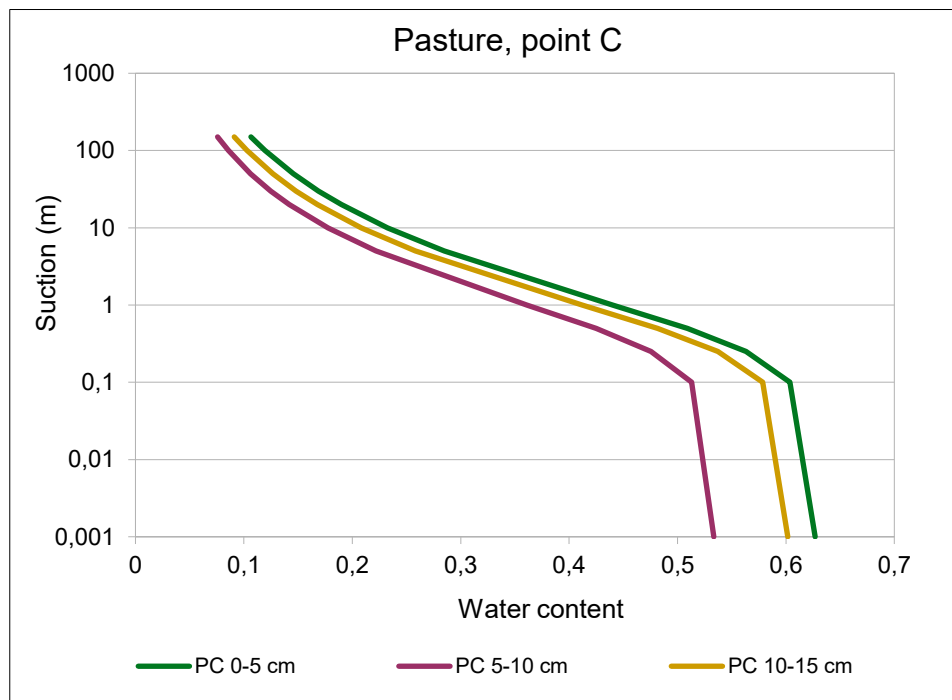


Figure 3.18 - Water retention curves of the samples of point C, in the pasture, at depths down to 15 cm.

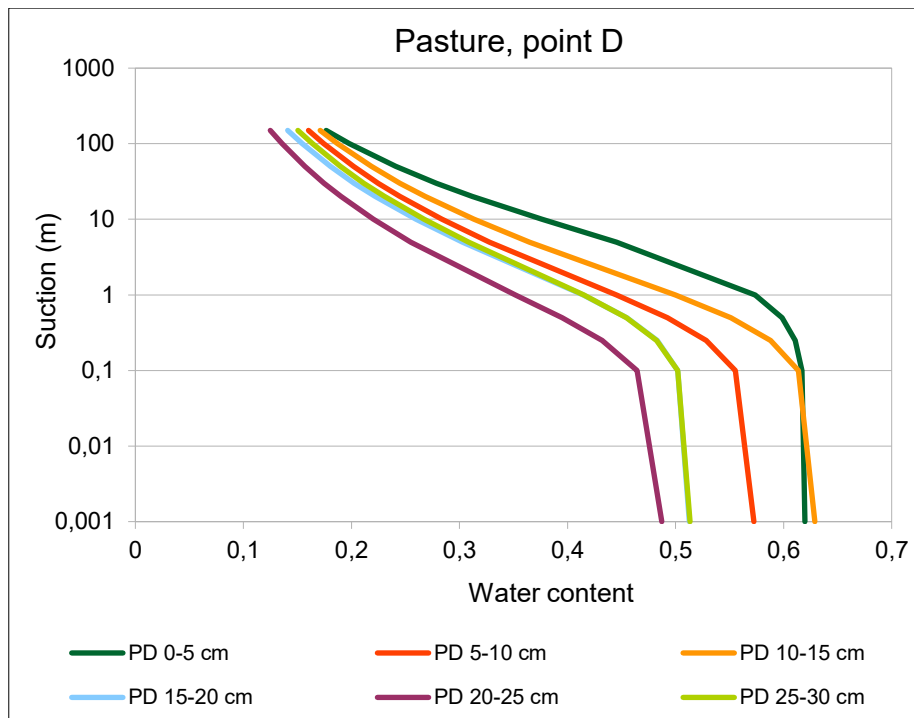


Figure 3.19 - Water retention curves of the samples of the point D, in the pasture, at depths down to 15 cm.

## 3.2. Soil moisture dynamics in the two units

### 3.2.1. Modelling results of the two units

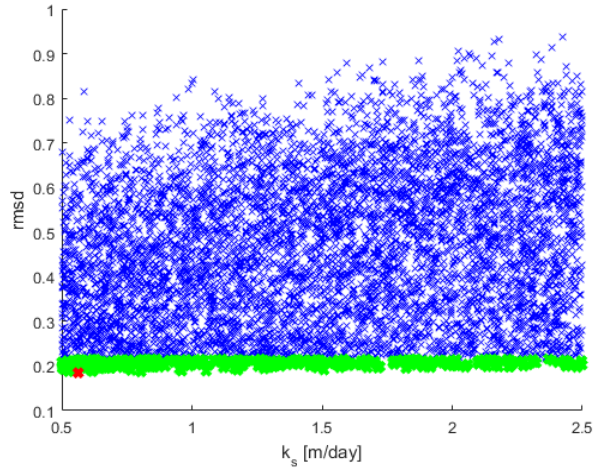
The minimum and maximum RMSE of the behavioural simulations (which are the 5% best simulations) of the two models are reported in Table 3.10.

Table 3.10 – Minimum and maximum objective function among the behavioural simulations of the models of the two units

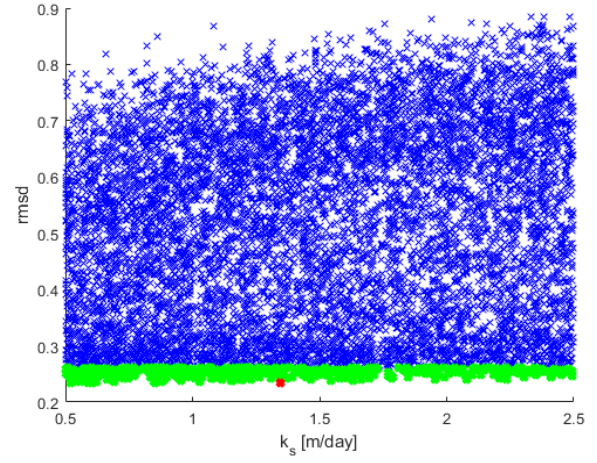
	RMSE min	RMSE max
Cropped fields	0,185	0,216
Pasture	0,234	0,262

Figure 3.20 illustrates the dotty plots produced by the Monte Carlo code; each dot represents one simulation, the green ones represent the behavioural and the red dot represents the best simulation (namely, the one with the minimum RMSE).

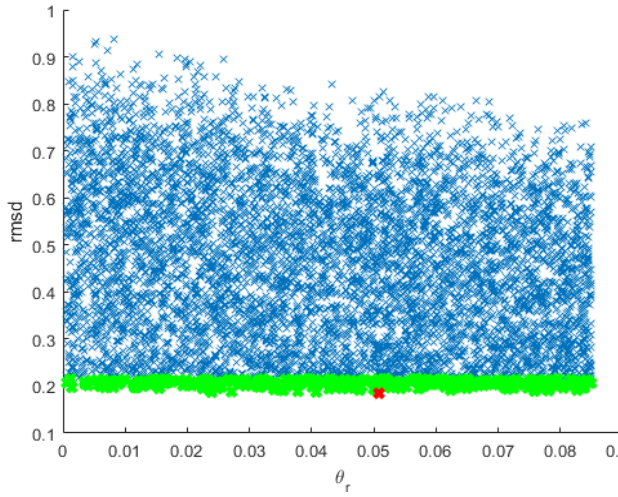
a)  $K_s$  (m/day), cropped fields



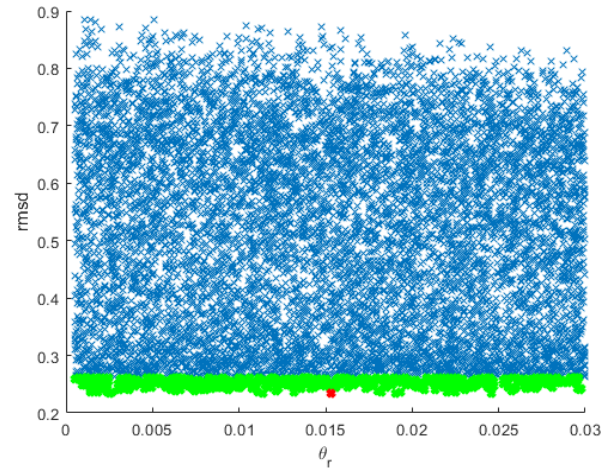
b)  $K_s$  (m/day), pasture



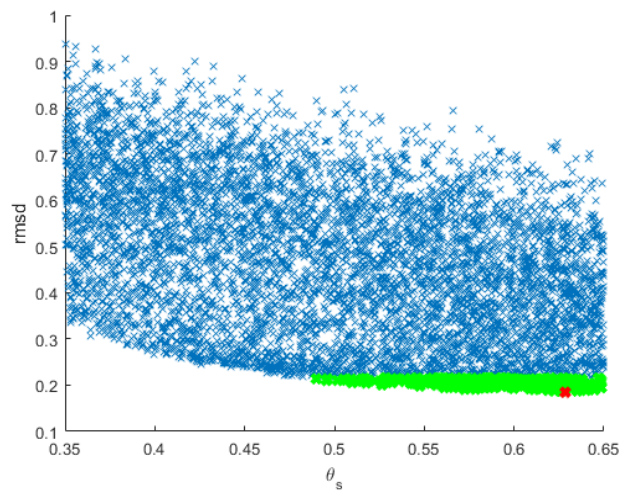
c)  $\theta_r$ , cropped fields



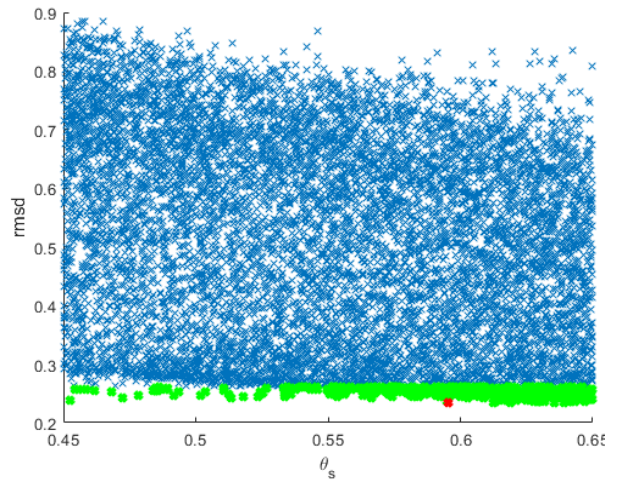
d)  $\theta_r$ , pasture



e)  $\theta_s$ , cropped fields



f)  $\theta_s$ , pasture





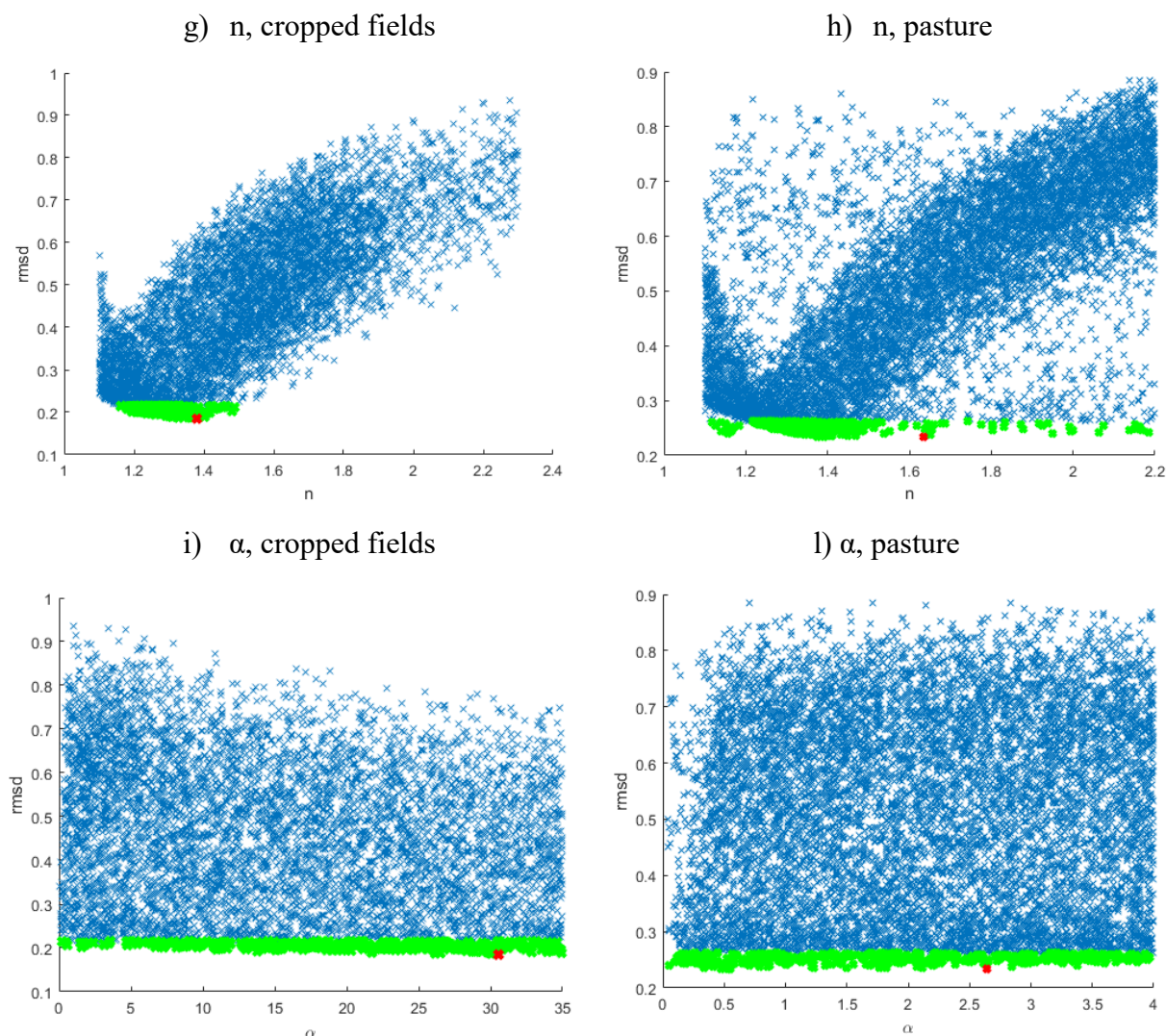


Figure 3.20 – Dotty plots representing the variation of performance of the models of the two units (indicated by RMSD) within the pre-set ranges of the parameters  $K_s$ ,  $\theta_r$ ,  $\theta_s$ ,  $n$  and  $\alpha$

The envelopes reported in the Figures 3.21 and 3.22 are the minimum and maximum soil moisture values at 2.5, 7.5 and 12.5 cm depth, among the behavioural simulations of the model of the cropped fields and of the pasture, respectively. They are plotted together with the observation points. It should be noted that the model simulates soil moisture for all the time-period considered, for each element the profile is divided into, namely every 0.5 cm down to 0.5 m depth. Among all the simulated data, only the values corresponding to 2.5, 7.5 and 12.5 are selected, in order to be compared with the calibration points.

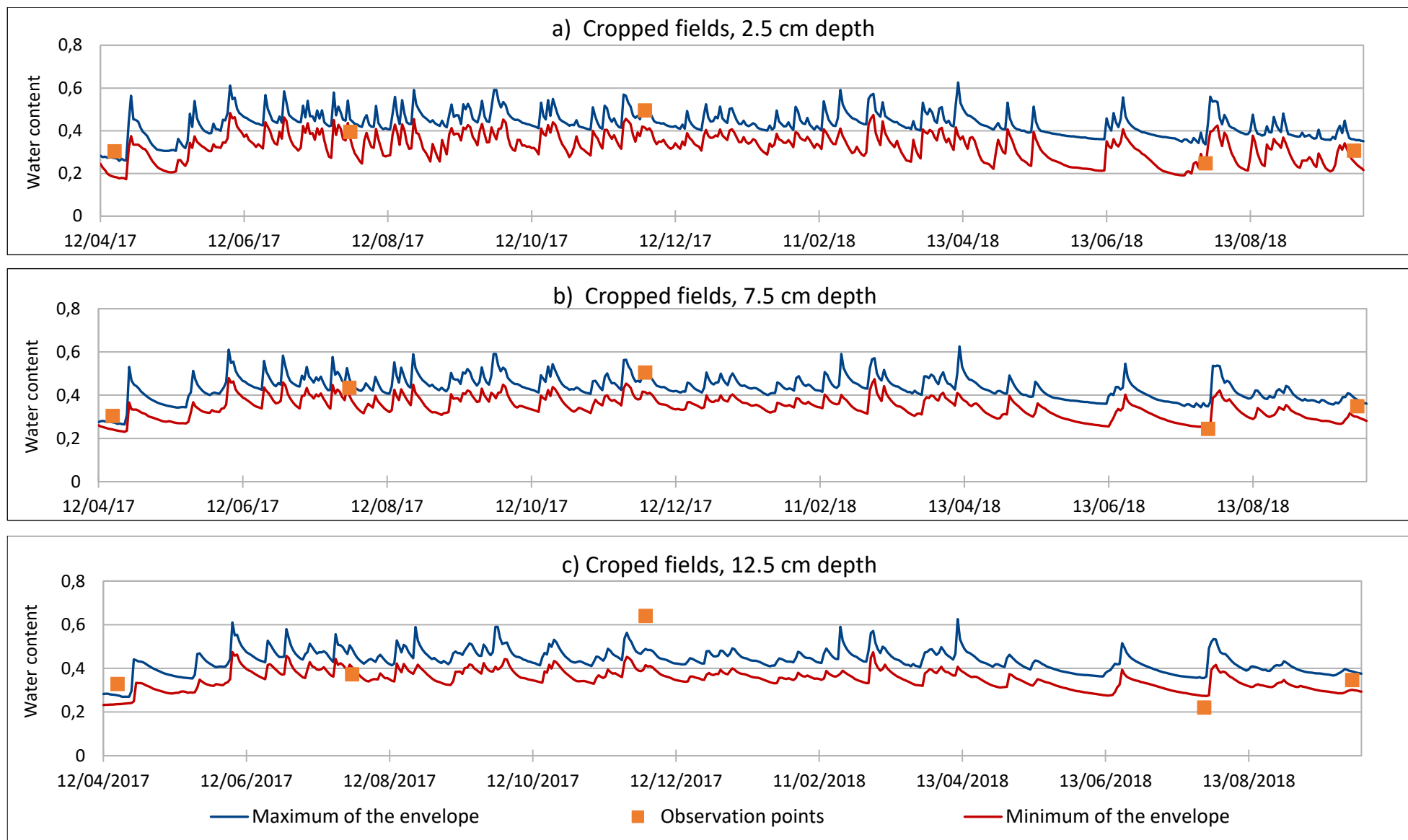


Figure 3.21 a, b c - Observation data at three depths and envelopes of the simulated soil moisture at the corresponding depths, for the cropped fields.

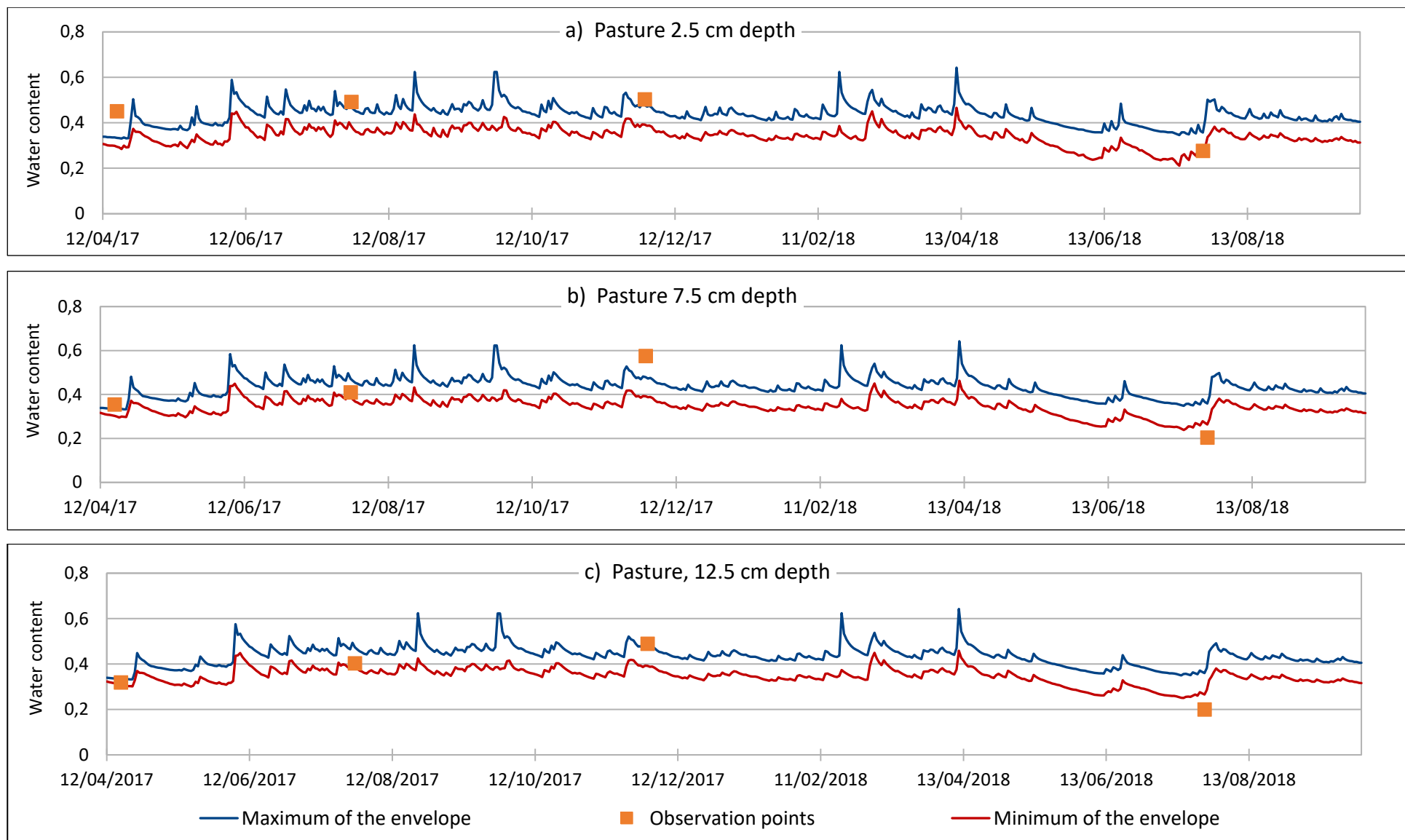


Figure 3.22 a, b, c - Observation data at three depths and envelopes of the simulated soil moisture at the corresponding depths, for the pasture model.

## Evaluation of the models of the two units

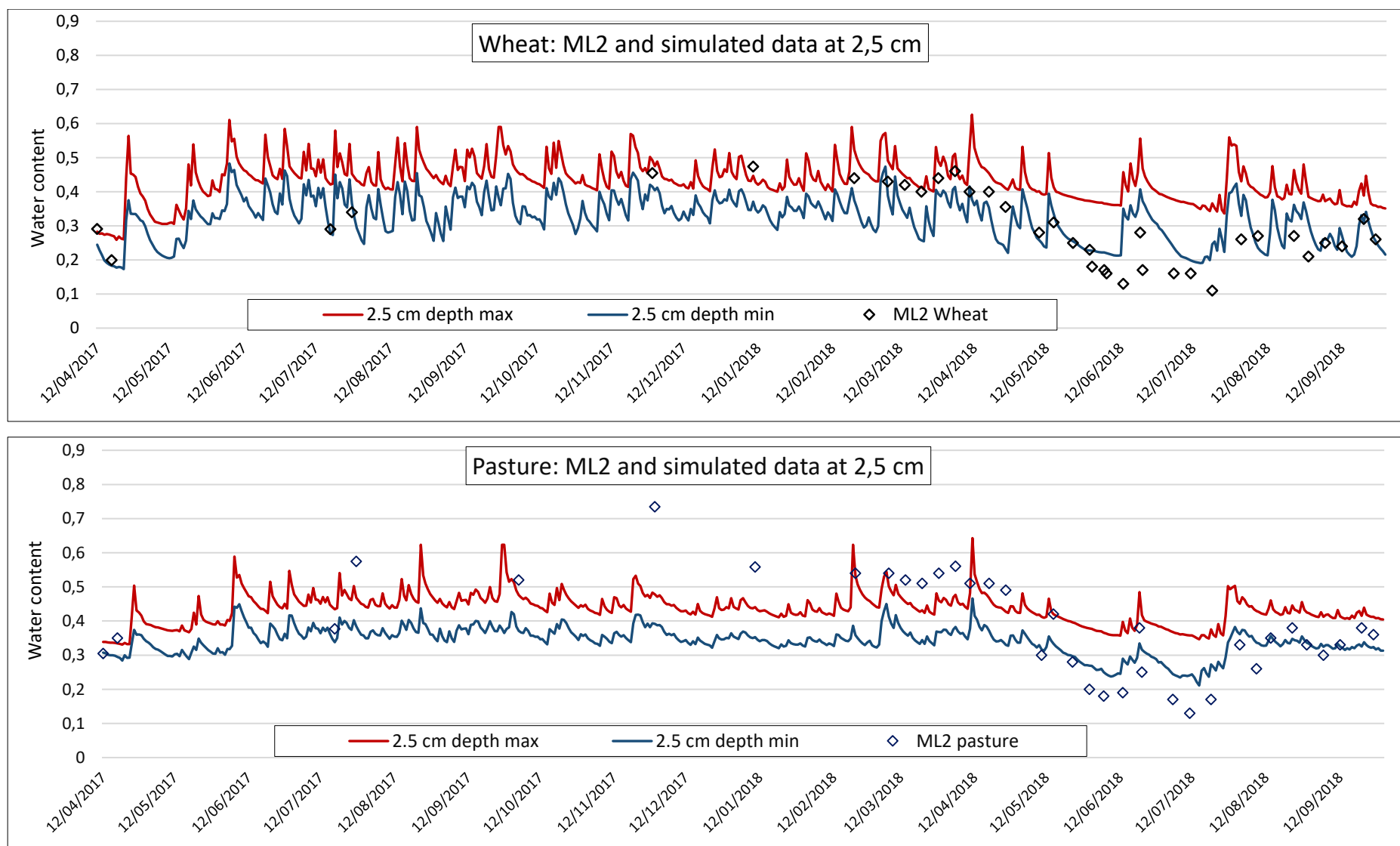
To evaluate the two models, each envelope of the simulated soil moisture at 2.5 cm depth was compared with the ML2 measurements taken on the corresponding field, as illustrated by Figures 3.23 and 3.24. The model representing the cropped fields was evaluated by using the ML2 measurements taken in the wheat field, while the pasture model was evaluated by using the measurements from the pasture.

The model of the cropped fields seems to compare better with the ML2 measurements than the model of the pasture. No one of the models represents well the ML2 data during June and July 2018,

In addition to that, the RMSE between the median of the simulated values and the ML2 measurements was calculated for each model. The RMSE values are reported below, resulting to be lower than the RMSE between the simulated data and the calibration points.

Table 3.11 – RMSE values obtained by the evaluation of the two models

	RMSE
Cropped fields	0,107
Pasture	0,110



Figures 3.23, 3.24 – Evaluation of the model for the cropped fields (3.23) and for the pasture (3.24) by using the data collected with the ML2 probe from the wheat field and the pasture, respectively.



### 3.3. Simulated large scale dynamics

The dotted plots resulted from the CRS calibration are reported in Figure 3.25 (from a to e); the green dots represent the behavioural simulations and the red one represent the best simulation.

Figure 3.26 illustrates the envelope of the simulated CRS data and the observed CRS data, divided into the three years of the simulation period. The envelope compares well with the observed data, except the period from January to March 2016 and from June to September 2018.

The minimum and maximum RMSE of the behavioural simulations are:

- Minimum RMSE=0.063;
- Maximum RMSE=0.065.

#### *Evaluation of the CRS model*

To evaluate the CRS model, an area-weighted average of the ML2 measurements was calculated (the weight is the proportion of each field in the CRS' footprint). It was then plotted together with the envelope of the CRS model, for the period from 12/04/2017 to 30/09/2018 (Figure 3.27).

Like the models of the two units, the CRS model don't represent well the ML2 measurements of June and July 2018.

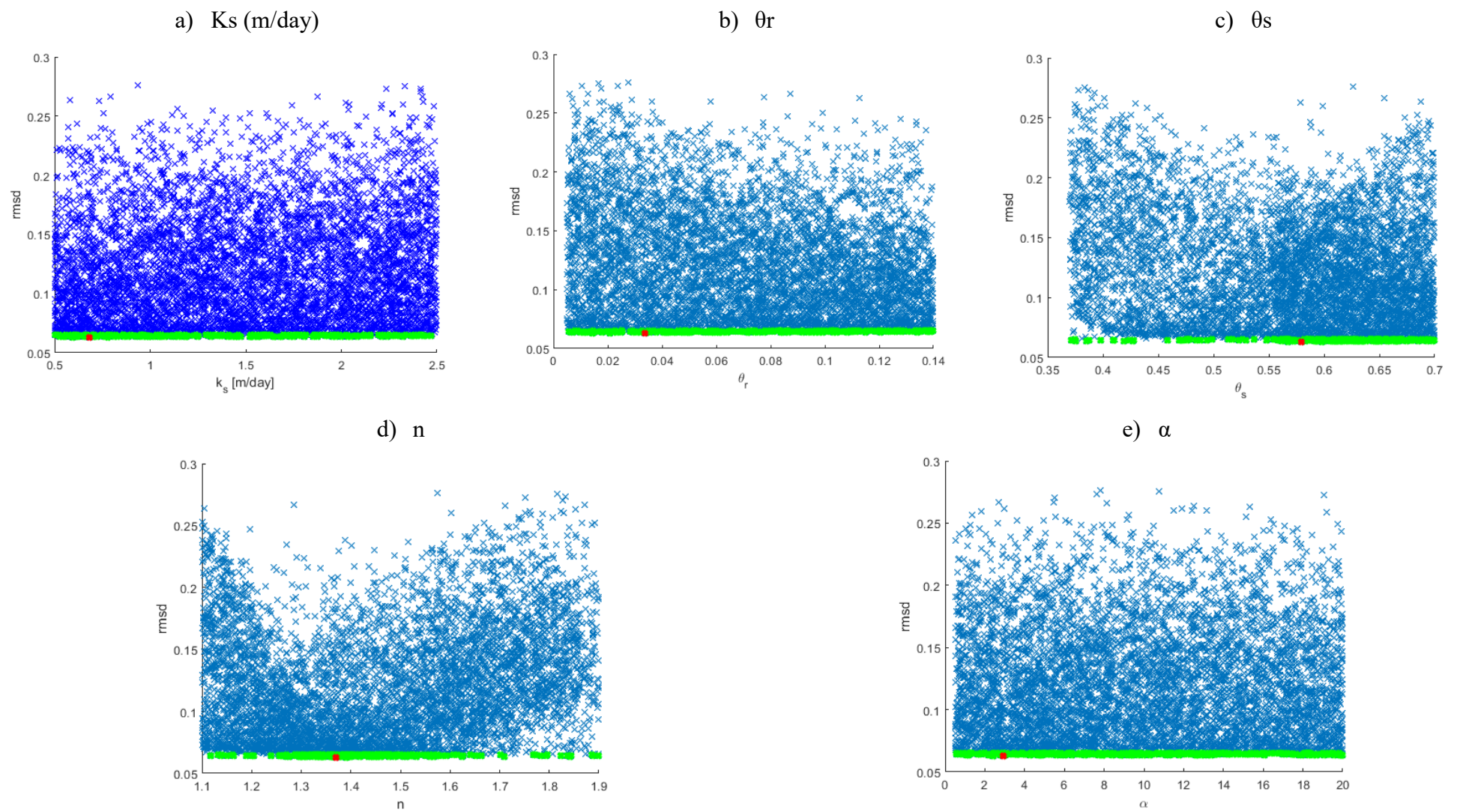
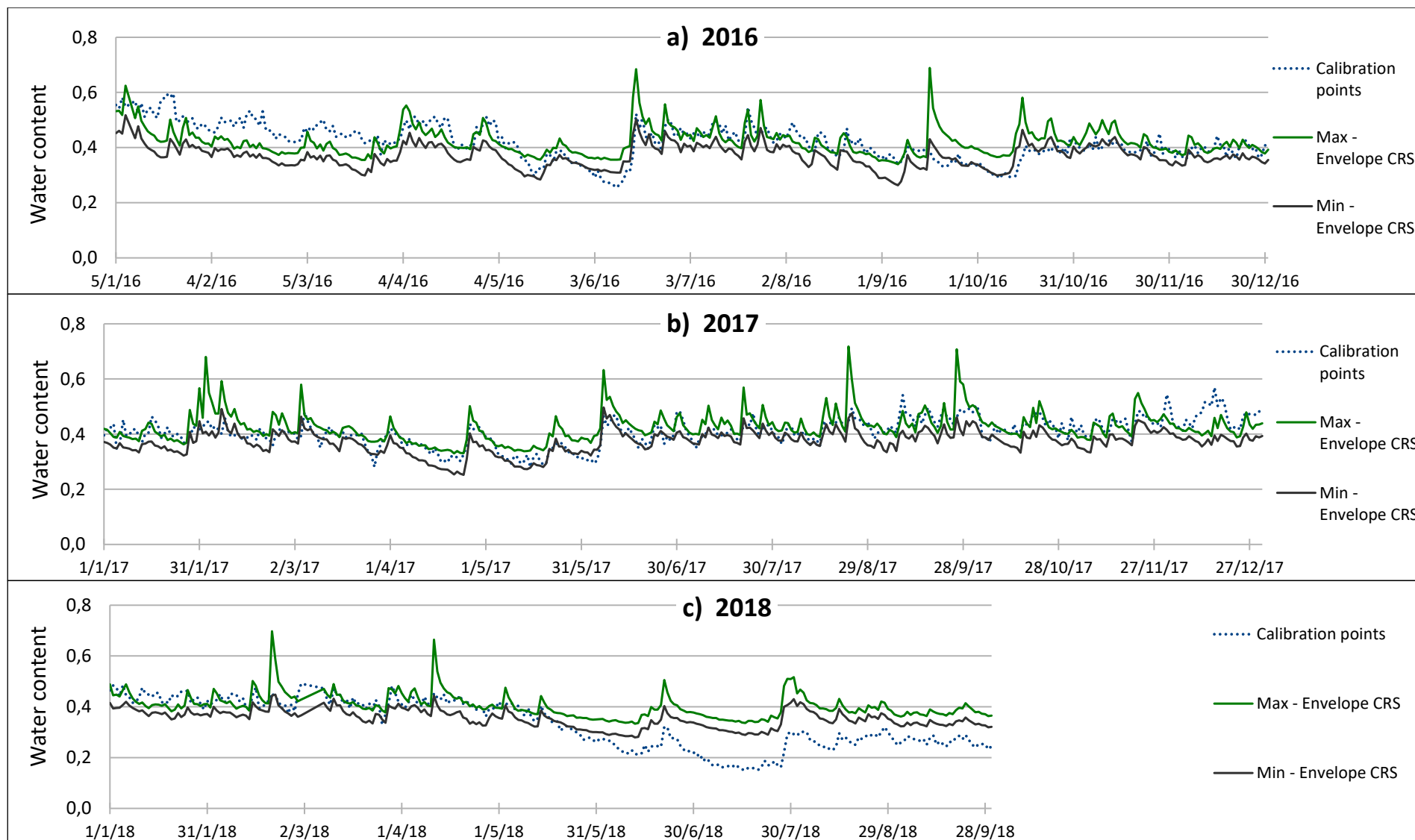


Figure 3.25 – Dot plots representing the variation of the performance of the CRS model (indicated by RMSD) within the pre-set ranges of the parameters  $K_s$ ,  $\theta_r$ ,  $\theta_s$ ,  $n$  and  $\alpha$



Figures 3.26 a, b, c – Simulates CRS dynamics and observed CRS data, divided into the three years of the simulation period.

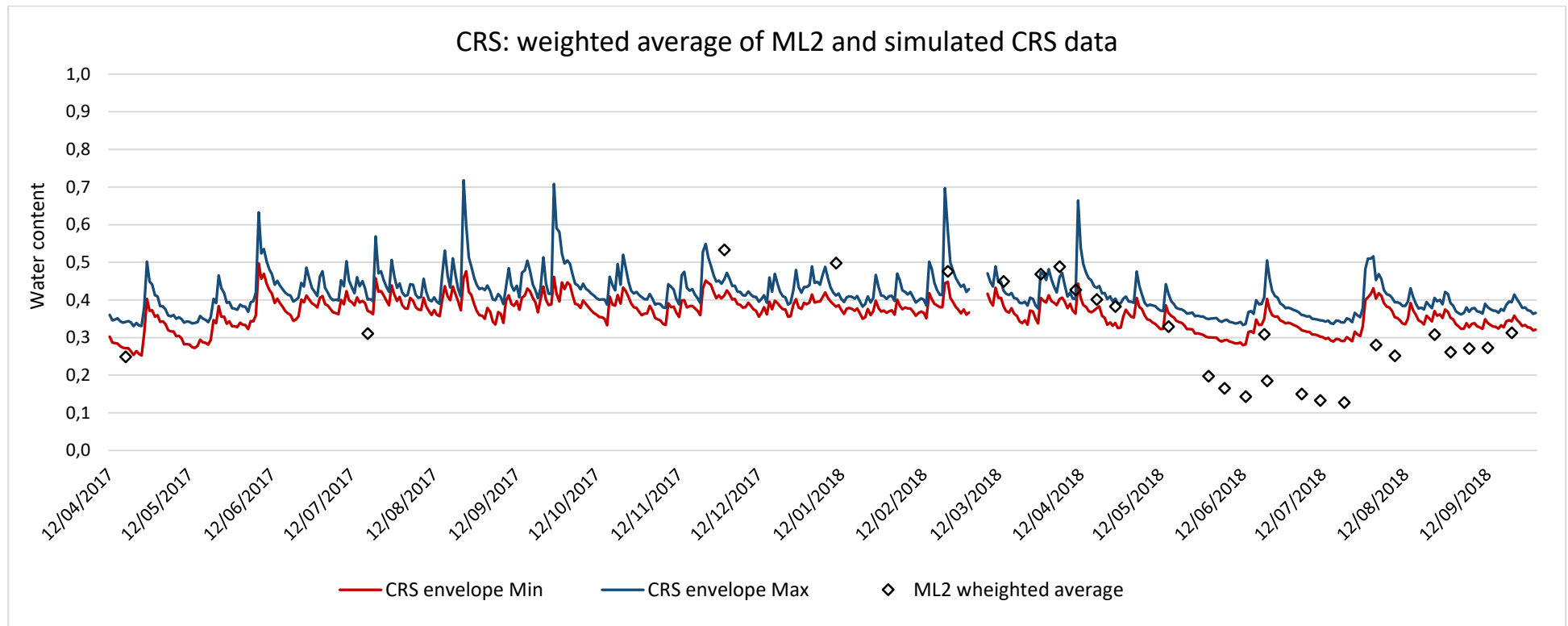


Figure 3.27 – Evaluation of the CRS model by using an area-weighted average of the ML2 measurements taken from the three units.

## 1.1. Comparison of the results of the CRS model and of the models of the two units

As explained in section 2.5, an area-weighted average was calculated using the envelopes of the soil moisture simulated for the cropped fields and the pasture. It was then plotted together with the simulated CRS envelope, for the period from 12/04/2017 to 30/09/2018 (Figure 3.27).

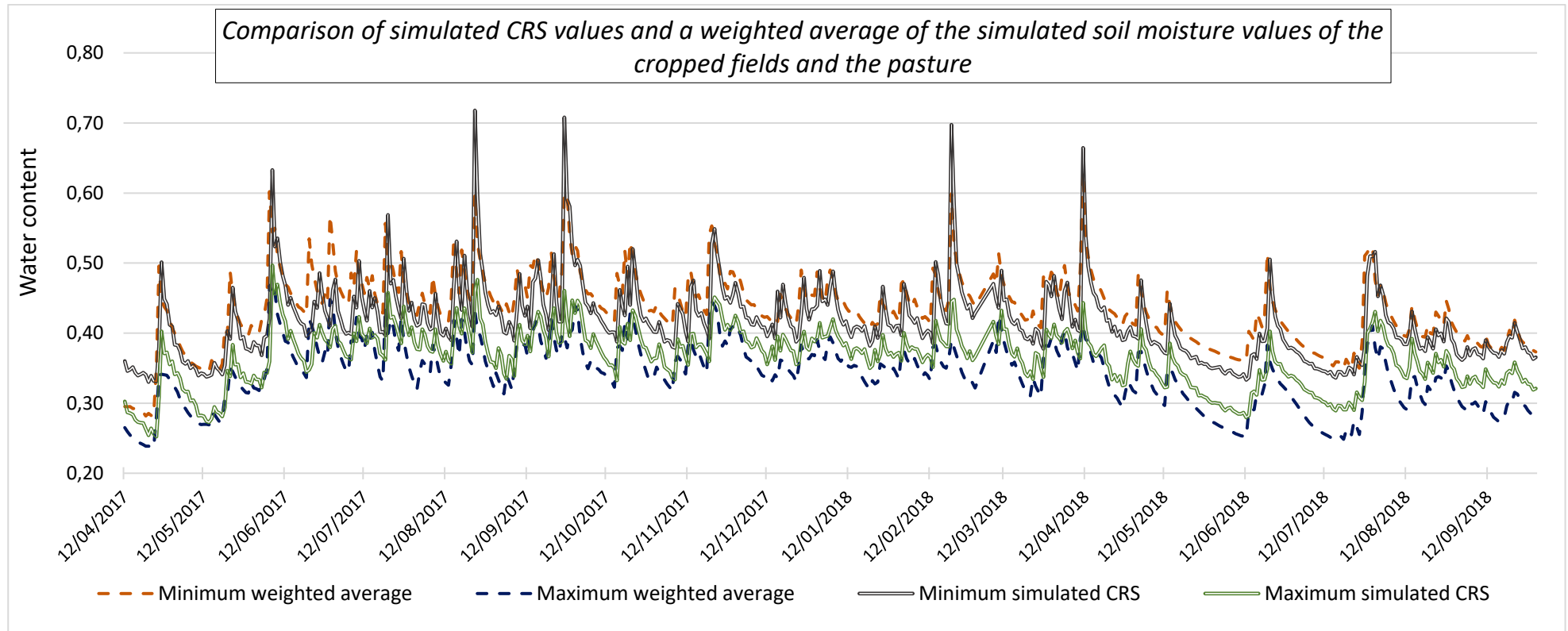


Figure 3.27 – Envelope of the CRS model plotted together with an area-weighted average of the envelopes of the models of the two units.

## 4. Discussion of the results

### 4.1. Discussion of the soil hydraulic properties and texture results

#### *Texture*

The texture was found to be sandy-loam for all the analysed samples and this is in agreement with **1:250 000 texture map of Scotland, by the James Hutton Institute (1988)**.

No clear change along the vertical profile was either found in the study of the water retention curves, confirming that the soil down to 30 cm depth could be assumed to be of just one type.

#### 4.1.1. Discussion of the water retention curve results

#### *Estimated parameters*

All the estimated parameters present wide ranges, reflecting a high variability of the soil capacity to retain water in the study area.

Some consideration could be made about each parameter, as a consequence of the comparison between the estimated parameters and the literature values and by observing the box-and-whiskers plots of the Figures from 3.3 to 3.6:

- $\theta_r$ : a low value of this parameter (out of literature ranges) is obtained for several samples (namely every sample from the pasture field, the majority of the samples from the barley field and some samples from the wheat field). As explained in section 2.2.1.,  $\theta_r$  is the amount of water that can't be drained from the soil because it's retained in disconnected pores and immobile films. A low value of this parameter could mean that in some points just a very low amount of water is retained at low suction;
- $\theta_s$ : a high variability of this parameter was found among the collected samples, ranging from 0.37 to 0.63. The maximum values found are out of literature ranges. However, the reliability of the estimates is confirmed by the porosity values previously estimated on 216 samples from the Elswick site (72 samples from each field), presenting ranges that match the ones obtained in this thesis.

- $\alpha$ : the values found for the majority of the samples are within literature ranges. However, also pretty low values, out of literature ranges, were found for some samples. This parameter is related to the inverse of the air entry pressure, so, a low value of  $\alpha$  could mean a high air entry pressure and hence a low pore-size in some points of the field.
- $n$ : different sampling points were found to be characterized by considerably different values of this parameter. Although the majority of the samples show values that are within the literature ranges, some samples present pretty high values of this parameter (about 2). The parameter  $n$  is a measure of the pore-size distribution and the high values found may denote that the distribution is narrow and pores are not very connected (Verrot et al., 2018). The wide range of values obtained could mean a high variability of the connectivity between pores between different points of the site.

### *Discussion about the variability of the curves*

Figures from 3.12 to 3.19 provide some insights into the horizontal variability of the soil capacity to retain water.

From Figures from 3.12 to 3.14, concerning the first 15 cm of soil, two clusters are recognizable: one corresponding to the wheat field and the other one to the pasture. An interesting aspect is that the pasture curves in the first 15 cm show a  $\theta_s$  value that is higher than in the other fields, as visible by the box-and-whiskers plot of Figure 3.4.

Moreover, at depths higher than 15 cm, a cluster formed by the curves from the barley field is recognizable (Figures 3.15 and 3.16).

Figures from 3.12 to 3.19 offer some insights into the vertical variability along seven soil profiles, each one corresponding to a sampling point.

Both the points A and B from the wheat field (Figures 3.12 and 3.13) are characterized by curves with a constant shape with depth.  $\theta_s$  is the only parameter that considerably changes along the profile. However, no clear correlation was found between  $\theta_s$  and depth.

Concerning the barley field, the effect of ploughing was identifiable: the first 10 cm of points E and F, indeed, present curves that are very different from the rest (Figures 3.14, 3.15), probably due to the fact that the soil was disturbed, so it lost its natural characteristics.

By contrast, point G (collected after a further soil treatment; Figure 3.16), show very low vertical variability, suggesting that the treatment left the soil more homogeneous. In addition to that, the

soil from point G and the deeper soil of point F show a very similar retention capacity (Figure 3.17), probably meaning that deeper soil was less affected by the ploughing.

Summarizing, the shapes of the water retention curves show a horizontal variability that is higher than the vertical one. Moreover, the horizontal variability between fields was found to be higher than the one within fields in the majority of cases. In addition to that, no greater similarity was found between the two cropped fields, although classified as the same soil type and with similar land use.

## **4.2. Discussion about the models of the two units**

The RMSE values ( $0.185 \div 0.216$  for the cropped fields and  $0.234 \div 0.262$  for the pasture) are quite high for both the models. However, to interpret these values, the low number of data available and the length of the simulation period should be considered. Given these two factors, the models could be considered satisfying. Also Beven (2012) points out that if the number of calibration data is low, there may not be enough information to support a robust calibration of several parameters. In addition to that, the observed points were not equally spaced in time. There was indeed a lack of data from 29/11/2017 to 25/07/2018, meaning that almost 8 months weren't represented by the calibration data, possibly negatively affecting the results.

Another possible reason is that some of the calibration data were affected by error. Beven (2012) asserts that disinformative calibration data could lead to biased estimates. However, each one of the calibration data was obtained by calculating the average of soil moisture values estimated on six samples, that were collected in different positions of the fields, and no outlier was found among these values. It's then unlikely that any of these data was affected by a high error.

As concerns the dotted plots from Figure 3.20, both the models seem to be sensitive only to the parameters  $\theta_s$  and  $n$ , while the others seem to generate behavioural simulations for any value of the preset range. It follows that it's not possible to identify a unique set of parameters that could be assumed to be the most realistic one, with the present hydraulic model and observation data (as explained in "The concept of equifinality", in section 2.3.2.).

Another reason why behavioural simulations are found also close to the boundary of the parameters' ranges could be that the range was not wide enough (Beven 2012). However, since the ranges were set pretty wide and were predetermined by laboratory experiments on samples from the study site, this option could be presumed as unlikely.



Regarding Figures 3.21 and 3.22, the majority of the observation points seem to be located within the corresponding envelope, or close to it, with some exceptions. In particular, the trends simulated by the model of the cropped fields at 12.5 cm depth and by the pasture model at 7.5 cm don't seem to represent extreme conditions properly, namely November 2017 (wettest condition) and July 2018 (driest condition). In addition to that, neither the pasture simulated data at 12,5 cm match the dry conditions on 25/07/2018.

### *Discussion of the evaluation of the two models*

The comparison between the data simulated at 2,5 cm and the ML2 measurements, plotted in Figures 3.23 and 3.24, show that both the models are lacking in representing the dry conditions from the beginning of June to the end of July 2018. Furthermore, the pasture model is also deficient in representing some other points corresponding to wet conditions.

However, the RMSE between the median of the envelopes and the ML2 measurements was higher than the one with the calibration points, suggesting that the models acceptably simulate soil moisture during the periods when no calibration data were available.

## **4.3. Discussion about the CRS model**

The RMSE values obtained for the CRS model ( $0.063 \div 0.065$ ) are low enough to consider the CRS model acceptable. The difference between them and the RMSE values of the models of the two units is noticeable and the greater availability of data for the calibration has to be considered as the main cause.

As concerns the dotted plots (Figure 3.25), the only parameters the model seem to be sensitive to are  $\theta_s$  and  $n$ , similarly to the models of the two units. However, the CRS model seems to be less sensitive to them than the other two models.

It follows the considerations made before: it's not possible to identify a unique set of parameters that could be considered representative of the real conditions.

The envelope illustrated in Figure 3.26 show a good match with the observed data, except some periods, namely from January to the end of March 2016 and from June to the end of September 2018 (drought process). Also the models of the two units were found to be lacking in reproducing the dry conditions during the second of the two periods.

### *Discussion about the evaluation of the CRS model*

Figure 3.27 should be interpreted in a qualitative way, because the ML2 measurements and the CRS simulated data actually refer to different volumes. The main point is that the comparison confirms that the model is lacking in representing the dry conditions from May to September 2018.

## **4.4. Discussion about the comparison of the modelling results**

Figure 3.27 shows that the CRS simulated data compares well with the weighted average of the data simulated for the two units. Specifically, the CRS envelope is more narrow than the other and for the majority of the days is within the range of the weighted average. However, almost all the higher peaks constitute exceptions to this, with the CRS data being higher than the weighted average. The CRS model could possibly overestimate soil moisture for highest precipitation values or, it could be the other models that underestimate it.

## 5. Conclusion

Soil hydraulic properties were found to be very heterogeneous in the study site, generally showing a greater variability between fields than within each field. Moreover, they were found to vary more horizontally than vertically.

Regarding the hydrological models, the CRS model was found to represent field data better than the models of the two units. The main cause is likely to be the limited number of observed points in time used for the calibration of the last two models.

Moreover, all the models were found to be lacking in representing the dry conditions from the end of May to the beginning of August 2018. The CRS model was additionally found to be lacking in representing the subsequent observed points, until the end of September 2018.

Concerning the information contained in the dot plots, every calibration showed the model to be sensitive only to the parameters  $\theta_s$  and  $n$ , while the other parameters present equally good fit to the observed data in the whole pre-set range. It follows that a single set of parameters that could represent the real system can't be identified.

Finally, the simulated CRS data were found to compare well with the weighted average calculated with the simulations of the two units, presenting some exception at the peaks.

Since soil hydraulic properties were found to be highly variable between different points of the study site, also soil moisture should be assumed to present a similar variability. It follows that local soil moisture dynamics can't be assumed to be representative of a whole field. Consequently, point-scale measurement techniques such as the PR2 probe, even if providing a high number of data in time, are not useful to infer soil moisture dynamics at larger scale.

The classic method of deriving soil moisture from a large number of samples manually collected from different points of the field is a way to provide spatial representativeness, but only a few points in time could be obtained in this way. The model calibration of the two units showed how the lack of data in time negatively affects the results, providing no simulation with a really good match to the observed values.

This thesis verified the spatio-temporal representativeness offered by the new Cosmic Ray Sensor technique by studying its operating in an area where different land uses and soil types were involved. The results showed that the data obtained by the use of CRS integrate the soil moisture dynamics of the different units of the footprint.

## 6. Bibliography

- Allen, R. G., Pereira, L., Raes, D. and Martin S.. 1998. "Crop Evapotranspiration : Guidelines for Computing Crop Water Requirements." *FAO Irrigation and Drainage Paper*: 56, 1–15.
- Asner, G.P, Scurlock, J. M. O. and Hicke, J. 2003. "Global Synthesis of Leaf Area Index Observations :." *Global Ecology and Biogeography* 12 (3): 191–205.
- Baroni, G., Scheffele, L. M., Schrön, M., Ingwersen, J. and Oswald, S. E. 2018. "Uncertainty, Sensitivity and Improvements in Soil Moisture Estimation with Cosmic-Ray Neutron Sensing." *Journal of Hydrology* 564 (July 2017): 873–87.
- Beven, K. 2006. "A Manifesto for the Equifinality Thesis." *Journal of Hydrology* 320 (1–2): 18–36.
- Beven, K. 2012. *Rainfall-Runoff Modelling*. John Wiley & Sons, Ltd
- Beven, K. 2016. "Advice to a Young Hydrologist." *Hydrological Processes* 30 (20): 3578–82.
- Boorman, D. B., Hollis, J. M., and Lilly, A. 1995. "Hydrology of Soil Types: A Hydrologically-Based Classification of the Soils of United Kingdom." *Institute of Hydrology Report* 126 (126): 137.
- Zheng, C., Hill, M. C., Cao, G. and Ma, R. 2013. "HYDRUS: Model Use, Calibration, and Validation." *Transactions of the ASABE* 55 (4): 1549–59.
- Willmott, J.C. and Matsuura K. 2005. "Advantages of the Mean Absolute Error (MAE) over the Root Mean Square Error (RMSE) in Assessing Average Model Performance." *Climate Research* 30 (1): 79–82.
- Creutzfeldt, B., Peter, A. T., Güntner, A., Ferré, T.P.A., Graeff, T. and Merz, B.. 2014. "Storage-Discharge Relationships at Different Catchment Scales Based on Local High-Precision Gravimetry." *Hydrological Processes* 28 (3): 1465–75.
- Delta-T Devices Ltd. 1998. "Delta - T Devices - ML2 User Manual."
- Delta-T Devices Ltd. 2016. "User Manual for the Profile Probe Type PR2."
- Desilets, D, and Zreda, M. 2013. "Footprint Diameter for a Cosmic-Ray Soil Moisture Probe: Theory and Monte Carlo Simulations." *Water Resources Research* 49 (6): 3566–75.
- Desilets, D., Zreda, M. and Ferré, T. P. A. 2010. "Nature's Neutron Probe: Land Surface Hydrology at an Elusive Scale with Cosmic Rays." *Water Resources Research* 46 (11): 1–7.
- Evans, J. G., Ward, H. C., Blake, J. R., Hewitt, E. J., Morrison, R., Fry, M., Ball, L. A. et al. 2016. "Soil Water Content in Southern England Derived from a Cosmic-Ray Soil Moisture Observing System – COSMOS-UK." *Hydrological Processes* 30 (26): 4987–99.
- Feddes, R.A., Penning de Vries, F. W. T. and Van. Laar, H. H. 1978. "Simulation of Plant Growth

- and Crop Production,” 308.
- Franz, T. E., Zreda, M., Rosolem, R. and Ferre, T. P. A. 2013. “A Universal Calibration Function for Determination of Soil Moisture with Cosmic-Ray Neutrons.” *Hydrology and Earth System Sciences* 17 (2): 453–60.
- Van Genuchten, M.T. 1980. “A Closed-Form Equation for Predicting the Hydraulic Conductivity of Unsaturated Soils.” *Soil Science Society of America Journal*.
- Brunetti, G., Šimůnek, J., Boga, H., Baatz, B., Huisman, J.A., Dahlke, H., Vereecken, H. 2018. “On The Information Content of Cosmic-Ray Neutron Data in The Inverse Estimation of Soil Hydraulic Properties.” *Vadose Zone Journal*, no. September: 1–72.
- European Commission. 2012. “Crop Monitoring in Europe”, MARS Bulletin Vol. 21 No. 6.
- Heidbuchel, I., Guntner, A. and Blume, T. 2016. “Use of Cosmic-Ray Neutron Sensors for Soil Moisture Monitoring in Forests.” *Hydrology and Earth System Sciences* 20 (3): 1269–88.
- International Atomic Energy Agency. 2017. “Cosmic Ray Neutron Sensing: Use, Calibration and Validation for Soil Moisture Estimation.” Vienna: IAEA.
- J. Šimůnek, M. Š., Saito, H., Sakai, M. and Van Genuchten, M.T. 2013. “Hydrus1D - 4.17 Manual.”
- Zotarelli, L., Dukes, M.D., Romero, C., Migliaccio, K.W. and Morgan, K.T. 2016. “Step by Step Calculation of the Penman-Monteith Evapotranspiration (FAO-56 Method),” 1–10.
- Ling, L., Franz, T.E., Robinson, D.A. and Jones, S. B. 2014. “Measured and Modeled Soil Moisture Compared with Cosmic-Ray Neutron Probe Estimates in a Mixed Forest.” *Vadose Zone Journal*, 1–13.
- Ma, Y., Yan Li, X., Guo, L. and Lin, H. 2017. “Hydropedology: Interactions between Pedologic and Hydrologic Processes across Spatiotemporal Scales.” *Earth-Science Reviews* 171 (19): 181–95.
- Peters-Lidard, Christa, D., Clark, M., Samaniego, L., Verhoest, N., Van Emmerik, T., Uijlenhoet, R., Achieng, K., Franz, T.E. and Woods, R. 2017. “Scaling, Similarity, and the Fourth Paradigm for Hydrology.” *Hydrology and Earth System Sciences* 21 (7): 3701–13.
- Rawls, W.J., and Brakensiek, D.L. 1985. “Prediction of Soil Water Properties for Hydraulic Modeling” 21 (4): 162.
- Ritchie, J.T. 1972. “Model for Predicting Evaporation from a Row Crop with Incomplete Cover.” *Water Resources Research* 8 (5): 1204–13.
- Villarreyes, R., Baroni, C.G. and Oswald, S. E. 2014. “Inverse Modelling of Cosmic-Ray Soil Moisture for Field-Scale Soil Hydraulic Parameters.” *European Journal of Soil Science* 65 (6): 876–86.

- Robinson, D. A., Campbell, C. S., Hopmans, J. W., Hornbuckle, B. K., Jones, S. B., Knight, R., Ogden, F., Selker, J., and Wendroth, O. 2008. "Soil Moisture Measurement for Ecological and Hydrological Watershed-Scale Observatories: A Review." *Vadose Zone Journal* 7 (1): 358.
- Rodríguez, B., Castro, T. 2012. "Rainfall–runoff Response and Event-Based Runoff Coefficients in a Humid Area (Northwest Spain)." *Hydrological Sciences Journal* 57 (3): 445–59.
- Schrön, M., Köhli, M., Scheiffele, L., Iwema, J., Bogaen, H. R., Ling, L., Martini, E., et al. 2017. "Improving Calibration and Validation of Cosmic-Ray Neutron Sensors in the Light of Spatial Sensitivity – Theory and Evidence." *Hydrology and Earth System Sciences Discussions*, no. March: 1–30.
- Song, L., Zhuang, Q., Yunhe, Y., Shaohong, W., and Xudong, Z. 2017. "Intercomparison of Model-Estimated Potential Evapotranspiration on the Tibetan Plateau during 1981–2010." *Earth Interactions* 21 (11).
- Tarboton, D. G. 2003. "Chapter 4 - Soil Properties." In *Rainfall-Runoff Processes*, 1–30.
- The James Hutton Institute. 1988. "1:250 000 UKSO Texture Map of Scotland.Pdf."
- Vereecken, H., Huisman, J. A., Hendricks, H. J., Franssen, N., Bogaen, H. R., Kollet, S., M. Javaux, J. van der Kruk, and J. Vanderborght. 2015. "Soil Hydrology: Recent Methodological Advances, Challenges, and Perspectives." *Water Resources Research* 51: 2616–33.
- Vereecken, H., Huisman, J. A., Bogaen, H., Vanderborght, J., Vrugt, J. A., and J. W. Hopmans. 2010. "On the Value of Soil Moisture Measurements in Vadose Zone Hydrology: A Review." *Water Resources Research* 46 (4): 1–21.
- Verrot, Lucile et al. 2018. "Importance of Temporal Variability in Soil Physical Properties for Soil Water Modelling", manuscript submitted for publication
- Western, A.W., Grayson, R.B., and Blöschl, G. 2002. "Scaling of Soil Moisture: A Hydrologic Perspective." *Annual Review of Earth and Planetary Sciences* 30 (1): 149–80.
- Zreda, M., Desilets, D., Ferré, T. P.A. and Scott, R. L. 2008. "Measuring Soil Moisture Content Non-Invasively at Intermediate Spatial Scale Using Cosmic-Ray Neutrons." *Geophysical Research Letters* 35 (21): 1–5.

## 7. Acknowledgements

I would first like to thank my supervisor from Politecnico, Prof. Pierluigi Claps, for his supervision and for giving me the unique possibility to work at my thesis project in a foreign research group. I will always be grateful to him and Thea Piovano for introducing me in the Hydrology department of the school of Geoscience, at the University of Aberdeen.

Secondly, I would like to offer my special thanks to my supervisor at the University of Aberdeen, Dr. Jeris Gosie. She followed me with dedication during all my project, motivating me and effectively clarifying any doubt that I had. She also introduced me in field work activities and different laboratory experiments giving me the possibility to enhance my practical skills.

I would like to express another special thank to the PhD student Katya Dimitrova, who introduced me in the Hydrology research group of the University of Aberdeen, explained me everything needed about the monitoring of Elsick site and let me cooperate with her in the field work. She also provided me with data about the site that she collected and estimated during the first 1 and a half year of her PhD project; these data were exploited as the basis of this thesis project. She additionally gave me useful advices during all my project.

I would also like to thank the Postdoctoral researcher Lucile Verrot, who provided the Matlab code used to implement the Monte Carlo method for the calibrations of the Hydrus-1D models, adjusting the code to the different models and helping me to run it. She also gave me the code to fit the Van Genuchten function to the laboratory experiments.

I would then like to thank the laboratory staff of the Cruickshank building, who helped me during the laboratory experiments to determine the soil texture and the water retention curves.

Of course, I would also like to express my gratitude to my family, that has always supported me and my choices and helped me during all my years of study.

A special thank should be given to my boyfriend, who supported and encouraged me during my project and patiently waited for my coming back.

The results I have obtained would not have been possible without all of them.

Finally, I would like to thank all my closest friends, who have been by my side both in happy moments and hard times, with faithful affection.